2018

Precision radio-frequency and microwave dielectric spectroscopy and characterization of ionic aqueous solutions

Amin Gorji-Bandpy
Iowa State University

Precision radio-frequency and microwave dielectric spectroscopy and characterization of ionic aqueous solutions

by

Amin Gorji-Bandpy

A dissertation submitted to the graduate faculty

in partial fulfillment of the requirements for the degree of

DOCTOR OF PHILOSOPHY

Major: Electrical Engineering
(Electromagnetics, Microwave and Nondestructive Evaluation)

Program of Study Committee:
Nicola Bowler, Major Professor
Brian K. Hornbuckle
Amy L. Kaleita-Forbes
Nathan M. Neihart
Jiming Song

The student author, whose presentation of the scholarship herein was approved by the program of study committee, is solely responsible for the content of this dissertation. The Graduate College will ensure this dissertation is globally accessible and will not permit alterations after a degree is conferred.

Iowa State University

Ames, Iowa

2018

DEDICATION

To all of the dedicated personnel and volunteers of Moulton Elementary School, Des Moines, IA, who strive to improve the lives of disadvantaged children and families. Interacting with these students has been a lesson in humility as I reflected on the accomplishments and sacrifices I have made in pursuit of my doctorate degree.

TABLE OF CONTENTS

Page

LIST OF FIGURES vi

LIST OF TABLES x

ACKNOWLEDGMENTS xiv

ABSTRACT xvi

CHAPTER 1. GENERAL INTRODUCTION 1
1.1. Research Question 1
1.2. Problem Statement 1
1.3. Current Ion Monitoring Systems 3
1.3.1. Ion-Selective Electrode (ISE) Technology 3
1.3.2. Ultraviolet (UV) Absorption Technology 4
1.4. Dielectric Spectroscopy 6
1.5. Research Objectives 10
1.5.1. Develop Precision Laboratory-Based Measurement Techniques for RF and MW Dielectric Spectroscopy of Ionic Aqueous Solutions 10
1.5.2. Collection of RF and MW Dielectric Spectral Data with Low Uncertainty and Rigorous Uncertainty Analysis 11
1.5.3. Exploit Potential Indicators to Estimate Ion-Specific Concentration 11
1.5.4. Develop Concentration- and Temperature-Dependent Models for RF and MW Spectral Parameters of Aqueous Ionic Solutions 12
1.6. Dissertation Organization 12
1.7. References 13

CHAPTER 2. STATIC PERMITTIVITY OF ENVIRONMENTALLY-RELEVANT LOW-CONCENTRATION AQUEOUS SOLUTIONS OF SODIUM CHLORIDE, SODIUM NITRATE, AND SODIUM SULPHATE 16
2.1. Abstract 16
2.2. Introduction 17
2.3. Experimental Method 19
2.3.1. Apparatus and Sample Preparation 19
2.3.2. Data Analysis 21
2.3.3. Uncertainty Analysis 24
2.4. Modeling Static Permittivity 27
2.4.1. Dilution and Internal Depolarizing Field 28
2.4.2. Kinetic Depolarization 29
2.4.3. Dielectric Saturation 32
2.4.4. Ionic Atmosphere Polarization 35
2.4.5. Complete Model of Static Permittivity 37
2.5. Results 38

2.6. Discussion 40
2.6.1. Evaluation of Semi-Empirical Model 40
2.6.2. Irrotationally Bound Water Molecules 44
2.6.3. Debye-Falkenhagen Effect 47
2.7. Conclusion 48
2.8. References 49

CHAPTER 3. DIELECTRIC MEASUREMENT OF LOW-CONCENTRATION AQUEOUS SOLUTIONS: ASSESSMENT OF UNCERTAINTY AND ION-SPECIFIC RESPONSES 54
3.1. Abstract 54
3.2. Introduction 55
3.3. Experimental Setup 58
3.4. Fitting Procedure 62
3.5. Uncertainty Analysis 64
3.5.1. Compilation of Uncertainty Elements 64
3.5.1.1. Random errors 65
3.5.1.2. Systematic errors 66
3.5.1.3. Reference data uncertainty 68
3.5.1.4. Combined standards uncertainties 69
3.5.2. Covariance Matrix Method 72
3.5.3. Monte Carlo Method 74
3.5.3.1. Generating random errors 75
3.5.3.2. Generating trial permittivity data 76
3.5.3.3. Generating trial fitting parameters 76
3.5.4. Results 76
3.6. Ion-Specific Indicators 80
3.7. Conclusion 85
3.8. References 87

CHAPTER 4. CONCENTRATION AND TEMPERATURE DEPENDENT MODELS OF DIELECTRIC SPECTRAL PARAMETERS FOR LOW-CONCENTRATION IONIC AQUEOUS SOLUTIONS 91
4.1. Abstract 91
4.2. Introduction 91
4.3. Measurement and Analysis 94
4.3.1. Experimental Setup 94
4.3.2. Data Fitting 95
4.4. Results 96
4.5. Conductivity Modeling 96
4.6. Relaxation Time Modeling 102
4.6.1. Temperature Dependence of Deionized Water 102
4.6.2. Temperature Dependence of Ionic Aqueous Solutions 107
4.7. Static Permittivity Modeling 110
4.7.1. Temperature Dependence of Deionized Water 110
4.7.1.1. Infinite permittivity 113
4.7.1.2. Kirkwood correlation factor 115

4.7.1.3. Hydrogen-bonded molecules concentration 118
4.7.1.4. Model 119
4.7.2. Temperature Dependence of Ionic Aqueous Solutions 119
4.8. Three-Dimensional Trajectory Plots 126
4.9. Conclusion 126
4.10. References 129

CHAPTER 5. GENERAL CONCLUSION 132
5.1. Summary 132
5.2. Feasibility of Potential Sensor 135
5.3. Future Directions 137

LIST OF FIGURES

Page

Figure 1.1 Drawing of a cropland without a tile drainage-system (a), and with a tile-drainage system (b). The perforated pipes are typically deployed 1 m below the soil surface and spaced 10 to 30 m apart. This picture is redrawn from the original source [5]. 2

Figure 1.2 Ion-selective electrode (ISE) sensor and membrane. The membrane allows sodium ions to cross and, therefore, a concentration-dependent voltage is generated across the membrane. The ISE sensor photo used in the figure, at right, is from Neulog [12]. 4

Figure 1.3 General design and key components of field-deployable ultraviolet (UV) sensor. This picture is modified and redrawn from the original source [10]. UV sensor photo used in the figure is from Hach [13]. 5

Figure 1.4 Types of water-based molecular dipoles and charge carriers present in a simple ionic aqueous solution of sodium chloride (NaCl). 8

Figure 1.5 A schematic of dielectric spectra of a simple ionic aqueous solution and relaxation processes corresponding to different dipolar mechanisms. The three-state model mentioned for mechanism 3 comprises the relaxation processes of hydrogen-bonded water molecules, hydration water molecules of cation, and hydration water molecules of anion [21]. 9

Figure 2.1 Dielectric dispersion $\varepsilon'(f)$ (a) and loss $\varepsilon''(f)$ (b) spectra of aqueous solutions of NaCl with c = 7.052 mmol/L; $NaNO_3$ with c = 7.139 mmol/L; and Na_2SO_4 with c = 7.797 mmol/L at T = 25 °C. The symbols represent the measured permittivity data. The lines represent the fitted curves (single Debye relaxation model). The contributions due to the conductivity term ($\sigma/2\pi f\varepsilon_0$) and the dipolar relaxation process $\varepsilon_d''(f)$ are shown separately in the inset of (b). 22

Figure 2.2 Hypothetical graph representing the dependence of static permittivity (2.22) on concentration. The effects of Debye-Falkenhagen effect, δ_{DF}, dilution and internal depolarizing field, δ_{MW}, dielectric saturation, δ_{sat}, kinetic depolarization, δ_{KD}, and ion-pair, δ_{IP}, are shown in the figure. 38

Figure 2.3 Experimental data (open circles) of the static permittivity, ε_{dc}, and fitted semi-empirical model of static permittivity (2.22) (solid line) with parameters listed in Table 2.5, of aqueous solutions of (a) NaCl, (b)

$NaNO_3$, and (c) Na_2SO_4 at T = 25 °C. Theoretical discernment term Δ_1 (2.23) accounts for the contributions of dilution and kinetic depolarization (dash-dot line) and Δ_2 (2.24) accounts for the contributions of dilution, kinetic depolarization, and dielectric saturation, where Z_{IB} values are taken from literature [19] and are treated as input variables (dashed line).....43

Figure 2.4 Number of irrotationally bound water molecules, Z_{IB}, of NaCl (circle), $NaNO_3$ (square), and Na_2SO_4 (triangle) at 25 °C. Z_{IB} values are corrected for kinetic depolarization (hollow symbols), and corrected for kinetic depolarization and Debye-Falkenhagen effect (filled symbols). The 68% confidence intervals, representing the uncertainties in deriving Z_{IB} values, are also shown (dashed line). Fitted static permittivities (2.22) are used to calculate Z_{IB} through (2.14)-(2.16). 45

Figure 3.1 Experimental setup for measuring the dielectric spectrum and conductivity of an aqueous ionic solution at controlled temperature. The vector network analyzer is not shown in the picture.....61

Figure 3.2 Calculated individual relative (%) standard uncertainties in permittivity measured over the frequency range 200 MHz to 20 GHz for a sample $NaNO_3$ solution with concentration c = 7.139 mmol/L at 25 °C. (a) Real, and (b) imaginary parts. Random and systematic sources of uncertainty are due to repeatability u'_{rand} (u'_{meth}) and u''_{rand} (u''_{meth}), deviation from reference data represented by recovery terms $|R'\text{-}1|$ and $|R''\text{-}1|$, uncertainty in best-fit values of reference data u'_{BF} and u''_{BF}, and temperature uncertainty of reference data u'_T and u''_T. The uncertainties of reference data are provided only up to 5 GHz; refer to Table 3.1 for further details. 71

Figure 3.3 The procedure followed for computing each trial permittivity data set for evaluation of the standard uncertainties associated with the Debye fitting parameters, (3.4). In the Monte Carlo modeling in this work, 10^4 trials are generated. The relative standard uncertainties and recovery (Table 3.1) can be best described by a normal (Gaussian) distribution, norm(μ,σ), where μ is the mean and σ is the variance of the population. The standard deviation of a set of samples is denoted 'std'.....75

Figure 3.4 Residual discrepancies between Monte Carlo trial permittivity data and measured permittivity data (a) real part ($\varepsilon' - \varepsilon'_{\text{Trial}}$) (b) imaginary part ($\varepsilon''_d - \varepsilon''_{d\,\text{Trial}}$), over the measured frequency range 200 MHz to 20 GHz for a sample $NaNO_3$ solution with c = 7.139 mmol/L at 25 °C. For clarity, only 100 trials are plotted in this figure.....77

Figure 3.5 Experimental data (symbols) and fitted (solid lines) semi-empirical model, (3.18), of static permittivity ε_{dc} with parameters listed in Table 3.7 for aqueous solutions of NaCl, $NaNO_3$ and Na_2SO_4 at T = 25 °C. The error bars represent the calculated standard uncertainty based on the Monte Carlo method (Tables 3.3 to 3.5) and reflect a level of confidence of approximately 68 %. 82

Figure 3.6 As for Figure 3.5 but for relaxation time, (3.19). 82

Figure 3.7 As for Figure 3.5 but for conductivity κ, (3.20), employing parameters listed in Table 3.6. The error bars that represent the calculated standard uncertainty (Tables 3.3 to 3.5) are too small to be visible in the figure. 83

Figure 3.8 3D trajectory plot mapped from extracted measured (symbols) and fitted (solid lines) static permittivity ε_{dc}, relaxation time τ, and conductivity κ of NaCl, $NaNO_3$ and Na_2SO_4 solutions at T = 25 °C. The 2D contour plots of each pair of fitted parameters are projected onto the corresponding planes for NaCl (dashed-dotted line), $NaNO_3$ (solid line) and Na_2SO_4 (dashed line). For clarity, error bars that represent the standard uncertainty of the data (Tables 3.3 to 3.5) are not shown in this figure. 85

Figure 4.1 Experimental setup for measuring the dielectric spectra and conductivity of an aqueous ionic solution at a controlled temperature. (a) Test tube containing high-concentrated stock solution, (b) Sample beaker containing diluted solutions. 95

Figure 4.2 Experimental data (symbols), Tables 4.1 to 4.3, and analytical model (solid lines), (4.7), of specific conductivity σ for aqueous solutions of NaCl, $NaNO_3$, and Na_2SO_4 at (a) 5 °C, (b) 10 °C, (c) 15 °C, (d) 20 °C, (e) 25 °C, and (f) 30 °C. The error bars that represent the calculated standard uncertainty (Tables 4.1 to 4.3) are too small to be visible in the figures. 103

Figure 4.3 Surface plot of specific conductivity (4.7) and experimental data (Tables 4.1 to 4.3) for aqueous solutions of (a) NaCl, (b) $NaNO_3$, and (c) Na_2SO_4. The 2D contour plots of σ-vs-c and σ-vs-T are also projected onto the corresponding planes. 104

Figure 4.4 Relaxation time τ^0, data (symbols), Arrhenius (4.8), and Eyring (4.9) fitting equations of deionized water as a function of temperature T. The Eyring equation can better predict the relaxation time at higher temperatures than the Arrhenius equation. 106

Figure 4.5 Experimental data (symbols), Tables 4.1 to 4.3, and empirical model (solid lines), (4.11) and Table 4.6, of relaxation time for aqueous solutions of NaCl, $NaNO_3$, and Na_2SO_4 at (a) 5 °C, (b) 10 °C, (c) 15 °C, (d) 20 °C, (e) 25 °C, and (f) 30 °C. The error bars represent the calculated standard uncertainty based on the Monte Carlo method (Tables 4.1 to 4.3) and reflect a level of confidence of approximately 68 %. 111

Figure 4.6 Surface plot of temperature- and concentration-dependent relaxation time model (4.12) and experimental data (Tables 4.1 to 4.3) for aqueous solutions of (a) NaCl, (b) $NaNO_3$, and (c) Na_2SO_4. 112

Figure 4.7 Measured ε_∞ values for the deionized water, various authors. The standard uncertainty ranges corresponding to 68% confidence interval are also shown. 114

Figure 4.8 Static permittivity, data (symbols) of various authors, and temperature-dependent model (4.28) of deionized water as a function of temperature T. 120

Figure 4.9 Experimental data (symbols), Tables 4.1 to 4.3, and semi-empirical model (solid lines), (4.30) and Table 4.10, of static permittivity for aqueous solutions of NaCl, $NaNO_3$, and Na_2SO_4 at (a) 5 °C, (b) 10 °C, (c) 15 °C, (d) 20 °C, (e) 25 °C, and (f) 30 °C. The error bars represent the calculated standard uncertainty based on the Monte Carlo method (Tables 4.1 to 4.3) and reflect a level of confidence of approximately 68 %. 124

Figure 4.10 Surface plot of temperature- and concentration-dependent static permittivity model (4.31) and experimental data (Tables 4.1 to 4.3) for aqueous solutions of (a) NaCl, (b) $NaNO_3$, and (c) Na_2SO_4. 125

Figure 4.11 3D trajectory plot mapped from extracted measured (symbols) and fitted (solid lines) static permittivity ε_{dc}, relaxation time τ, and conductivity σ of NaCl (c = 0 to 10.275 mmol/L), $NaNO_3$ (c = 0 to 14.31 mmol/L) and Na_2SO_4 (c = 0 to 11.36 mmol/L) solutions at (a) 5 °C, (b) 10 °C, (c) 15 °C, (d) 20 °C, (e) 25 °C, and (f) 30 °C. For clarity, error bars that represent the standard uncertainty of the data (Tables 4.1 to 4.3) are not shown in the figures. The 2D contour plots of each pair of fitted parameters are projected onto the corresponding planes for NaCl (dashed-dotted line), $NaNO_3$ (solid line) and Na_2SO_4 (dashed line) 127

LIST OF TABLES

Page

Table 2.1 A summary of most recent previous studies of dielectric properties for aqueous (aq) solutions of NaCl, $NaNO_3$, and Na_2SO_4. The table summarizes the studied range of concentration c, frequency f, and temperature T. 18

Table 2.2 Contributions of uncertainty components (real and imaginary parts) over the measured frequency range from 200 MHz to 20 GHz. The method and analysis were taken from GUM guideline [21]. Type A evaluation of uncertainty is based on statistical analysis of series of observations whereas Type B evaluation of uncertainty is relied on scientific judgement of any other information other than Type A. 25

Table 2.3 Input quantities required to model the specific conductivity and kinetic depolarization contribution to the static permittivity of NaCl, $NaNO_3$, and Na_2SO_4 at 25 °C according to (2.11) and (2.12). For NaCl and $NaNO_3$, $z_1 = 1$ and $z_2 = -1$ whereas for Na_2SO_4, $z_1 = 1$ and $z_2 = -2$. $\eta = 8.934\times10^{-4}$ (kg m^{-1} s^{-1}) [42], ρ = 997.06 (g/L) [42]. Ionic conductivity values λ_1 and λ_2 are taken from [43]. Debye-Falkenhagen (DF) coefficient D is also calculated from (2.18) for each electrolyte system. 32

Table 2.4 Parameters of single-term Debye model (ε_{dc}, τ, and ε_∞), specific conductivity (σ), and reduced variance of the fit (s^2) to (2.22) for various concentrations (c) of aqueous NaCl, $NaNO_3$, and Na_2SO_4 solutions at T = 25 °C. The specific conductivity was measured directly up to 500 μS/cm. For concentrations corresponding to specific conductivity greater than 500 μS/cm, σ was treated as an additional fitting parameter. The standard uncertainties correspond to approximately 68 % confidence interval. 39

Table 2.5 Concentration, ε^0_{dc}, and parameters of semi-empirical static permittivity model (2.22) of aqueous NaCl, $NaNO_3$, and Na_2SO_4 solutions at 25 °C. The sum of squared error (SSE) for each fitted curve is also shown. 44

Table 2.6 Number of irrotationally bound water molecules per anion, Z^-_{IB}, corrected for kinetic depolarization ($Z^-_{IB}{}^{KD}$), and corrected for kinetic depolarization and Debye-Falkenhagen effect ($Z^-_{IB}{}^{KD+DF}$). Fitted static permittivities (2.22) are used to calculate Z_{IB} through (2.14)-(2.16). Z^+_{IB} = 4.2 ± 0.3 for Na^+ [12] is assumed for all calculations. The

coordination number (CN) and Z^{-}_{IB} for each anion according to corresponding reference are also given. 45

Table 3.1 Compilation of relative standard uncertainties over the frequency range 200 MHz to 20 GHz for measuring the permittivity of aqueous ionic solutions. The nomenclature and methodology are taken from NIST [25] and GUM [26]. Type A evaluation of uncertainty is based on statistical analysis of a series of observations whereas Type B evaluation of uncertainty relies upon scientific assessment of information other than Type A. Each source of uncertainty is composed of a real and an imaginary part.....70

Table 3.2 Debye model parameters for methanol data at 25 °C, various authors.....70

Table 3.3 Parameters of the single-term Debye model (ε_{dc}, τ, and ε_{∞}), the associated standard uncertainties ($u(\varepsilon_{dc})$, $u(\tau)$, and $u(\varepsilon_{\infty})$) calculated from Monte Carlo and covariance matrix methods, and mean squared error (s^2) of aqueous NaCl solutions at T = 25 °C. The standard uncertainties provide a level of confidence of approximately 68 %. The specific conductivity was measured independently up to 500 μS/cm with ± 0.5 % instrument uncertainty. For concentrations corresponding to specific conductivity greater than 500 μS/cm, κ was treated as an additional fitting parameter, and the covariance matrix and Monte Carlo methods give similar uncertainty values within reported significant figures.....79

Table 3.4 As for Table 3.3 but for aqueous $NaNO_3$ solutions. 79

Table 3.5 As for Table 3.3 but for aqueous Na_2SO_4 solutions.....80

Table 3.6 Input quantities for calculation of the volume fraction and conductivity (3.20), of NaCl, $NaNO_3$, and Na_2SO_4 solutions at 25 °C. Water density is ρ = 997.06 (g/L) at 25 °C [49]. The infinite molar conductivity values Λ^{∞} are taken from [50], and the values of non-ideality coefficient B are calculated through the steps stated in [40].....83

Table 3.7 Concentration, parameters of semi-empirical static permittivity model (3.18), and parameters of empirical relaxation time model (3.19) for aqueous NaCl, $NaNO_3$, and Na_2SO_4 solutions at 25 °C. The standard uncertainties of the fitting parameters are calculated based on the covariance matrix method and provide a level of confidence of approximately 68 %. 83

Table 4.1 Specific conductivity (σ) and parameters of single-term Debye model (ε_{dc}, τ, and ε_{∞}) for various concentrations (c) and temperatures (T) of aqueous NaCl solutions. The specific conductivity was measured directly up to 500 μS/cm with ± 0.5 % instrument uncertainty. For concentrations corresponding to specific conductivity greater than 500 μS/cm, σ was treated as an additional fitting parameter. The standard uncertainties were calculated from Monte Carlo method and correspond to approximately 68 % confidence interval.....97

Table 4.2 As for Table 4.1 but for aqueous $NaNO_3$ solutions. 98

Table 4.3 As for Table 4.1 but for aqueous Na_2SO_4 solutions.....99

Table 4.4 Linear model of cation $\lambda_1(T)$ and anion $\lambda_2(T)$ conductivities at infinite dilution for NaCl and $NaNO_3$ aqueous solutions with $z_1 = 1$ and $z_2 = -1$, and Na_2SO_4 aqueous solution with $z_1 = 1$ and $z_2 = -2$. Ionic conductivity values are taken from [18].....100

Table 4.5 Eyring fitting parameters for the temperature-dependent model of relaxation time $\tau^0(T)$, (4.9), of deionized water, various authors. The uncertainties represent the standard uncertainty and reflect a level of confidence of approximately 68 %. The sum of squared errors (sse) of the fit corresponding to values calculated by each author is shown. Also see Figure 4.4 for plots representing Arrhenius, (4.8), and Eyring, (4.9), equations as a function of temperature.....105

Table 4.6 Parameters of empirical relaxation time model, (4.11), of aqueous NaCl (c = 0 to 10.275 mmol/L), $NaNO_3$ (c = 0 to 14.31 mmol/L), and Na_2SO_4 (c = 0 to 11.36 mmol/L) solutions for discrete temperatures from 5 °C to 30 °C. The relaxation time of deionized water τ^0 at each temperature is taken from Table 4.1. The standard uncertainties of the fitting parameters were calculated based on Monte Carlo method and provide a level of confidence of approximately 68 %.....109

Table 4.7 Parameters of temperature- and concentration-dependent relaxation time model, (4.12), for aqueous NaCl (c = 0 to 10.275 mmol/L), $NaNO_3$ (c = 0 to 14.31 mmol/L), and Na_2SO_4 (c = 0 to 11.36 mmol/L) solutions. The standard uncertainties of the fitting parameters were calculated based on Monte Carlo method and provide a level of confidence of approximately 68 %. The sum of squared errors (sse) of the surface-plot fits and the measured data are also shown. 110

Table 4.8 Estimates of ε_{∞} (4.18) from available literature values for ε^0_{dc}, g, c_d, and μ within the lowest and highest reported temperature range available. c_d

is approximated by analytical water concentration c_s (refer to Section 4.6.1.3). 114

Table 4.9 Fitting parameters for the temperature-dependent model of static permittivity $\varepsilon^0_{dc}(T)$, (4.28), of deionized water. The fitting procedure was performed for the measured data within 5 °C to 30 °C. The sum of squared errors (sse) of the fit is also shown. Also see Figure 4.8. 120

Table 4.10 Parameters of semi-empirical static permittivity model, (4.30), of aqueous NaCl (c = 0 to 10.275 mmol/L), $NaNO_3$ (c = 0 to 14.31 mmol/L), and Na_2SO_4 (c = 0 to 11.36 mmol/L) solutions for discrete temperatures from 5 °C to 30 °C. The specific conductivities σ for each solution are taken from Tables 4.1 to 4.3. The relaxation time τ^0 and static permittivity ε^0_{dc} of deionized water at each temperature are taken from Table 4.1. The standard uncertainties of the fitting parameters were calculated based on Monte Carlo method and provide a level of confidence of approximately 68 %. 123

Table 4.11 Parameters of temperature- and concentration-dependent static permittivity model, (4.31), for aqueous NaCl (c = 0 to 10.275 mmol/L), $NaNO_3$ (c = 0 to 14.31 mmol/L), and Na_2SO_4 (c = 0 to 11.36 mmol/L) solutions. In (4.31), $\sigma(T, c)$ (S/m) is calculated from (4.7), $\tau^0(T)$ (s) from (4.9) and the parameters in Table 4.5, and $\varepsilon^0_{dc}(T)$ from (4.28) and the parameters in Table 4.9. The standard uncertainties of the fitting parameters were calculated based on Monte Carlo method and provide a level of confidence of approximately 68 %. The sum of squared errors (sse) of the surface-plot fits and the measured data are also shown. 123

ACKNOWLEDGMENTS

My heartfelt gratitude extends to my major professor, Prof. Nicola Bowler, who has been the greatest of advisors, for her encouragement, dedicated help, integral view on research, and her mission for providing high-quality work. Her continuous support, both professionally and personally, confidence in my work, motivation, cooperation, and kindness have always kept me going ahead, believing in myself, and pursuing the best course of my life. Words are powerless to express my deepest appreciation, now, and in future, for everything she did for me. I will owe her forever.

My special words of thanks also go to Prof. Amy Kaleita-Forbes, our project leader, not only for providing the USDA funding which allowed me to undertake this research, but also for her prompt responses to my questions and queries at any time, which is truly exemplary. I am also so appreciative of Dr. Brian Hornbuckle, my mentor, for his enthusiasm, guidance, and resources he provided for me to gain knowledge and deeper understanding of becoming a better teacher, a role-model as he is. I must also give up my deep thanks to Prof. Jiming Song and Dr. Nathan Neihart, teachers of my core courses, for their immense knowledge, attention to details, and friendly personalities, who have instructed me the best fundamental tools I needed to conduct my research.

I would like to acknowledge the Center for Nondestructive Evaluation (CNDE). It was fantastic to work the majority of my research in these facilities. With a special mention to Prof. John Bowler whom we had enjoyable chats together there. I also thank Ms. Leigh-Ann Long from Water Quality Research lab (WQRL) for providing the ionic sample solutions used in this research. Special thanks to Ms. Zohre Motevalli for creating

some of the figures used in Chapter 1 of this dissertation, and to Mr. Subhanwit Roy and Mr. Brett Zimmerman for sharing their related research materials.

My humble thanks go to Dr. Robert (Bob) Sheldon, Dr. Shuaishuai Liu, and Mr. Vincent Waters who have unlimitedly helped me as friends from the beginning I arrived in the US. Their constant support and cooperation shall always be remembered. I also wish to thank my fellow group members, past and present, including Bob and Subhanwit for stimulating discussions we always had, Shuaishuai, Dr. Chamila DeSilva, Ms. Trishelle Copeland-Johnson, Ms. Aishwarya Sriraman for all the fun we have had, Dr. Connor Daily, Dr. Weixing Sun, Dr. Rui Ding, Mr. Tyler Antony, Ms. Sara Neshani, and many more of friends, classmates, and officemates, for sharing a great relationship as compassionate friends.

My family friends, Mr. and Mrs., Brennan and Selia Buss, Ms. Judy Newhouse, and Pastor Mark Heilman, people who provided a much-needed form of escape from my studies, also deserve thanks for helping me keep things in perspective.

Last but not least, I must express my deepest gratitude to my sister and parents who encouraged and supported me at every stage of my personal and academic life. To my family-in-law for supporting me morally throughout this course. Above all, I am very much indebted to my wife, Zohre, who has been a constant source of encouragement and emotional support in my life and experienced all of the ups and downs of my research. I am truly thankful for having you in my life, and let's buckle up for the next chapter of our life!

ABSTRACT

Excessive amounts of chemicals and ions flowing into water sources, which are mainly due to efflux from agricultural lands, cause serious environmental and human-health related concerns. The lack of affordable and real-time monitoring systems for these contaminants limits effective conservation and management strategies. To establish a basis for developing an effective, fast, real-time, and affordable sensing system, dielectric spectroscopy has been applied to characterize agriculturally-relevant aqueous solutions of most commonly found ions in tile drainage water. Dielectric spectra of aqueous sodium chloride (NaCl), sodium nitrate ($NaNO_3$), and sodium sulphate (Na_2SO_4) ionic solutions, which are the common pollutants found in agricultural tile drainage waters in Iowa and the United States, were measured over the frequency range from 200 MHz to 20 GHz, at temperatures 5 °C to 30 °C in 5 °C increments and for concentrations in the range 0 to 20 millimoles per liter.

In this work, the measured dielectric spectra were fitted with a Debye model using a non-linear, weighted, least-squares analysis. Uncertainties due to random and systematic errors, that contribute to the measured dielectric spectra and become critical in the context of low concentration aqueous solutions, have been assessed. Moreover, two methods of calculating associated uncertainties of the fitting parameters, covariance matrix and Monte Carlo methods have been performed. The results show that the numerical approach taken by the Monte Carlo method, while yielding the same estimates, reduces the tediousness associated with the analytical covariance matrix method.

Next, the fitting parameters for the Debye model, which include static permittivity, relaxation time, and specific conductivity, have been extracted as potential

indicators of ion concentration and type. A method of judiciously exploiting these indicators, by means of a 3D trajectory plot, is proposed to uniquely identify an ion and infer its concentration from the benchmark data provided in this work.

In addition, for separate ionic aqueous solutions of NaCl, $NaNO_3$, and Na_2SO_4, concentration- and temperature-dependent parametric models of static permittivity, relaxation time, and specific conductivity that account for physical chemistry and molecular dynamics present in these systems have been developed. These models provide an accurate representation of the radio-frequency (200 MHz to 1 GHz) and microwave (1 to 20 GHz) dielectric spectrum for any of these agriculturally-relevant solutions at a particular concentration and temperature within the ranges studied. The research presented in this dissertation lays a foundation upon which an efficient, real-time, field-deployable, and economically feasible electrical sensing system can be designed for the efficient monitoring and analysis of agricultural run-off.

CHAPTER 1. GENERAL INTRODUCTION

1.1. Research Question

The research presented herein addresses the concept of employing the method of dielectric spectroscopy (DS) within radio-frequency (RF) and microwave (MW) frequency ranges to identify ions and estimate their concentrations in agriculturally-relevant aqueous solutions. The goal of this research is to conduct precision and high-accuracy laboratory-based measurements to characterize the dielectric properties of target ions, as well as, to perform a careful assessment of the measurement uncertainties for reliable interpretation of measurement data. Another goal of the research is to extract meaningful indicators and develop a model from the dielectric spectra that allow the concentration and type of ions to be uniquely determined. This research is important in view of the need for monitoring systems that enable efficient management of excessive pollutants in water run-off in the Midwestern United States. The DS-based method lays a foundation upon which an effective, fast, real-time, and affordable sensor can be designed to operate in agriculturally-relevant conditions.

1.2. Problem Statement

In November 2014 it was publicly reported that the nitrate level in the Des Moines and Raccoon Rivers, IA, has reached its recent historic and unprecedented high [1]. These two rivers are the main sources of drinking water for the city of Des Moines [2]. High levels of nitrates in drinking water can be extremely lethal to infants a few months old [3]. It can also be a cause of thyroid cancer, miscarriage, and toxic to fish and other forms of aquatic life, affecting Midwestern lakes, streams, and rivers all the way to the Gulf of Mexico [4]. The excessive concentration of nitrate, and potentially other contaminant substances, is due

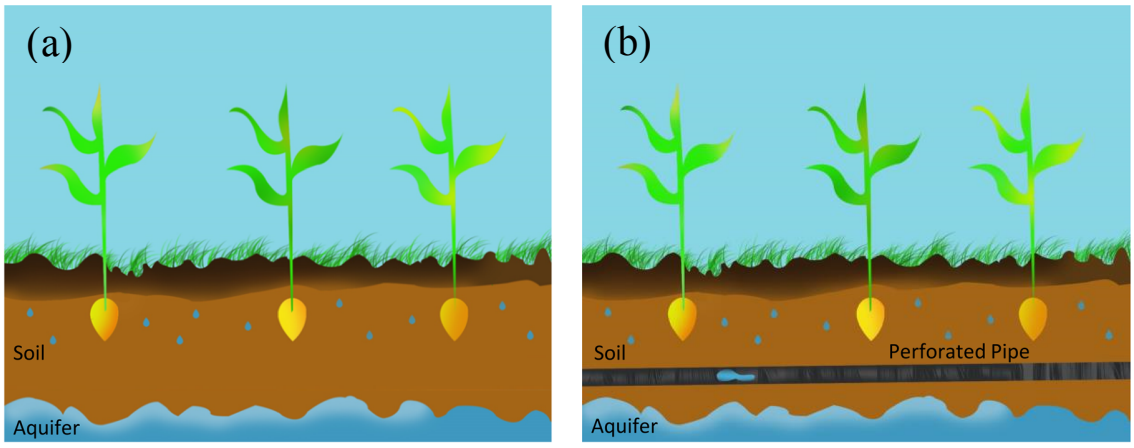

Figure 1.1 Drawing of a cropland without a tile drainage-system (a), and with a tile-drainage system (b). The perforated pipes are typically deployed 1 m below the soil surface and spaced 10 to 30 m apart. This picture is redrawn from the original source [5].

to efflux from subsurface tile drainage systems of agricultural lands [6]. Tile drainage systems, which are designed to control the height of the water table to provide suitable conditions for crop production and field operations [7], is a type of drainage system (Figure 1.1) that allows for removal of the excess amount of water from the soil by using a network of perforated pipes that are typically deployed about 1 m below the soil surface. However, owing to the fact that a tile drainage system provides a flow-path to the surface streams, soluble nutrients and contaminants from the croplands may be washed directly into those streams [6]. A 1987 USDA report [8] estimates that nearly 110 million acres of U.S. farmland are artificially drained. The report also suggests that this quantity will continue to grow with the increasing trend for adoption of tile drainage on previously undrained lands.

In order to make significant strides in developing effective conservation and management systems designed to limit chemical efflux from agricultural lands, especially in tile-drained regions where chemical export through the subsurface drainage lines is a major concern, it is critical that the monitoring system be able to accurately track chemicals' dynamics. Since the concentration of the chemicals is tightly linked to the local hydrology

and changes rapidly in time, space, and with temperature, 'spot and send-to-lab' analysis yields incomplete data. All of these issues reinforce the need for effective monitoring that can inform real-time mitigation strategies for unwanted chemicals (ions) in water. Such a system needs cheap sensors that can be deployed on a relatively fine spatial scale. In the next section, a brief review of current monitoring systems and their principles is presented.

1.3. Current Ion Monitoring Systems

In recent years, great efforts have been devoted to the development of effective ion monitoring systems that are capable of operating with very low (~ millimoles per liter), agriculturally relevant concentrations. Of all the methods found in literature, the two principle approaches are ion-selective-electrode (ISE) [9] and ultraviolet (UV) absorption [10] technologies.

1.3.1. Ion-Selective Electrode (ISE) Technology

In ion-selective electrode (ISE) technology, which is an electrochemical method, the particular ion of interest interacts directly with a specialized electrode membrane. As shown in Figure 1.2, a small voltage is developed across the membrane when the target ion diffuses through from the high concentration side to the lower concentration side. This voltage is proportional to the concentration of the target ion [9].

In ISE technology, the type of the membrane determines which ion can be detected. The types of membranes are generally based on silicate glass to detect Na^+ and H^+ ions, crystalline (solid state) membranes to detect Cl^- and F^- ions, organic liquid membranes to detect Ca_2^+ and divalent ions, and polymer membranes composed of polyvinylchloride (PVC) to detect K^+, Ca_2^+, Cl^-, and NO_3^- ions [11]. Even though this approach has a few key

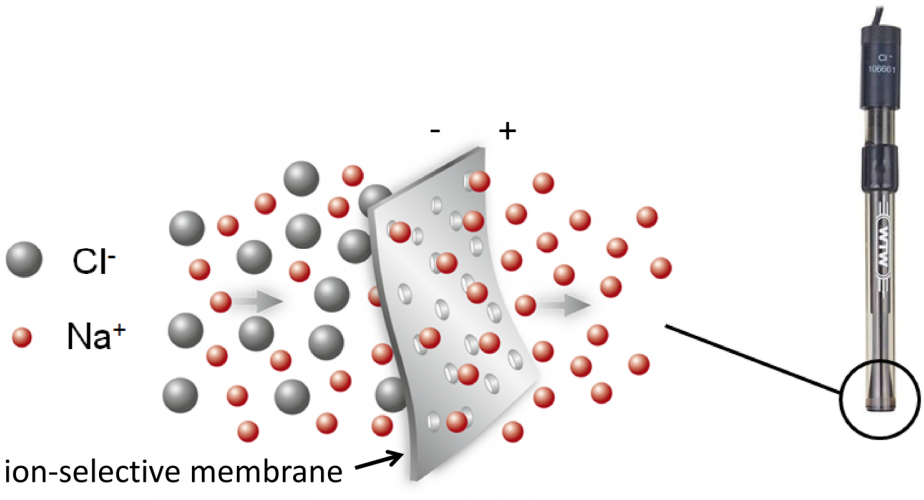

Figure 1.2 Ion-selective electrode (ISE) sensor and membrane. The membrane allows sodium ions to cross and, therefore, a concentration-dependent voltage is generated across the membrane. The ISE sensor photo used in the figure, at right, is from Neulog [12].

advantages like being easy to use and relatively inexpensive[1] compared to its counterparts, in practice, it can experience serious interference from the presence of other ions because no membrane is selective to only one ion. Moreover, there is a need for low solubility of the membrane so that it does not dissolve in the sample solution, which diminishes the suitability of this approach for long continuous periods of deployment in the field environment [9].

1.3.2. Ultraviolet (UV) Absorption Technology

In ultraviolet (UV) absorption technology, the sensors rely on the principle that absorbing substance in solution (in this case the dissolved ions) absorb electromagnetic radiation in the UV spectral range, allowing the ions to be identified according to their spectral fingerprint. These sensors can measure nitrate concentration, over a wide range of environmental conditions from ocean to runoff in rivers and stream [10]. As illustrated in Figure 1.3, a built-in photometer is designed to measure the intensity of the UV light passing through a sample in comparison with that of a reference light, in order to allow the

[1] At the time of writing, a typical ISE sensor "Neulog-241 Nitrate Sensor [12]" costs around $400.

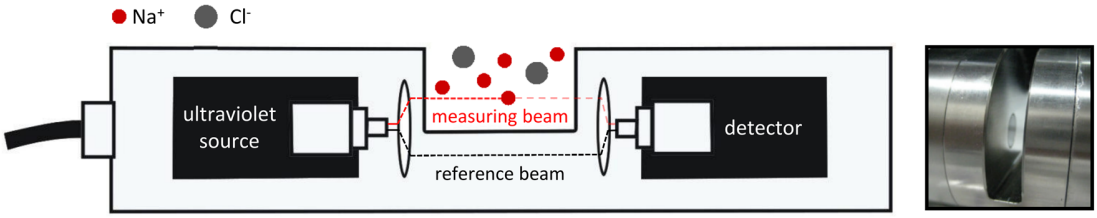

Figure 1.3 General design and key components of field-deployable ultraviolet (UV) sensor. This picture is modified and redrawn from the original source [10]. UV sensor photo used in the figure is from Hach [13].

absorbance of the substance to be calculated. The concentration of an absorbing substance can be calculated according to Beer-Lambert law [14] that provides a direct correlation between the absorbance, the concentration, and the path length of the sample.

This technology, however, requires highly monochromatic UV radiation which is difficult to realize in practice, leading to prohibitive installation and maintenance costs[1] of the sensor. The cost of these instruments prohibits their deployment at multiple points in a study area and the risk of damage to unattended instruments makes them impractical for watershed monitoring. Moreover the UV sensor may also suffer from the interference of other ions and organic compounds with similar absorbance as the ion of interest. At high concentrations of ions, an increase in inter-ionic interactions, e.g., creation of ion-pairs [16], also causes interference and limits the capability of UV sensor to predict the concentration accurately.

In summary, current ion monitoring systems do not meet all criteria for an effective, fast, real-time, and affordable monitoring system to operate in agriculturally relevant conditions. Therefore, there is a need to develop a new technique and sensing strategy to tackle the problem. In the next section, the method proposed in this project, based upon radio-frequency (RF) and microwave (MW) dielectric spectroscopy, which lays a foundation

[1] At the time of writing, a typical UV sensor "SUNA v2 UV Nitrate Sensor [15]" costs around $25,000.

toward a real-time, potentially low-cost, and nondestructive ionic monitoring system, is introduced.

1.4. Dielectric Spectroscopy

Dielectric spectroscopy (DS), which probes the interaction of a sample with an applied time-varying electric field with frequency f, is a powerful technique to characterize the physical and chemical properties of ionic aqueous solutions, particularly at radio and microwave frequencies [17]. The dielectric spectral response, i.e., broadband complex relative permittivity $\varepsilon_T(f) = \varepsilon'(f) - j\varepsilon''(f)$ of an ionic aqueous solution, is determined by its molecular structure and available polarization mechanisms therein. Real relative permittivity $\varepsilon'(f)$ indicates the extent to which electrical energy is stored by the sample, while imaginary relative permittivity $\varepsilon''(f)$ indicates the extent to which electrical energy is dissipated in the sample. By measuring dielectric properties, therefore, we can relate the effect of structure-influencing parameters such as ion concentration, ion type, and temperature, to the characteristics of the dielectric spectral response.

Dielectric spectroscopy is able to probe dynamic processes over a broad range of frequencies from hundreds of hertz to hundreds of gigahertz and is therefore a widely used tool in materials science to characterize solids, polymers, and liquids. For ionic aqueous solutions, the polarization – related to $\varepsilon'(f)$ – and the dissipation of energy – related to $\varepsilon''(f)$ - can be essentially separated into three additive contributions:

i. Always present are the intra-molecular forces, also known as permanent molecular dipoles. This contribution is associated with the bonds between atoms which create a molecule.

ii. Second are the inter-molecular forces which correspond to the forces present between adjacent molecules or ions, in the form of molecule-molecule, ion-molecule, or ion-ion interactions. As a result, we will have different types of permanent molecular dipoles, each experiencing a different type of inter-molecular forces.

iii. The third contribution comes from the migration of charge carriers, also known as conductivity, under the influence of an applied electric field. Note that the conductivity term contributes solely to the energy dissipation in the dielectric spectral responses.

Under the influence of a time-varying applied electric field, each type of permanent molecular dipole tries to align with the direction of the applied field. At sufficiently low frequency, all molecular dipoles contribute to the polarization of the sample [18]. For each molecular dipole, there exists a characteristic frequency, which is the inverse of a characteristic parameter called relaxation time, around which the molecular dipole loses its ability to follow the reorientations of the applied field, due to viscous forces at work on it, for example. When for a particular molecular dipole the frequency of the applied electric field exceeds the inverse of the relaxation time, the dipoles cannot keep up the pace with the change in direction of the applied field. The molecular dipole, thus, does not contribute to the total polarization for frequencies well above this relaxation frequency. This effect manifests itself as a drop in the real part of permittivity, and is observed to be paired with a peak in the imaginary part. Such a process is called a dipolar (rotational) relaxation process and can provide information concerning the structure of the sample. In DS, any molecular dipole, whether permanent or induced, produces a relaxation process that exhibits $d\varepsilon'/df < 0$ and whose relaxation frequency is defined by the condition $d\varepsilon_d''/df = 0$. For different molecules,

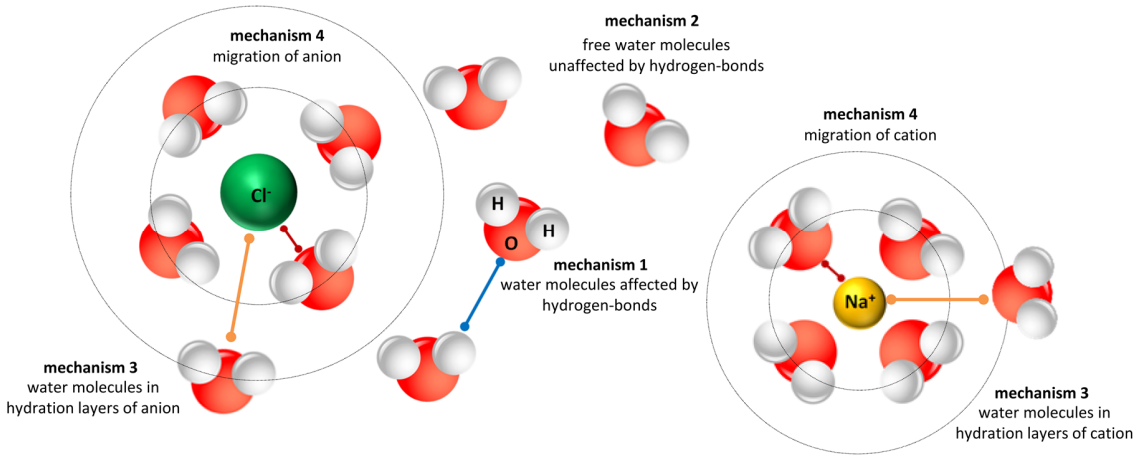

Figure 1.4 Types of water-based molecular dipoles and charge carriers present in a simple ionic aqueous solution of sodium chloride (NaCl).

these relaxation processes can occur at different frequencies far from each other, in which case they can easily be distinguished, or they can overlap with each other, in which case a meticulous task of accurate decomposition of the spectrum is required.

As demonstrated in Figure 1.4, the principle types of permanent molecular dipoles in low concentration (~ mmol/L) ionic aqueous solution are [19] :

1) Water molecules affected by inter-molecular hydrogen-bond forces (mechanism 1)

2) Free (bulk) water molecules not connected to any hydrogen bond (mechanism 2)

3) Water molecules affected by ion-molecule forces. These molecular dipoles are in the hydration layers of positive charge (cation) and the hydration layers of negative charge (anion) (mechanism 3).

4) In addition, anion as an electron carrier and cation as a hole carrier [20] both contribute to conductivity constructively (equivalent to electrical current).

Experiments show that the relaxation processes of molecules associated with mechanism 1, i.e., hydrogen-bonded water molecules, and those associated with mechanism 3, i.e., water molecules in the hydration layers of cations and anions, occur within the micro-

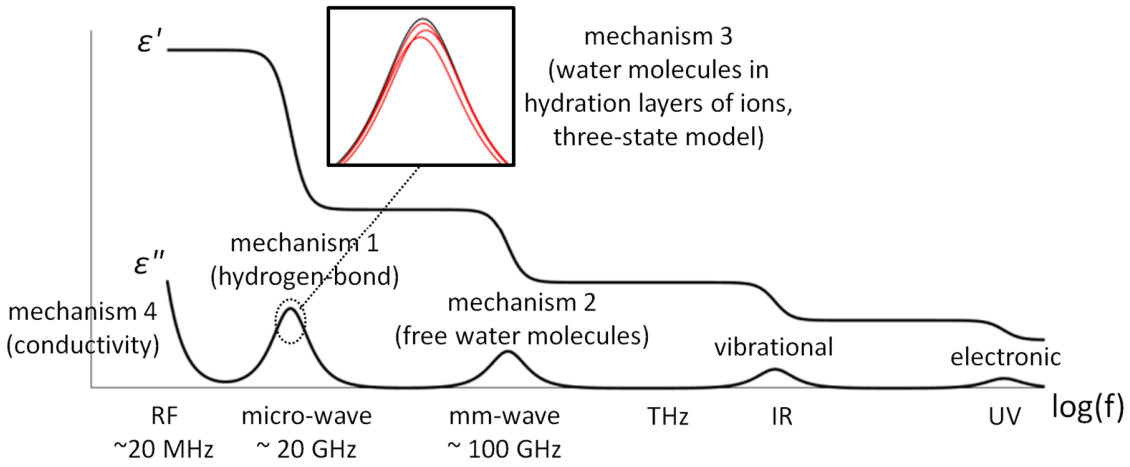

Figure 1.5 A schematic of dielectric spectra of a simple ionic aqueous solution and relaxation processes corresponding to different dipolar mechanisms. The three-state model mentioned for mechanism 3 comprises the relaxation processes of hydrogen-bonded water molecules, hydration water molecules of cation, and hydration water molecules of anion [21].

wave frequency range at around 18 GHz [21]. Free water molecules (mechanism 2) are able to keep pace with the external field and their relaxation process happens to be in mm-wave regions at around 110 GHz [22]. Conductivity (mechanism 4) is manifested at lower frequencies of the imaginary dielectric spectra, $\varepsilon''(f)$. Non-rotational relaxation processes which are due to vibrational and electronic transitions of intra-molecule forces take place at infrared (IR) and ultraviolet (UV) regions of the frequency spectrum. Figure 1.5 depicts, qualitatively, the dielectric spectrum of a simple low-concentration ionic aqueous solution and the relaxation processes corresponding to the different dipolar mechanisms illustrated in Figure 1.4.

The RF and MW frequency regions (as specified in Figure 1.5) of the dielectric spectra, where three of the relaxation mechanisms take place, i.e., mechanisms 1, 3 and 4 (Figure. 1.5), offer low cost and high portability in terms of electronics, compared with higher frequencies. A method based on dielectric spectroscopy, therefore, can be employed

as a foundation upon which a prototype sensor will be designed to operate at RF and MW frequencies [23]. In the next section, the research objectives are set.

1.5. Research Objectives

The dielectric properties of various moderate- and high-concentration solutions of mono/bi-valent ions dissolved in water have been characterized in prior works [16, 24-26]. The most frequently occurring ions in subsurface drainage water generally are, in decreasing order, chloride Cl^-, nitrate NO_3^-, sulphate SO_4^{2-}, and, to a lesser degree, nitrite NO_2^- and phosphate PO_4^{3-} [27]. Recent research conducted at Iowa State University [28] has also found that the most common dissolved ions present in the agricultural tile drainage waters of central Iowa are, in descending order, bicarbonate HCO_3^-, calcium Ca^{2+}, magnesium Mg^{2+}, nitrate NO_3^-, chloride Cl^-, sodium Na^+, and sulphate SO_4^{2-}. In this dissertation, thus, Na^+, Cl^-, NO_3^-, and SO_4^{2-} ions, are selected for study as four common pollutants found in agricultural tile drainage waters in Iowa and the United States. The main objectives of this research can now be expressed as follows.

1.5.1. Develop Precision Laboratory-Based Measurement Techniques for RF and MW Dielectric Spectroscopy of Ionic Aqueous Solutions

The existing studies of dielectric properties of ionic aqueous solutions have been limited by the lack of available data in the literature for very low, agriculturally-relevant concentration levels. For solutes sodium chloride (NaCl), sodium nitrate ($NaNO_3$), and sodium sulphate (Na_2SO_4), available dielectric spectroscopy data do not span the relevant concentration levels which are on the order of millimoles per liter (mmol/L). Laboratory-based measurement techniques, including test fixtures, instrumentation, temperature control, and methodology, therefore, will be developed for measuring the dielectric properties of

ionic aqueous solutions of different composition with varying concentrations across radio-frequency (200 MHz to 1 GHz) and microwave frequency (1 to 20 GHz) regions.

1.5.2. Collection of RF and MW Dielectric Spectral Data with Low Uncertainty and Rigorous Uncertainty Analysis

Many of the existing data of dielectric spectra of ionic aqueous solutions are subject to large uncertainties. Careful assessment of the measurement uncertainties is necessary for reliable interpretation of measurement data in general and is particularly important in this case concerning the dielectric properties of ionic aqueous solutions at agriculturally-relevant low concentrations. The ability to resolve the variations in $\varepsilon'(f)$ and $\varepsilon''(f)$ that arise for small changes in concentration is governed by the requirement that they must exceed the experimental uncertainties for $\varepsilon'(f)$ and $\varepsilon''(f)$. A careful assessment of uncertainty which, to the best knowledge, has not been previously applied in the context of RF and MW dielectric spectroscopy of ionic aqueous solutions, will be performed, leading to a high quality set of data for these solutions with thorough uncertainty analysis.

1.5.3. Exploit Potential Indicators to Estimate Ion-Specific Concentration

The dielectric spectra of ionic aqueous sodium chloride (NaCl), sodium nitrate ($NaNO_3$), and sodium sulphate (Na_2SO_4) solutions will be characterized for various ranges of environmentally-relevant concentration and temperature. On this basis, methods of extracting meaningful indicators from the dielectric spectra through fitting procedures will be explained. To my knowledge, no prior investigation has attempted the inverse problem of exploiting the dielectric spectral features to estimate the ion-specific concentration of aqueous solutions. The following work indeed lays a foundation upon which a prototype real-time monitoring system can be built to target the most effective indicators. Such a system can be, e.g., based on a resonant sensor using an open-ended coaxial transmission line. Interested

readers are referred to recent research at Iowa State University [29] for more information regarding the details of sensor design using the dielectric spectral features provided by this dissertation.

1.5.4. Develop Concentration- and Temperature-Dependent Models for RF and MW Spectral Parameters of Aqueous Ionic Solutions

A semi-empirical concentration- and temperature-dependent parametric model of each dielectric spectral feature accounting for physical chemistry and molecular dynamics of the ionic aqueous solution will be developed. Such models can be employed to estimate dielectric spectral features, including static permittivity ε_{dc}, relaxation time τ, conductivity σ, and complex permittivity for agriculturally-relevant concentrations and temperatures at RF and MW frequencies. The methodology taken here can also be generalized for other types of ions.

1.6. Dissertation Organization

The research presented in the rest of this dissertation starts in Chapter 2 with a systematic study of the RF and MW dielectric spectra of aqueous solutions of sodium chloride (NaCl), sodium nitrate ($NaNO_3$), and sodium sulphate (Na_2SO_4) at a constant temperature. A semi-empirical model to represent the static permittivity, ε_{dc}, of multivalent electrolyte systems is introduced. This concentration-dependent model expresses the contributions of distinct mechanisms to static permittivity in the low concentration regime.

In Chapter 3, a thorough assessment of uncertainty in the context of low-concentration agriculturally-relevant ionic aqueous solutions is presented. Two methods of calculating associated uncertainties of the dielectric spectral indicators, covariance matrix and Monte Carlo methods, are described. A method of judiciously exploiting the dielectric

spectral indicators is proposed, that allows the concentration and type of ions to be uniquely determined.

In Chapter 4, the dielectric spectra of aforementioned ionic aqueous solutions are measured and characterized for the extended range of temperatures. Complete analytical and semi-empirical models for static permittivity ε_{dc}, relaxation time τ, and specific conductivity σ as a function of concentration and temperature are then derived. A detailed discussion on the molecular dynamics of these parameters with respect to temperature is also given.

In Chapter 5, conclusions drawn from the entire work are summarized and recommendations for extended study are provided.

1.7. References

[1] D. Eller, "Raccoon River nitrate level peaked Saturday," ed: The Des Moines Register, 24 Nov. 2014.

[2] [Accessed: 2018, March 29]. *Des Moines and Raccoon river watersheds*. Available: http://www.dmww.com/water-quality/watershed

[3] M. H. Ward, B. A. Kilfoy, P. J. Weyer, K. E. Anderson, A. R. Folsom, and J. R. Cerhan, "Nitrate intake and the risk of thyroid cancer and thyroid disease," *Epidemiology (Cambridge, Mass.),* vol. 21, p. 389, 2010.

[4] G. Randall and M. Goss, "Nitrate losses to surface water through subsurface, tile drainage," *Nitrogen in the environment: sources, problems, and management, 2nd edn. Elsevier, New York,* pp. 145-175, 2008.

[5] AgPhD. [Accessed: 2018, March 29]. Available: https://www.youtube.com/watch?v=L7zkkXIklHU

[6] E. Maxwell, E. W. Peterson, and C. M. O'Reilly, "Enhanced Nitrate Reduction within a Constructed Wetland System: Nitrate Removal within Groundwater Flow," *Wetlands,* vol. 37, pp. 413-422, 2017.

[7] S. V. Veen. [Accessed: 2018, March 29]. *Operating and Maintaining a Tile Drainage System*. Available: http://www.omafra.gov.on.ca/english/engineer/facts/10-091.htm

[8] G. A. Pavelis, *Farm drainage in the United States: History, status, and prospects*: US Department of Agriculture, Economic Research Service, 1987.

[9] W. E. Morf, *The principles of ion-selective electrodes and of membrane transport* vol. 2: Elsevier, 2012.

[10] B. A. Pellerin, B. A. Bergamaschi, B. D. Downing, J. F. Saraceno, J. D. Garrett, and L. D. Olsen, "Optical techniques for the determination of nitrate in environmental waters," *Quality Assurance, and Data Reporting. In: Techniques and Methods,* pp. 1-D5, 2013.

[11] E. M. Gross, R. S. Kelly, and D. M. Cannon, "Analytical Electrochemistry: Potentiometry," *The Journal of the Analytical Sciences Digital Library,* 2008.

[12] [Accessed: 2018, March 29]. *Nitrate logger sensor NUL-241*. Available: https://neulog.com/nitrate

[13] [Accessed: 2018, March 29]. *NITRATAX™ sc UV nitrate sensors*. Available: https://www.hach.com/asset-get.download.jsa?id=7639981839

[14] M. Silberberg, *Chemistry: The Molecular Nature of Matter and Change With Advanced Topics*: McGraw-Hill, 2018.

[15] [Accessed: 2018, March 29]. *SUNA V2 UV nitrate sensor*. Available: http://www.seabird.com/suna

[16] S. Schrödle, W. W. Rudolph, G. Hefter, and R. Buchner, "Ion association and hydration in 3: 2 electrolyte solutions by dielectric spectroscopy: Aluminum sulfate," *Geochimica et Cosmochimica Acta,* vol. 71, pp. 5287-5300, 2007.

[17] R. Buchner and G. Hefter, "Interactions and dynamics in electrolyte solutions by dielectric spectroscopy," *Physical Chemistry Chemical Physics,* vol. 11, pp. 8984-8999, 2009.

[18] N. Vinh, M. S. Sherwin, S. J. Allen, D. George, A. Rahmani, and K. W. Plaxco, "High-precision gigahertz-to-terahertz spectroscopy of aqueous salt solutions as a probe of the femtosecond-to-picosecond dynamics of liquid water," *The Journal of Chemical Physics,* vol. 142, p. 164502, 2015.

[19] R. Buchner, "What can be learnt from dielectric relaxation spectroscopy about ion solvation and association?," *Pure and Applied Chemistry,* vol. 80, pp. 1239-1252, 2008.

[20] K. Oldham and J. Myland, *Fundamentals of Electrochemical Science*: Elsevier, 2012.

[21] R. Buchner, G. T. Hefter, and P. M. May, "Dielectric relaxation of aqueous NaCl solutions," *The Journal of Physical Chemistry A,* vol. 103, pp. 1-9, 1999.

[22] R. Buchner, J. Barthel, and J. Stauber, "The dielectric relaxation of water between 0 C and 35 C," *Chemical Physics Letters,* vol. 306, pp. 57-63, 1999.

[23] S. Roy, N. Neihart, and N. Bowler, "Coaxial microwave resonant sensor design for monitoring ionic concentration in aqueous solutions," in *Instrumentation & Measurement Technology Conference (I2MTC), 2018 IEEE*, Houston, TX, USA, 2018, pp. 1-4.

[24] R. Buchner, S. G. Capewell, G. Hefter, and P. M. May, "Ion-pair and solvent relaxation processes in aqueous Na2SO4 solutions," *The Journal of Physical Chemistry B,* vol. 103, pp. 1185-1192, 1999.

[25] T. Chen, G. Hefter, and R. Buchner, "Dielectric spectroscopy of aqueous solutions of KCl and CsCl," *The Journal of Physical Chemistry A,* vol. 107, pp. 4025-4031, 2003.

[26] A. Lileev, Z. Filimonova, and A. Lyashchenko, "Dielectric permittivity and relaxation in aqueous solutions of alkali metal sulfates and nitrates in the temperature range 288–313 K," *Journal of Molecular Liquids,* vol. 103, pp. 299-308, 2003.

[27] M. E. Fernández-Boy, F. Cabrera, and F. Moreno, "Analysis of inorganic anions in drainage water and soil solution by single-column ion chromatography," *Journal of Chromatography A,* vol. 823, pp. 285-290, 1998.

[28] B. A. Zimmerman, "Exploration of ion species in agricultural subsurface drainage waters," Iowa State University, 2016.

[29] S. Roy, "Microwave resonant sensor for measurement of ionic concentration in aqueous solutions," Iowa State University, 2017.

CHAPTER 2. STATIC PERMITTIVITY OF ENVIRONMENTALLY-RELEVANT LOW-CONCENTRATION AQUEOUS SOLUTIONS OF SODIUM CHLORIDE, SODIUM NITRATE, AND SODIUM SULPHATE

To be submitted to *Journal of Chemical Physics*

Amin Gorji[1, 2, a] and Nicola Bowler[1, 2, 3, a]

2.1. Abstract

In this work, result of a systematic study of the dielectric spectra of aqueous solutions of NaCl, $NaNO_3$, and Na_2SO_4 with environmentally-relevant concentrations (~ mmol/L) are presented, for frequencies from 200 MHz up to 20 GHz and at temperature 25.00 ± 0.01 °C. The measured spectra were fitted with a Debye relaxation model using a non-linear, weighted, least-squares analysis. Conductivity was measured independently, to reduce uncertainty in obtaining other parameters by spectral fitting. A Monte Carlo modeling method was used to evaluate the associated fitting uncertainties. This process incorporates uncertainty contributions of repeated measurements and calibration validation based on a priori known reference data. Careful experimentation provided dielectric data of sufficiently low uncertainty to enable observation of polarization mechanisms that emerge only in the low-concentration regime. The data were fitted by a concentration-dependent parametric model that includes terms accounting for internal depolarizing fields and the solvent dilution effect (mixture relation), the kinetic depolarization effect, the dielectric saturation effect, and the Debye-Falkenhagen effect that accounts for the contribution of ionic atmosphere polarization. It has been shown here that, in NaCl and $NaNO_3$ solutions at sufficiently low concentrations, the static permittivity increases due to the Debye-Falkenhagen effect. It has

[1] Department of Electrical and Computer Engineering, Iowa State University, Ames, Iowa, 50011, USA
[2] Center for Nondestructive Evaluation, Iowa State University, Ames, Iowa, 50011, USA
[3] Department of Materials Science and Engineering, Iowa State University, Ames, Iowa, 50011, USA
[a] Email: amingorji68@gmail.com, nbowler@iastate.edu

also been shown that, to calculate the number of irrotationally bound water molecules Z_{IB}, the measured static permittivity values should be corrected to account for the contributions of kinetic depolarization and Debye-Falkenhagen effects. Otherwise, unrealistic values of Z_{IB} are obtained. An explanation for the different strengths of the Debye-Falkenhagen effect observed for the different electrolyte solutions, essentially due to the electrophoretic effect and coordination number, is also presented.

2.2. Introduction

Excessive amounts of unwanted chemicals and ions flowing into water sources are concerning, for environmental and human-health related reasons. Electrolyte solutions of nitrate (NO_3^-), chloride (Cl^-), and sulfate (SO_4^{2-}) ions in water are among the most common pollutants [1] that can cause serious environmental and human health problems. Understanding the dielectric properties of such electrolytes is of considerable interest, providing information about molecular (polarization) and ionic (charge-transport) dynamics [2]. Dielectric spectroscopy (DS), which monitors the response of a sample, i.e., its complex relative permittivity $\varepsilon(f) = \varepsilon'(f) - j\varepsilon''(f)$, to an applied time-harmonic electric field oscillating with frequency f is a powerful technique for characterizing unique properties of the nature and dynamics of electrolyte solutions [3]. At sufficiently low frequency, DS detects all mechanisms that contribute to the polarization of the sample [4]. As frequency increases, relaxation or resonance events take place at their characteristic frequencies. At frequencies higher than those characteristic frequencies, the contribution of the particular polarization mechanism associated with that relaxation or resonance, to the overall polarization of the sample, is lost. Real relative permittivity $\varepsilon'(f)$ indicates to what extent electrical energy may be stored in the material, while imaginary relative permittivity $\varepsilon''(f)$ indicates the degree of

dissipation of electrical energy (dielectric loss) in the sample, whether by conduction or polarization loss.

The dielectric properties of various moderate- and high-concentration solutions of mono/bi-valent nitrate, chloride, and sulfate-based ions dissolved in water have been characterized in prior work [5-7]. Table 2.1 summarizes results of most recent dielectric studies of sodium-based nitrate, chloride, and sulfate ions. Of note, the dielectric properties of $NaNO_3$(aq) reported by Lileev *et al*. [8] are of very high concentration samples $c \sim 0.52$ to 8.54 mol/L over five discrete frequencies between 7 to 25 GHz and different temperatures from 10 °C to 40 °C. Wachter *et al*. [9], however, covered a broad frequency range up to 89 GHz within concentration range $c \sim 0.05$ to 1.5 mol/L at $T = 25$ °C. Most of the previous studies, however, did not consider environmentally-relevant concentration levels of NaCl(aq), $NaNO_3$(aq), and Na_2SO_4(aq) which are on the order of millimoles per liter. Conclusions drawn from previous studies on moderate- and high-concentration solutions do not provide a picture of the dielectric properties in the low concentration regime. A need for dielectric data for low concentrations of these ions has arisen in the context of a need for real-time monitoring of contaminant ions in water sources [10]. In addition, the data obtained

Table 2.1 A summary of most recent previous studies of dielectric properties for aqueous (aq) solutions of NaCl, $NaNO_3$, and Na_2SO_4. The table summarizes the studied range of concentration c, frequency f, and temperature T.

Reference	Sample	c (mol/L)	f (GHz)	T (°C)
Nörtemann *et al.* [11]	NaCl(aq)	0.05-0.6	0.02-40	20
Buchner *et al.* [12]	NaCl(aq)	0.1-5	0.2-20	5, 20, 25, 35
Levy *et al.* [13]	NaCl(aq)	0.1-1	0.5-50	25
Lileev *et al.* [8]	$NaNO_3$(aq)	0.52-8.54	7-25 [a]	10, 15, 25, 35, 40
Wachter *et al.* [9]	$NaNO_3$(aq)	0.05-1.5	0.2-89	25
Barthel *et al.* [14]	Na_2SO_4(aq)	0.1-1	0.95-89	25
Buchner *et al.* [15]	Na_2SO_4(aq)	0.025-1.6	0.95-89	25

[a] Measured at five discrete frequencies

for low concentrations should be of higher accuracy than is currently available in literature because the small variations in ε' and ε'' in low concentration solutions may otherwise be concealed by the experimental uncertainties of ε' and ε''.

In this work, the dielectric properties of environmentally-relevant, low-concentration, aqueous solutions of NaCl, $NaNO_3$, and Na_2SO_4 are characterized in a well-controlled laboratory experiment. In Section 2.3, the details of the experimental setup to perform broadband dielectric spectroscopy over the frequency range 200 MHz to 20 GHz and to measure specific conductivity are presented. Methods of extracting meaningful permittivity parameters from the dielectric spectra are also presented in Section 2.3, along with a summary of Monte Carlo modeling employed to evaluate the associated uncertainties. This approach to uncertainty analysis which, to the knowledge of authors, has not been previously applied in the context of electrolyte solutions, enables us to deduce possible mechanisms that emerge in the dielectric properties of the electrolyte solutions at low concentrations. In Section 2.4, a semi-empirical model to represent the static permittivity, ε_{dc}, of multivalent electrolyte systems is introduced. This concentration-dependent model expresses the contributions of distinct mechanisms to static permittivity in the low concentration regime. Results of extracted permittivity parameters and their associated uncertainties are presented in Section 2.5. Section 2.6 is devoted to discussion, and the chapter is drawn to conclusion in Section 2.7.

2.3. Experimental Method

2.3.1. Apparatus and Sample Preparation

Dielectric property measurements were made with a Speag open-ended coaxial DAK3.5 Dielectric Probe Kit (200 MHz to 20 GHz recommended bandwidth) and an Anritsu 37347C Vector Network Analyzer (40 MHz to 20 GHz nominal bandwidth) whose drivers

were specially programmed for compatibility with the DAK probe. The DAK software provided with the probe kit was used to calculate the relative permittivity ε' and ε'' of the sample from the complex reflection coefficient (S_{11}) measured at the interface between the immersed coaxial probe and the liquid sample. The system was calibrated using three standards: a shorting block, air, and deionized water at 25 °C. For each sample, the frequency was swept and recorded ten times at 100 points between 200 MHz and 20 GHz with equal logarithmic frequency steps. Instead of obtaining the conductivity σ as an adjustable parameter in the fitting procedure, it was measured separately using a Mettler Toledo Seven2Go^{TM} Conductivity meter with InLab720 probe (operating range 0.1 to 500 µS/cm with relative uncertainty ± 0.5 %), to reduce uncertainty in obtaining other dielectric parameters by spectral fitting (discussed in Section 2.3.3). The conductivity probe was calibrated using a Mettler Toledo 84 µS/cm standard potassium chloride solution at 25 °C.

The sample beaker was placed in a temperature-controlled Anova R10 Refrigerated and Heating Circulator, stable to within ± 0.01 °C, and the temperature held at 25 °C ± 0.01 °C during this experiment. Dowtherm SR-1 Ethylene Glycol oil (18.1 vol. %) was used as the bath fluid in order to minimize the influence of ambient temperature fluctuations. It was observed that the temperature fluctuation can significantly affect the quality of the measured dielectric spectra and mask the concentration/ion-dependent responses particularly for low ion concentration. Thus, an electric stirrer was immersed in the sample beaker and the sample liquid stirred continuously but gently, avoiding turbulence (bubbles), to mitigate against temperature gradients and promote a uniform temperature through the entire sample.

To perform the experiments, three sets of environmentally-relevant electrolyte solutions were prepared and 14 concentrations c of each (including de-ionized water as zero

concentration) were tested: (i) aqueous sodium chloride (NaCl) with concentration ranging from c = 0 to 11.26 mmol/L, (ii) aqueous sodium nitrate ($NaNO_3$) with c = 0 to 17.83 mmol/L, (iii) aqueous sodium sulfate (Na_2SO_4) with c = 0 to 12.45 mmol/L. These ranges, despite being different, correspond to 0 to 400 mg/L concentration of sodium chloride as chloride (NaCl-Cl), sodium nitrate as nitrogen ($NaNO_3$-N), and sodium sulfate as sulfur (Na_2SO_4-S), which is the commonly represented unit in agricultural societies. The samples were tested from lower to higher concentrations by successively titrating (± 0.05 ml) the required amount of each stock electrolyte into a specified starting volume of deionized water.

2.3.2. Data Analysis

Combining the frequency dependence of polarization $\varepsilon'(f)$ and energy dissipation $\varepsilon''(f)$ of an electrolyte solution in response to an applied electric field, the total complex relative permittivity $\varepsilon_T(f)$ can be written

$$\begin{aligned}\varepsilon_T(f) &= \varepsilon'(f) - j\varepsilon''(f) \\ &= \varepsilon'(f) - j\left[\varepsilon_d''(f) + \frac{\sigma}{2\pi\varepsilon_0 f}\right]\end{aligned} \tag{2.1}$$

where the energy dissipation component $\varepsilon''(f)$ is composed of dipolar loss $\varepsilon_d''(f)$ and specific conductivity σ (dc conductivity) terms. The measured dielectric spectra (total complex relative permittivity) for three examples of NaCl, $NaNO_3$, and Na_2SO_4 with approximately the same concentration, $c \sim 7$ mmol/L, are presented in Figure 2.1. The loss spectra $\varepsilon''(f)$ are also decomposed into the contributions from the conductivity term $\sigma/2\pi f\varepsilon_0$, where σ is the specific conductivity, and dipolar loss $\varepsilon_d''(f)$.

The fitting of dielectric spectra requires care, especially for low concentrations of solute for which the dielectric spectrum varies only slightly from that of pure water. By subtracting the specific conductivity contribution from $\varepsilon''(f)$ to obtain the dipolar loss only

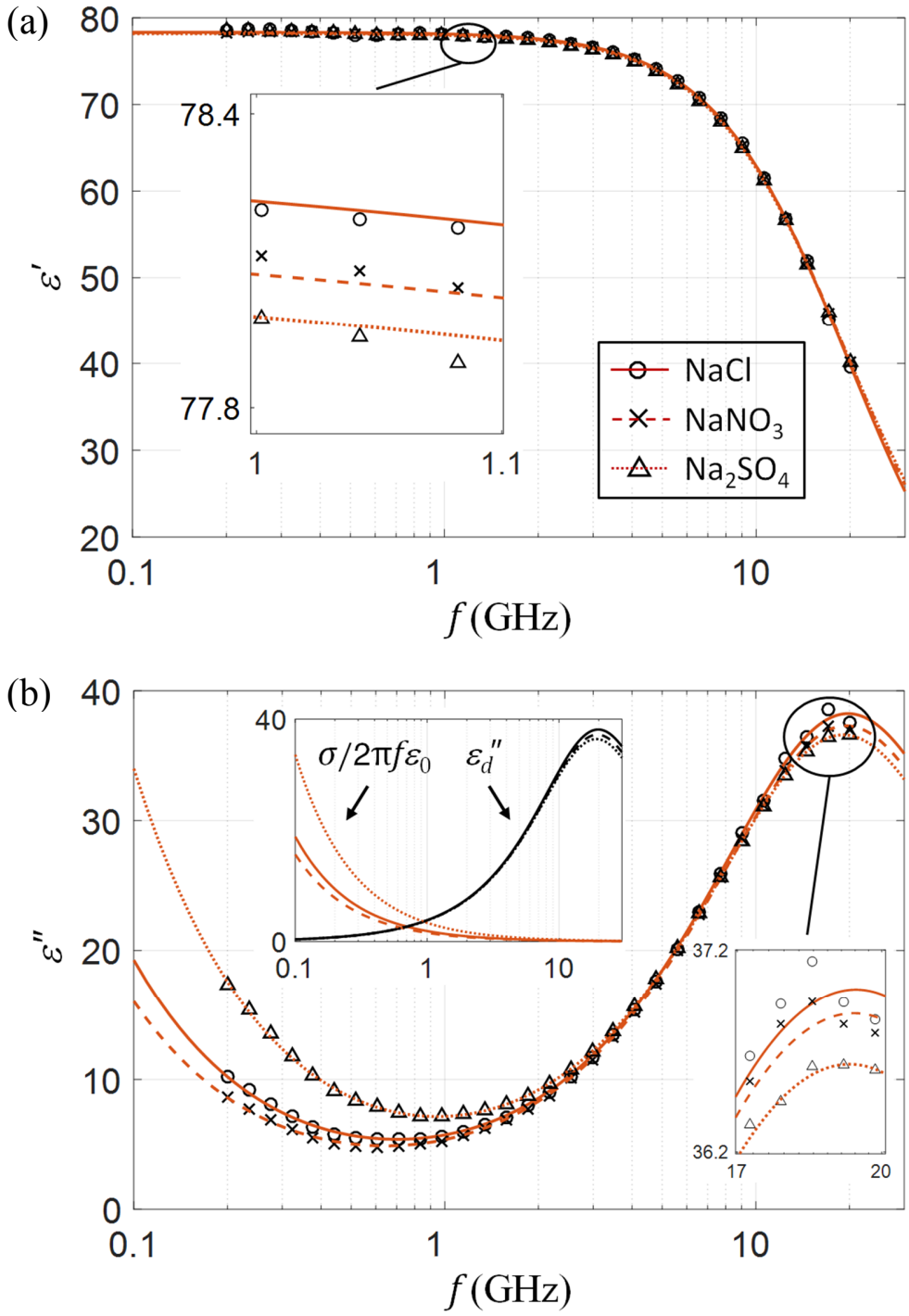

Figure 2.1 Dielectric dispersion $\varepsilon'(f)$ (a) and loss $\varepsilon''(f)$ (b) spectra of aqueous solutions of NaCl with c = 7.052 mmol/L; $NaNO_3$ with c = 7.139 mmol/L; and Na_2SO_4 with c = 7.797 mmol/L at T = 25 °C. The symbols represent the measured permittivity data. The lines represent the fitted curves (single Debye relaxation model). The contributions due to the conductivity term ($\sigma/2\pi f\varepsilon_0$) and the dipolar relaxation process $\varepsilon_d''(f)$ are shown separately in the inset of (b).

$\varepsilon_d''(f)$, and within the frequency range under consideration, the corrected complex relative permittivity $\varepsilon_c(f) = \varepsilon'(f)\text{-}j\varepsilon_d''(f)$ can be approximated by a single-term Debye relaxation model as

$$\begin{aligned} \varepsilon_{Debye}(f) &= \varepsilon'_{Debye}(f) - j\varepsilon''_{Debye}(f) \\ &= \varepsilon_\infty + \frac{\varepsilon_{dc} - \varepsilon_\infty}{1 + j2\pi f\tau} \end{aligned} \tag{2.2}$$

where ε_{dc} is the static permittivity, ε_∞ is the permittivity at a frequency well above that of the relaxation frequency f_r, and $\tau = 1/(2\pi f_r)$ is the relaxation time. The reason for correcting for the specific conductivity is to subtract the ionic migration (i.e. conductivity) contribution from $\varepsilon''(f)$ in order to deal separately with dipolar polarizations represented by $\varepsilon_d''(f)$. Among other relaxation models [16], the dielectric spectra of the present electrolyte solutions can be best described by a single-term Debye relaxation model in the low concentration range (~ mmol/L). In principle, ε_∞ is identified as the plateau reached by $\varepsilon'(f)$ when all polarization contributions associated with inter-molecular dynamics are no longer effective [7]. Thus, ε_∞ reflects only contributions from intra-molecular polarizability that could be obtained from dielectric spectroscopy in the terahertz region [17]. Since this is far above our upper limit of measured frequency, ε_∞ was treated as an additional fitting parameter in (2.2). This treatment results in slightly increased values of the reduced variance of the fit, s^2, but also produces a smoother progression of the fitting parameters as a function of concentration. An alternative approach in which the value of ε_∞ is fixed during the fitting procedure, depending on particular scenarios, has also been reported in the literature [11, 12].

A simultaneous, non-linear, weighted, unconstrained, least-squares analysis to minimize the residuals χ^2 was performed, based on the Gauss-Marquardt algorithm [18]:

$$\chi^2 = \frac{1}{n-m-1}\sum_{i=1}^{n}\left\{\left[w_i'(f_i)\left(\varepsilon_d'(f_i)-\varepsilon_{Debye}'(f_i)\right)\right]^2+\left[w_i''(f_i)\left(\varepsilon_d''(f_i)-\varepsilon_{Debye}''(f_i)\right)\right]^2\right\} \quad (2.3)$$

where f_i (i = 1, ..., n) denotes each of n frequencies at which permittivity is measured; m is the number of adjustable parameters of the Debye relaxation model, and w_i' = $1/\delta\varepsilon'(f_i)$ and w_i'' = $1/\delta\varepsilon_d''(f_i)$ are the weighting factors which are inversely proportional to the standard deviations of ten recorded spectra of $\varepsilon'(f)$ and $\varepsilon_d''(f)$. The uncertainty of the fitting parameters $u(\varepsilon_{dc})$, $u(\tau)$, and $u(\varepsilon_\infty)$, which returned the 68% confidence interval, was also calculated via Monte Carlo (MC) modeling described in the following section.

2.3.3. Uncertainty Analysis

A careful analysis of the uncertainty is necessary to deduce reliable interpretations of the dielectric properties of electrolyte solutions at low concentrations. Currently, an instrument uncertainty of ~ 1-3 % in ε' and ~ 2-4 % in ε'' is common at frequencies below 100 GHz and they may easily reach ~ 10 % for both quantities in the THz region [19]. The resolution of small variations in $\varepsilon'(f_i)$ and $\varepsilon''(f_i)$ in low concentration solutions is limited by the requirement that they must at least exceed the experimental uncertainties $u'(f_i)$ and $u''(f_i)$. In addition, as the number of parameters in the fitting equation increases (equivalent to reduced degrees of freedom), the associated uncertainty for each fitting parameter will subsequently increase [20]. One way that the latter difficulty was addressed was by measuring the conductivity independently at high-precision and subtracting the relevant contribution, i.e., $\sigma/2\pi f_i\varepsilon_0$ from the experimentally accessible $\varepsilon''(f_i)$ to obtain $\varepsilon_d''(f_i)$. By treating $\varepsilon_d''(f_i)$ rather than $\varepsilon''(f_i)$, the number of fitting parameters was reduced and the associated uncertainty for each fitting parameter was also reduced.

In this work, the combined standard uncertainties of the measured dielectric spectra, $u_c'(f_i)$ and $u_c''(f_i)$, were calculated in accordance with the established "Guide to the Expression

of Uncertainty in Measurement (GUM)" guideline [21]. As listed in Table 2.2, the individual standard uncertainties include contributions from 10 recorded spectra of repeatable measurements, calibration validation through measurement on a reference sample [22], and uncertainties associated with the reference data. The calibration validation was performed by measuring the complex permittivity of methanol CH_3OH at 25 °C. A hybrid set of reference data for methanol was created by combining the permittivity data reported by Gregory *et al*. [23] for frequency range 200 MHz to 10 GHz with that presented by Sato *et al*. [24] for 10 to 20 GHz. While the former incorporates the first relaxation of methanol, which occurs at 3 GHz, the latter covers the second relaxation which occurs at around 20 GHz at 25 °C. The combined standard uncertainties $u'(f_i)$ and $u''(f_i)$, associated with measured $\varepsilon'(f_i)$ and $\varepsilon_d''(f_i)$ values at each frequency, are the root sum of squares (RSSu) of individual standard uncertainties, as attained in Table 2.2. The combined standard uncertainties provide a level of confidence of approximately 68 %. In order to get a rough *single-number* estimate of the

Table 2.2 Contributions of uncertainty components (real and imaginary parts) over the measured frequency range from 200 MHz to 20 GHz. The method and analysis were taken from GUM guideline [21]. Type A evaluation of uncertainty is based on statistical analysis of series of observations whereas Type B evaluation of uncertainty is relied on scientific judgement of any other information other than Type A.

Source of uncertainty	Type of uncertainty	Probability distribution	Standard uncertainty (%)
Repeatability [a]	A	Normal	$u_1'(f_i)$, $u_1''(f_i)$
Uncertainty of reference data [b, c]	B	Normal	$u_2'(f_i)$, $u_2''(f_i)$
Deviation from reference data [d]	B	Normal	$\delta'(f_i)$, $\delta''(f_i)$
Combined standard uncertainty	$u_c'(f_i) = [u_1'(f_i)^2 + u_2'(f_i)^2 + \delta'(f_i)^2]^{1/2}$ $u_c''(f_i) = [u_1''(f_i)^2 + u_2''(f_i)^2 + \delta''(f_i)^2]^{1/2}$		

[a] Standard deviation of the mean (SDM) calculated from 10 recorded spectra of every test sample
[b] Gregory *et al*. [23]: combined "Best-fit" and temperature uncertainties
[c] Sato *et al*. [24]: no associated uncertainty was reported
[d] A set of permittivity data for methanol obtained by combining that of Gregory *et al*. [23] (f < 10 GHz) and Sato *et al*. [24] (f > 10 GHz)

overall uncertainty associated with ε' and ε'' presented in this work, the calculated combined standard uncertainties at each frequency were averaged over the entire frequency (200 MHz to 20 GHz) to get $\bar{u}_c' = \Sigma u_c'(f_i)/n$ = 0.98 % and $\bar{u}_c'' = \Sigma u_c''(f_i)/n$ = 1.46 %. These values demonstrate smaller uncertainties compared to common uncertainty ranges mentioned earlier (1-3 % in ε' and 2-4 % in ε'') which is an improvement toward more precise values for the measured dielectric spectra.

In order to calculate the standard uncertainties associated with the fitting parameters, i.e., $u(\varepsilon_{dc})$, $u(\varepsilon_\infty)$, and $u(\tau)$, we have chosen a Monte Carlo (MC) modeling technique based on the approach applied by Gregory *et al*. [25]. The MC modeling is performed according to the following procedure:

Step 1: Normally-distributed errors $\Delta\varepsilon'$ and $\Delta\varepsilon_d''$ are generated at each frequency ($\Delta\varepsilon'$ and $\Delta\varepsilon_d''$ can be positive or negative). The errors are sampled from a normal population with zero mean and variances equal to $u_c'(f_i)$ and $u_c''(f_i)$. These values are generated independently at every measured frequency to simulate random noise.

Step 2: The MC modeling requires a large number of trial datasets to be constructed which are representative of the expected statistical variations of the measured data. Therefore, 10^4 trial permittivity data sets are created at each frequency point $\varepsilon'_{\text{Trial}} = \varepsilon' + \Delta\varepsilon'$ and $\varepsilon''_{d\,\text{Trial}} = \varepsilon_d'' + \Delta\varepsilon_d''$.

Step 3: The Debye fitting procedure, according to (2.3), is performed on each trial permittivity spectrum to extract the trial fitting parameters. The standard deviations of 10^4 trial fitting parameters are taken to be their associated standard uncertainties, $u(\varepsilon_{dc})$, $u(\varepsilon_\infty)$, and $u(\tau)$. The reported uncertainty is based on a standard uncertainty multiplied by a coverage factor k = 1, providing a level of confidence of approximately 68 %.

2.4. Modeling Static Permittivity

The static permittivity ε_{dc} gives insight into possible polarization mechanisms present at the molecular level of electrolyte solutions. At an ideal zero frequency in which the applied electric field is constant, besides the thermal agitations of molecules, all dipolar moments in the solution tend to align with the direction of the field, thus contributing to the total polarization $\varepsilon'(f = 0) = \varepsilon_{dc}$. At zero concentration, i.e., for deionized water the value $\varepsilon_{dc}(c = 0) = \varepsilon^0_{dc}$ can be attributed to the total number of water molecules that could align with the applied field. Water molecules, due to the electric charge distribution of their electronic orbitals, form an almost tetrahedrally structured hydrogen-bond (H-bond) network [19] or are 'free', i.e., are not H-bonded. The ensemble of water molecules aligned with the applied field are thus either H-bonded water molecules or free water molecules. Buchner *et al.* [26] demonstrated experimentally the existence of a dominant relaxation process in water centered on ~ 18 GHz at T = 25 °C, which is generally attributed to the kinetics of H-bonded (bulk) water molecules, and a weaker high-frequency relaxation process at around ~ 120 GHz due to rotational diffusion of free (single) water molecules. Adding ionic solute to water, to form a solution, the behavior of $\varepsilon_{dc}(c)$ depends on the contribution of different mechanisms emerging with respect to the characteristics of the particular ions, including solute-solvent, solute-solute, and solvent-solvent interactions. Another mechanism observable at low concentrations of ionic solute is known as the Debye-Falkenhagen effect [27], which is an induced polarization due to charge cloud separations without any molecular association involved in the process [28]. We seek concentration-dependent parametric model to express the behavior of static permittivity over a given concentration range. It is common practice to construct the model by summing contributions of the distinct mechanisms that

contribute to static permittivity. These include terms accounting for solvent dilution and internal depolarizing fields, kinetic depolarization effect, dielectric saturation effect, and the Debye-Falkenhagen effect that accounts for the contribution of ionic atmosphere polarization. These contributions are considered in turn in each of the following Sections 2.4.1 through 2.4.4 after which the full model for $\varepsilon_{dc}(c)$ is presented in Section 2.4.5.

2.4.1. Dilution and Internal Depolarizing Field

In order for solute particles to dissolve in water, the positive (cation) and negative (anion) ions must break free from the crystal-lattice structure of the solid. When the ions dissolve in solution, they are surrounded by water molecules. This indeed yields to reduction (dilution) of free and H-bonded water molecules that could otherwise have contributed to the total polarization of the solution. The water molecules form layers of solvation around the ion. Friedman [29] proposed a classification of solvation models into three groups: Hamiltonian, continuous, and chemical. Due to complexity of solutions of the Hamiltonian model and limitations of the continuous model, the chemical models are more extensively used in dielectric studies [30]. In the chemical model, the volume around an ion is divided into two regions. In the exterior region the solvent molecules are treated as pure solution with zero ion concentration, while in the interior region they are affected by the presence of ions. In this regard, the early attempts to develop a model of the quantitative dielectric decrement of water due to dissolved ions were made by Sack [31], Ritson-Hasted [32], and Glueckauf [33] where the static permittivity of the solution was found to decrease linearly with ion concentration. In later theories, Pottel's ellipsoidal model [30] which is based on Onsager's spherical model [34] postulates an ellipsoidal exclusion zone containing hydration water molecules (water molecules immediately adjacent to a solute particle) together with the solute particle. This exclusion zone is surrounded by a homogeneous host medium with

permittivity equal to that of pure water. An additional internal depolarizing field [35], due to electronic polarization of the ion ($\varepsilon_e \sim 2$) is also introduced inside the ellipsoidal zone. The dilution of free and H-bonded water molecules due to solvation, along with the internal depolarizing fields makes the static permittivity of the solution (effective permittivity) decrease compared to static permittivity of pure water. Although a rigorous theoretical treatment of these mechanisms is not possible, a multitude of mixture relations (effective medium approximations) exist. For ease of calculation the Maxwell-Wagner relation [36] is employed in this work. The Maxwell-Wagner relation assumes, however, that the permittivity in the direct neighborhood of the exclusion zone equals that of the pure solvent. In other words, it ignores the long-range interactions between the solute particles and those water molecules outside the solvation layers that are weakly affected by the local fields of the ion charges. For binary mixtures of non-polar solute particles of permittivity ε_e, volume fraction $v(c)$ (= c[mol/L]M[g/mol]/ρ[g/L]), and a background host medium of permittivity ε^0_{dc}, the static permittivity decrement $\delta_{MW}(c)$ according to the Maxwell-Wagner relation is

$$\delta_{MW}(c) = \frac{3v(c)\varepsilon^0_{dc}\left(\varepsilon_e - \varepsilon^0_{dc}\right)}{2\varepsilon^0_{dc} + \varepsilon_e - v(c)\left(\varepsilon_e - \varepsilon^0_{dc}\right)} \tag{2.4}$$

where $\varepsilon_e = 2$ is a reasonable approximation in the case of a nonpolar spherical solute [36]. Other mixture relations including the Bruggeman relation and the Looyenga relation are formulated in [37] but, the same underlying assumptions hold for them.

2.4.2. Kinetic Depolarization

The measured static permittivity of electrolyte solutions clearly falls below the predictions of mixture relations, because, in an electrolyte solution, the migration of ions under the influence of an external electric field reduces the polarizability of the solvent [38].

In the theoretical framework of the Hubbard-Onsager model [38], a symmetrically charged impenetrable sphere (the ion) is moving in a viscous, incompressible, polarizable fluid continuum (the solvent) [39]. As an ion migrates and sets up a non-uniform flow, according to the laws of hydrodynamics, the surrounding water molecules in the outer regions of the solvation layer are perturbed and tend to rotate in the direction opposite to that promoted by the external field. This additional polarization deficiency is known as kinetic depolarization $\delta_{KD}(c)$ and is proportional to the specific conductivity $\sigma(c)$ of the solution and the relaxation time τ_s of the solvent. In the case of electrolyte solutions where perfect slip (p = 2/3) boundary conditions between the ion surface and solvent continuum are assumed [12], $\delta_{KD}(c)$ is given by

$$\delta_{KD}(c) = \xi(c)\sigma(c) \tag{2.5}$$

where $\xi(c)$ is the Hubbard-Onsager coefficient

$$\xi(c) = p\frac{\varepsilon_{dc}^{0} - \varepsilon_{\infty}(c)}{\varepsilon_0 \varepsilon_{dc}^{0}}\tau_s \tag{2.6}$$

The identity $\varepsilon_\infty(c) = \varepsilon_\infty(c = 0)$ is assumed throughout this work. The kinetic depolarization mechanism adds to the decrements due to dilution of free and H-bonded water molecules and the internal depolarizing fields. Recently, terahertz time-domain spectroscopy data also confirmed that hydrodynamic motions of water molecules resulting from movement of ions contribute significantly to polarization deficiency [40].

Considering a set of assumptions regarding the system of non-ideal electrolyte solutions, Debye, Huckel, and Onsager (DHO) derived a fundamental treatment to consider the total effects of non-ideality (friction, electrophoretic, and asymmetric relaxation effects) on the ionic conductivity. The complete derivation of DHO theory has been extensively

discussed by Wright [41]. In order to calculate the specific conductivity of a general multivalent electrolyte system A_xB_y composed of A^{y+} and B^{x-} ion species with electron valency $z_1 = y$ and $z_2 = -x$ for cation and anion, respectively, and at temperature T in kelvin (K), we start our analysis by defining the concentration-independent inverse Debye length κ_0 (m^{-1}) as

$$\kappa_0 = \sqrt{\frac{e^2 N_A}{\varepsilon_0 \varepsilon_{dc}^0 k_B T}\left(|z_2| z_1^2 + |z_1| z_2^2\right)} \tag{2.7}$$

where e = 1.60×10^{-19} C is the elementary charge, N_A = 6.02×10^{23} mol^{-1} is Avogadro's number, ε_0 = 8.85×10^{-12} F/m is the free space permittivity, and k_B = 1.38×10^{-23} J/K is the Boltzmann constant. After carefully performing a few mathematical steps, the electrophoretic coefficient, a ($m^{3.5}S/mol^{1.5}$), and the asymmetric relaxation coefficient, b ($m^{3.5}S/mol^{1.5}$), can be written as

$$a = |z_2| \frac{z_1^2 F e \kappa_0}{6\pi\eta} + |z_1| \frac{z_2^2 F e \kappa_0}{6\pi\eta} \tag{2.8}$$

$$b = |z_2| \frac{z_1^2 e^2 \kappa_0}{24\pi\varepsilon_0 \varepsilon_{dc}^0 k_B T} \frac{1}{1+\sqrt{0.5}} \lambda_1 + |z_1| \frac{z_2^2 e^2 \kappa_0}{24\pi\varepsilon_0 \varepsilon_{dc}^0 k_B T} \frac{1}{1+\sqrt{0.5}} \lambda_2 \tag{2.9}$$

where F = 96,485.33 C/mol is the Faraday constant, η (kg $m^{-1}s^{-1}$) is the dynamic viscosity of the pure water, and λ_1 (m^2S/mol) and λ_2 (m^2S/mol) are the ionic conductivities of cation and anion, respectively, at infinite dilution. The infinite molar conductivity of the whole system at infinite dilution, Λ^∞ (m^2S/mol), is then

$$\Lambda^\infty = |z_2| \lambda_1 + |z_1| \lambda_2 \tag{2.10}$$

The molar conductivity of the whole system, $\Lambda(c)$ (m^2S/mol), can be calculated as a function of solute concentration c (mol/L) according to

$$\Lambda(c) = \Lambda^{\infty} - B\sqrt{10^3 c} \tag{2.11}$$

$$B = a + b \tag{2.12}$$

where B is the coefficient combining the non-idealities of electrophoretic and relaxation effects. Finally, the specific conductivity $\sigma(c)$ (S/m) of the solution, calculated through theoretical formulations directly, can be expressed

$$\sigma(c) = 10^3 c\Lambda(c) \tag{2.13}$$

In cases of low concentration solutions for which concentration is of the order of mmol/L, it is more convenient to report the specific conductivity in μS/cm. Table 2.3 lists the input quantities required to theoretically calculate the specific conductivity and kinetic depolarization contribution.

2.4.3. Dielectric Saturation

Around the solvation layers of an ion the rotational ability of the electric dipole moment of solvent molecules appears to be reduced by proximity to the associated Columbic field. If the ion-solvent interactions of water molecules located in the hydration layers of an ion are much stronger than the interactions to outer H-bonded water molecules, the water

Table 2.3 Input quantities required to model the specific conductivity and kinetic depolarization contribution to the static permittivity of NaCl, $NaNO_3$, and Na_2SO_4 at 25 °C according to (2.11) and (2.12). For NaCl and $NaNO_3$, $z_1 = 1$ and $z_2 = -1$ whereas for Na_2SO_4, $z_1 = 1$ and $z_2 = -2$. $\eta = 8.934\times10^{-4}$ (kg m^{-1} s^{-1}) [42], $\rho = 997.06$ (g/L) [42]. Ionic conductivity values λ_1 and λ_2 are taken from [43]. Debye-Falkenhagen (DF) coefficient D is also calculated from (2.18) for each electrolyte system.

ion	M (gr/mol)	λ_1 (m^{2}S/mol)	λ_2 (m^{2}S/mol)	Λ^{∞} (m^{2}S/mol)	B (m$^{3.5}$S/mol$^{1.5}$)	D (m$^{1.5}$ mol$^{-0.5}$)
NaCl	58.4428	50.1×10^{-4}	76.4×10^{-4}	126.5×10^{-4}	1.113×10^{-4}	0.118
$NaNO_3$	84.9947	50.1×10^{-4}	71.4×10^{-4}	121.5×10^{-4}	1.076×10^{-4}	0.118
Na_2SO_4	142.0421	50.1×10^{-4}	160×10^{-4}	260.2×10^{-4}	8.706×10^{-4}	0.405

molecules in the hydration layers effectively become immobilized and may not be affected by the presence of an external applied field. A resulting polarization deficiency, known as dielectric saturation, can be evaluated in terms of the number of irrotational bonded (IB) water molecules Z^{+}_{IB} and Z^{-}_{IB} per cation and anion, respectively. For a general multivalent electrolyte system A_xB_y, the water molecules adjacent to cation and anion, numbered $Z_{IB} = xZ^{+}_{IB} + yZ^{-}_{IB}$, do not contribute to the static permittivity. The Z_{IB} values of monovalent ions reported in the literature [19] indicate that cations, which have smaller ionic radius than anions relatively, are more extensively surrounded by water molecules than anions, with the number of water molecules in the solvation layers decreasing with increasing ionic radius [37]. In addition, more highly charged cations and anions (multivalent ions) have greater Z_{IB} values than monovalent ions, suggesting the existence of irrotationally bound water molecules beyond the first solvation layer. Recent computer simulations [44, 45] and dielectric spectroscopy studies [19] of aqueous solutions also concluded that the ions influence the water molecules in the first hydration layer as well as the H-bonded water molecules nearby. Noting that effects of ionic radius, electron valency, and long-range interactions are not accounted for in the mixture relation (2.4), the contribution of dielectric saturation to a semi-empirical model describing static permittivity must be added separately. Although there have been yet no theoretical approaches to directly calculate Z_{IB} from the characteristics of solute particles, a comparison of the apparent solvent concentration $c_s^{ap}(c)$ calculated from measured $\varepsilon_{dc}(c)$, with the analytical solvent concentration c_s^0 (= ρ_{water}[gr/L]/M_{water}[gr/mol]) at zero solute concentration, leads to the calculation of $Z_{IB}(c)$ as [15]

$$Z_{IB}(c) = \frac{c_s^0 - c_s^{ap}(c)}{c} \tag{2.14}$$

In order to compare Z_{IB} values of the present samples in this work with the literature values used in Section 2.6, scaled Cavell equation [15, 46] is used for calculation of $c_s^{ap}(c)$ as follows

$$c_s^{ap}(c) = F_{Cav}^0 \frac{2\bar{\varepsilon}_{dc}(c)+1}{\bar{\varepsilon}_{dc}(c)}\left[\bar{\varepsilon}_{dc}(c) - \varepsilon_\infty(c)\right] \tag{2.15}$$

$$F_{Cav}^0 = c_s^0 \frac{\varepsilon_{dc}^0}{\left(2\varepsilon_{dc}^0+1\right)\left(\varepsilon_{dc}^0 - \varepsilon_\infty^0\right)} \tag{2.16}$$

where $\bar{\varepsilon}_{dc}(c) = \varepsilon_{dc}(c) + \delta_{KD}(c)$ is the static permittivity corrected for kinetic depolarization to prevent unreasonably large values of Z_{IB} for almost all electrolyte systems [47]. $\bar{\varepsilon}_{dc}(c)$, thus, is taking into account solvent-affiliated contributions due to dilution and internal depolarizing field as well as dielectric saturation. The field factor $f_i(c) = f_i(0)$ and $A_i = 1/3$ for spherical reaction field are assumed in the original equation [15]. Several other approaches including Kirkwood-Frohlich (KF) equation [12] and Bruggeman [11] relation have also been employed for the calculation of $c_s^{ap}(c)$. A direct comparison of Z_{IB} values from different models, however, requires careful attention since for a given electrolyte system the Z_{IB} value becomes model dependent [14] and thus no particular model is yet preferred. In order to form a semi-empirical model of the static permittivity with no *a priori* information of Z_{IB} values for the calculation of polarization deficiency due to dielectric saturation mechanism $\delta_{sat}(c)$, we treat it as a linear function of solute concentration

$$\delta_{sat}(c) = \gamma_{sat} c \tag{2.17}$$

where γ_{sat} is an adjustable parameter obtained through a data-fitting procedure, for each electrolyte systems.

2.4.4. Ionic Atmosphere Polarization

The concept of ionic atmosphere, as first dealt by the model presented by Debye and Huckel in 1927 for the conductivity of strong electrolyte systems, can be defined in terms of a chosen reference ion, with all the other ions including cations and anions distributed around it, making up the ionic atmosphere. In the absence of the external electric field the ionic atmosphere is symmetric with the charge distribution tending to zero with distance from the reference ion [41]. If the reference ion is a cation moving under the influence of an external electric field, however, it and the cations of the ionic atmosphere will move in the direction of the applied field, while the anions will move in the opposite direction. This movement therefore causes a deficit of negative charges in front of the moving reference cation and an excess of negative charge behind it, causing asymmetry in the ionic atmosphere around the moving reference ion. Under alternating electric field development of the asymmetric ionic atmosphere depends on the frequency, in particular on whether there is enough time available to reach the asymmetric state. The frequency-dependent asymmetric ionic atmosphere, as first theoretically predicted by Debye and Falkenhagen [27, 48], introduces additional polarization of quasi-elastic origin to the system, without any dipolar species resulting from ion association and chemical reaction (different from ion-pairs). The Debye-Falkenhagen (DF) effect suggests a rise in static permittivity above that of pure water at very low concentrations. For a typical ~ 10 mmol/L solution of a 1:1 electrolyte system, the relaxation of the asymmetric ionic atmosphere is predicted to occur below 100 MHz [49, 50]. The DF effect is, alternatively, recognized as increasing ionic conductivity at around the frequency corresponding to the relaxation of the asymmetric ionic atmosphere [50, 51]. Prior published works do not unambiguously establish any positive contribution of the DF effect to

static permittivity. This is mainly because, as frequency decreases, the loss tangent ($\propto \sigma/2\pi f\varepsilon_0$) is so great and the electrode effects so marked that the required accuracy is not available [52]. Indeed, prior dilute solution measurements have shown the static permittivity to be smaller than that of pure water [53, 54] and some have shown the opposite. Van Beek *et al*. [49] were first to experimentally reported the increment in static permittivity. For most aqueous solutions investigated in their work, including alkali chlorides in water, static permittivity shows an initial increase above the value of the pure solvent with the values up to concentrations of 25 mmol/L. Further initial evidence of the existence of DF effect in NaCl aqueous solutions was implicitly mentioned by Winsor *et al*. [55] and Nortemann *et al*. [11].

The static permittivity increment based on speculative estimation by Debye and Falkenhagen, which is equal to $Dc^{0.5}$ (c [mol.m^{-3}]) where D (m$^{1.5}$ mol$^{-0.5}$) is the Debye-Falkenhagen (DF) coefficient [48, 49]

$$D = \frac{|z_1 z_2| e^2 \kappa_0 q^{1.5}}{24\pi\varepsilon_0 k_B T \left(1+q^{0.5}\right)^2} \tag{2.18}$$

and q is

$$q = \frac{|z_1 z_2|\left(\lambda_1+\lambda_2\right)}{\left(|z_1|+|z_2|\right)\left(|z_1|\lambda_2+|z_2|\lambda_1\right)} \tag{2.19}$$

gives relatively larger effects at low concentrations [55]. As a result, we add an adjustable parameter γ_{DF_1} to correct for DF coefficient during the fitting procedure. Moreover, as the DF effect was originally derived for dilute range of concentration [49] and will be amplified as concentration increases, a decaying factor $\Gamma(c)$ should be introduced to correct for the theoretical expression as concentration increases. The decaying function, as will be shown in Section 2.6, is also necessary to be included to obtain reasonable values for irrotational

bonded (IB) water molecules Z_{IB}. In this work, an exponential-type decaying function $\Gamma(c)$, through the adjustable parameter γ_{DF_2}, is established. The net static permittivity increment due to DF effect $\delta_{DF}(c)$ can then be written as

$$\delta_{DF}(c) = \gamma_{DF_1} D\sqrt{10^3 c}\ \Gamma(c) \tag{2.20}$$

$$\Gamma(c) = \exp(-\gamma_{DF_2} c) \tag{2.21}$$

The rationale behind an exponential-type decaying factor comes from the fact that it provides finer goodness of fit between the measured data and the proposed model of the static permittivity in the given concentration range.

2.4.5. Complete Model of Static Permittivity

According to the discussions made through Sections 2.4.1 to 2.4.4, the semi-empirical model to represent the static permittivity of multivalent electrolyte systems in low concentration regime can be given as a combination of terms from (2.4), (2.5), (2.17), and (2.20)

$$\begin{aligned} \varepsilon_{dc}(c) &= \varepsilon_{dc}^0 + \delta_{DF}(c) - \delta_{MW}(c) - \delta_{KD}(c) - \delta_{sat}(c) \\ &= \varepsilon_{dc}^0 + \gamma_{DF_1} D\sqrt{10^3 c}\exp(-\gamma_{DF_2} c) - \delta_{MW}(c) - \delta_{KD}(c) - \gamma_{sat} c \end{aligned} \tag{2.22}$$

where $\delta_{MW}(c)$ and $\delta_{KD}(c)$ are directly calculated through (2.4)-(2.13), D is calculated from (2.18) and is given in Table 2.3, and $\delta_{DF}(c)$ along with $\delta_{sat}(c)$ are calculated empirically through the adjustable parameters γ_{DF_1}, γ_{DF_2}, and γ_{sat} by careful execution of the data-fitting procedure. A hypothetical graph representing the behavior of static permittivity (2.22) with respect to concentration is shown in Figure 2.2.

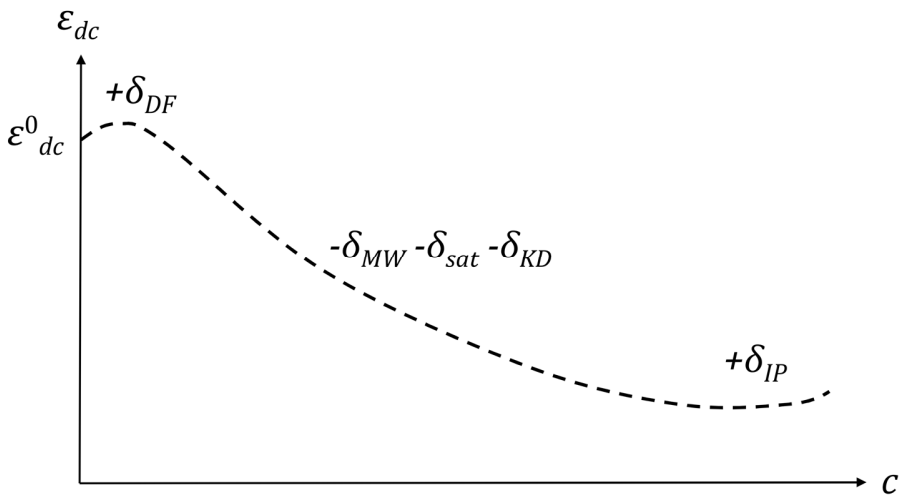

Figure 2.2 Hypothetical graph representing the dependence of static permittivity (2.22) on concentration. The effects of Debye-Falkenhagen effect, δ_{DF}, dilution and internal depolarizing field, δ_{MW}, dielectric saturation, δ_{sat}, kinetic depolarization, δ_{KD}, and ion-pair, δ_{IP}, are shown in the figure.

The effects discussed in Sections 2.4.1 to 2.4.4 have each been treated separately, effectively ignoring possible inter-relations between each other. Thus comparison with experimental results needs stringent attention. It is also worth mentioning that in highly concentrated solutions the ionic contributions, based on Bjerrum's concept of ion-pairs, generally increases. In the case of highly concentrated solutions, it may be necessary to add the incremental effect of ion-pairs (IP) $\delta_{IP}(c)$ to the model of static permittivity represented in (2.22). Analysis of dielectric spectra proves to be more complicated, but manageable, if ion-pairs and complex aggregates also contribute to the complex permittivity [56]. In the concentration ranges for the electrolyte systems studied in this work, however, no evidence of creation of strong ion-pairs has been observed.

2.5. Results

The fitted Debye relaxation parameters, specific conductivities, and reduced variance of the fits of the data to (2.22), along with the associated uncertainties for each of NaCl, $NaNO_3$, and Na_2SO_4 electrolyte systems at T = 25 °C, are listed in Table 2.4. The specific

Table 2.4 Parameters of single-term Debye model (ε_{dc}, τ, and ε_∞), specific conductivity (σ), and reduced variance of the fit (s^2) to (2.22) for various concentrations (c) of aqueous NaCl, $NaNO_3$, and Na_2SO_4 solutions at T = 25 °C. The specific conductivity was measured directly up to 500 μS/cm. For concentrations corresponding to specific conductivity greater than 500 μS/cm, σ was treated as an additional fitting parameter. The standard uncertainties correspond to approximately 68 % confidence interval.

c (mmol/L)	σ (μS/cm)	ε_{dc}	τ (ps)	ε_∞	s^2
NaCl					
0	8.184 ± 0.040	78.362 ± 0.078	8.275 ± 0.047	5.24 ± 0.16	0.002
0.294 ± 0.016	35.13 ± 0.18	78.380 ± 0.080	8.260 ± 0.047	5.07 ± 0.17	0.002
0.585 ± 0.024	69.91 ± 0.35	78.403 ± 0.078	8.254 ± 0.047	4.87 ± 0.16	0.004
0.873 ± 0.029	105.44 ± 0.52	78.421 ± 0.078	8.192 ± 0.046	4.26 ± 0.15	0.016
1.159 ± 0.033	138.18 ± 0.70	78.459 ± 0.080	8.175 ± 0.047	4.00 ± 0.16	0.041
1.722 ± 0.040	207.8 ± 1.0	78.444 ± 0.078	8.181 ± 0.046	4.00 ± 0.16	0.044
2.276 ± 0.045	273.1 ± 1.4	78.415 ± 0.079	8.172 ± 0.046	3.89 ± 0.16	0.047
2.820 ± 0.049	345.1 ± 1.7	78.387 ± 0.079	8.126 ± 0.046	3.53 ± 0.16	0.049
4.244 ± 0.049	517.0 ± 7.6	78.373 ± 0.079	8.129 ± 0.046	3.46 ± 0.16	0.065
5.653 ± 0.049	675.5 ± 8.4	78.357 ± 0.078	8.081 ± 0.045	3.07 ± 0.15	0.075
7.045 ± 0.049	838.2 ± 9.1	78.355 ± 0.078	8.104 ± 0.046	3.09 ± 0.15	0.120
8.462 ± 0.048	977.0 ± 9.4	78.340 ± 0.078	8.080 ± 0.046	2.85 ± 0.15	0.131
9.853 ± 0.047	1167 ± 10	78.315 ± 0.081	8.061 ± 0.046	2.69 ± 0.17	0.153
11.259 ± 0.047	1297 ± 10	78.266 ± 0.078	8.058 ± 0.045	2.66 ± 0.15	0.144
$NaNO_3$					
0	8.331 ± 0.042	78.363 ± 0.079	8.268 ± 0.047	5.19 ± 0.17	0.001
0.743 ± 0.043	84.77 ± 0.42	78.352 ± 0.077	8.258 ± 0.046	5.10 ± 0.15	0.002
1.479 ± 0.060	168.50 ± 0.84	78.344 ± 0.076	8.242 ± 0.046	4.96 ± 0.15	0.003
2.209 ± 0.073	250.5± 1.3	78.341 ± 0.078	8.235 ± 0.047	4.87 ± 0.16	0.005
2.932 ± 0.083	333.3 ± 1.7	78.325 ± 0.076	8.226 ± 0.046	4.73 ± 0.15	0.005
3.649 ± 0.092	414.6 ± 2.1	78.310 ± 0.077	8.209 ± 0.046	4.61 ± 0.15	0.006
4.36 ± 0.10	491.2 ± 2.5	78.292 ± 0.078	8.213 ± 0.047	4.66 ± 0.16	0.007
5.06 ± 0.11	566.9 ± 8.0	78.289 ± 0.078	8.196 ± 0.046	4.48 ± 0.16	0.011
5.76 ± 0.11	648.0 ± 8.1	78.275 ± 0.078	8.188 ± 0.046	4.39 ± 0.16	0.014
6.45 ± 0.12	728.8 ± 8.7	78.263 ± 0.079	8.177 ± 0.047	4.29 ± 0.17	0.018
7.14 ± 0.13	809.0 ± 9.0	78.270 ± 0.079	8.166 ± 0.046	4.16 ± 0.16	0.023
10.74 ± 0.13	1200± 10	78.185 ± 0.081	8.162 ± 0.047	4.13 ± 0.17	0.025
14.31 ± 0.13	1540 ± 13	78.014 ± 0.081	8.163 ± 0.047	4.31 ± 0.18	0.016
17.83 ± 0.12	1946 ± 13	77.975 ± 0.078	8.156 ± 0.046	4.27 ± 0.16	0.014
Na_2SO_4					
0	8.218 ± 0.041	78.362 ± 0.078	8.277 ± 0.047	5.26 ± 0.16	0.002
0.325 ± 0.019	78.44 ± 0.39	78.351 ± 0.082	8.271 ± 0.048	5.17 ± 0.19	0.002
0.965 ± 0.032	225.0 ± 1.1	78.322 ± 0.077	8.277 ± 0.046	5.25 ± 0.16	0.003
1.281 ± 0.036	297.0 ± 1.5	78.316 ± 0.079	8.270 ± 0.047	5.15 ± 0.17	0.002
1.594 ± 0.040	366.9 ± 1.8	78.305 ± 0.079	8.267 ± 0.047	5.15 ± 0.17	0.003
2.212 ± 0.047	496.7 ± 7.8	78.272 ± 0.078	8.273 ± 0.047	5.22 ± 0.16	0.003
2.819 ± 0.052	638.1 ± 8.5	78.240 ± 0.078	8.267 ± 0.047	5.21 ± 0.16	0.003
3.119 ± 0.054	703.0 ± 8.6	78.221 ± 0.078	8.280 ± 0.047	5.30 ± 0.16	0.003
4.693 ± 0.054	1038 ± 10	78.167 ± 0.079	8.266 ± 0.047	5.18 ± 0.17	0.003
6.250 ± 0.054	1320 ± 11	78.119 ± 0.079	8.265 ± 0.047	5.16 ± 0.17	0.005
7.789 ± 0.054	1596 ± 12	78.052 ± 0.078	8.252 ± 0.047	5.08 ± 0.16	0.005
9.356 ± 0.053	1904 ± 13	77.998 ± 0.077	8.245 ± 0.047	4.95 ± 0.15	0.007
10.895 ± 0.052	2163 ± 14	77.930 ± 0.076	8.238 ± 0.046	4.91 ± 0.15	0.010
12.449 ± 0.051	2394 ± 16	77.832 ± 0.077	8.221 ± 0.046	4.86 ± 0.15	0.022

conductivity σ was measured directly using a conductivity meter, as mentioned in Section 2.3. There were, however, a few concentrations for which σ was higher than the operating range of the conductivity meter, i.e., σ was greater than 500 μS/cm. In such cases the specific conductivity σ was treated as an additional adjustable parameter meaning that the sum of a single-term Debye relaxation model and a conductivity contribution ($\sigma/2\pi f\varepsilon_0$) was used to analytically represent the measured spectrum. According to Table 2.4, the major relaxation of the spectra for all three electrolyte systems occurs at around 18 GHz at T = 25 °C, corresponding to cooperative relaxation of the H-bond network of bulk water molecules. The minor high-frequency relaxation process (~ 120 GHz), which is due to free water molecules is beyond the upper frequency limit of the present work. The relaxation parameters of pure water obtained in this work are in a good agreement with the values presented in [13], based on a single-term Debye model, reported as ε^0_{dc} = 78.36 ± 0.2, τ = 8.27 ± 0.05 ps, and ε_∞ = 5.2 ± 0.1 at T = 25 °C. The uncertainties evaluated in this work are, however, smaller (Table2.4). Although a good quality fit to the measured spectra was achieved for each concentration, it should be noted that the reduced variance of the fit, $s^2 = \Sigma(\varepsilon_c - \varepsilon_{Debye})^2/(\text{n-m})$, increases with concentration.

2.6. Discussion

2.6.1. Evaluation of Semi-Empirical Model

In Figure 2.3 the static permittivity (column 3 in Table 2.4) for aqueous solutions of NaCl, $NaNO_3$, and Na_2SO_4 is plotted versus concentration. The fitted static permittivity modeled by (2.22) is also shown for each electrolyte system, with parameters given in Table 2.5. The permittivity of NaCl [11-13], $NaNO_3$ [8, 9], Na_2SO_4 [14, 15] and indeed most other strong electrolytes in water has already been found to follow a decreasing trend with

concentration for $c \approx 0.5$ to 5 mol/L (500 to 5,000 mmol/L). Within the concentration range of the present work, however, the static permittivities so obtained show a slight increase with concentration for both NaCl and $NaNO_3$, while they show almost linear decrease for Na_2SO_4. The positive contribution to static permittivity in this low concentration regime can be best attributed to the creation of ionic atmosphere polarization and the associated Debye-Falkenhagen (DF) effect, as discussed in Section 2.4. The contribution of the DF effect to the static permittivity represented by γ_{DF_1} (or $\gamma_{DF_1}D$) behave as NaCl > $NaNO_3$ > Na_2SO_4. The permittivity increment for NaCl is in conformity with the findings of van Beek *et al.* [49] and Winsor *et al.* [55], although Anderson [52] commented on the possible challenges that might in generally question the observation of DF effect through experiments. Static permittivity data in low concentration regions, which can potentially manifest the DF effect in $NaNO_3$ and Na_2SO_4, however, have not been yet reported in literature.

The resulting decrements in measured static permittivity, albeit with an initial increase in NaCl and $NaNO_3$ which will be discussed in Section 2.6, of all electrolyte systems shown in Figure 2.3 with concentration can be attributed to the sum of contributions from dilution and internal depolarizing field, kinetic depolarization, and dielectric saturation, as well as the vanishing effect of DF effect through $\exp(-\gamma_{DF_2}c)$. The dielectric saturation effect, represented by γ_{sat} follows the trend Na_2SO_4 > $NaNO_3$ > NaCl. In principle, such a sequence is connected to an increase in the number of irrotationally bound water molecules Z_{IB} within the concentration range studied.

Two theoretical decrement terms of static permittivity, Δ_1 and Δ_2, which are calculated according to

$$\Delta_1 = \varepsilon_{dc}^0 - \left(\delta_{MW}(c) + \delta_{KD}(c)\right) \tag{2.23}$$

and

$$\Delta_2 = \varepsilon_{dc}^0 - \left(\delta_{MW}(c) + \delta_{KD}(c) + \delta_{sat}(c)\right) \tag{2.24}$$

are also shown in Figure 2.3 for each electrolyte system. Therein ε^0_{dc} is the static permittivity of deionized water (Table 2.4), and $\delta_{MW}(c)$ and $\delta_{KD}(c)$ are calculated from (2.4) and (2.5), respectively. The theoretical calculation of $\delta_{sat}(c)$, i.e., $\delta_{sat}(c) = \varepsilon^0_{dc} - \bar{\varepsilon}_{dc}(c) - \delta_{MW}(c)$, where $\bar{\varepsilon}_{dc}(c)$ is implicitly calculated from (2.15), requires input values for Z_{IB}. The Z_{IB} values are measurable only for the whole system A_XB_Y, so it is necessary to split them into the ionic Z^+_{IB} and Z^-_{IB} values. Cationic irrotationally bound water molecules have Z^+_{IB} = 4.2 for Na^+ [12], and anionic irrotationally bound water molecules have Z^-_{IB} = 0 for Cl^- [12] , 0 for NO_3^-[19], and 10 for SO_4^{2-} [15]. These numbers, however, are obtained from experimental data for electrolyte systems with moderate to high concentrations, i.e., 0.5 mol/L < c < 5 mol/L. The decrement term Δ_1 accounts for reduction of static permittivity due to dilution and internal depolarizing field, and kinetic depolarization, while Δ_2, accounts for contributions of the same mechanisms as well as dielectric saturation.

Ideally, one would expect $\Delta_2 < \Delta_1$ as the sum of contributions from dilution and internal depolarizing field, kinetic depolarization, and dielectric saturation would be greater than the sum of the first two. This, however, is not held for the corresponding calculated results for NaCl and $NaNO_3$ (Figures 2.3.a and 2.3.b) within the entire concentration range as $\Delta_2 > \Delta_1$. This observation reflects that there are unrealistic negative values for dielectric saturation $\delta_{sat}(c)$ which are calculated theoretically from Z_{IB} values taken from literature. Therefore, it can be inferred that the number of irrotationally bound water molecules Z_{IB}

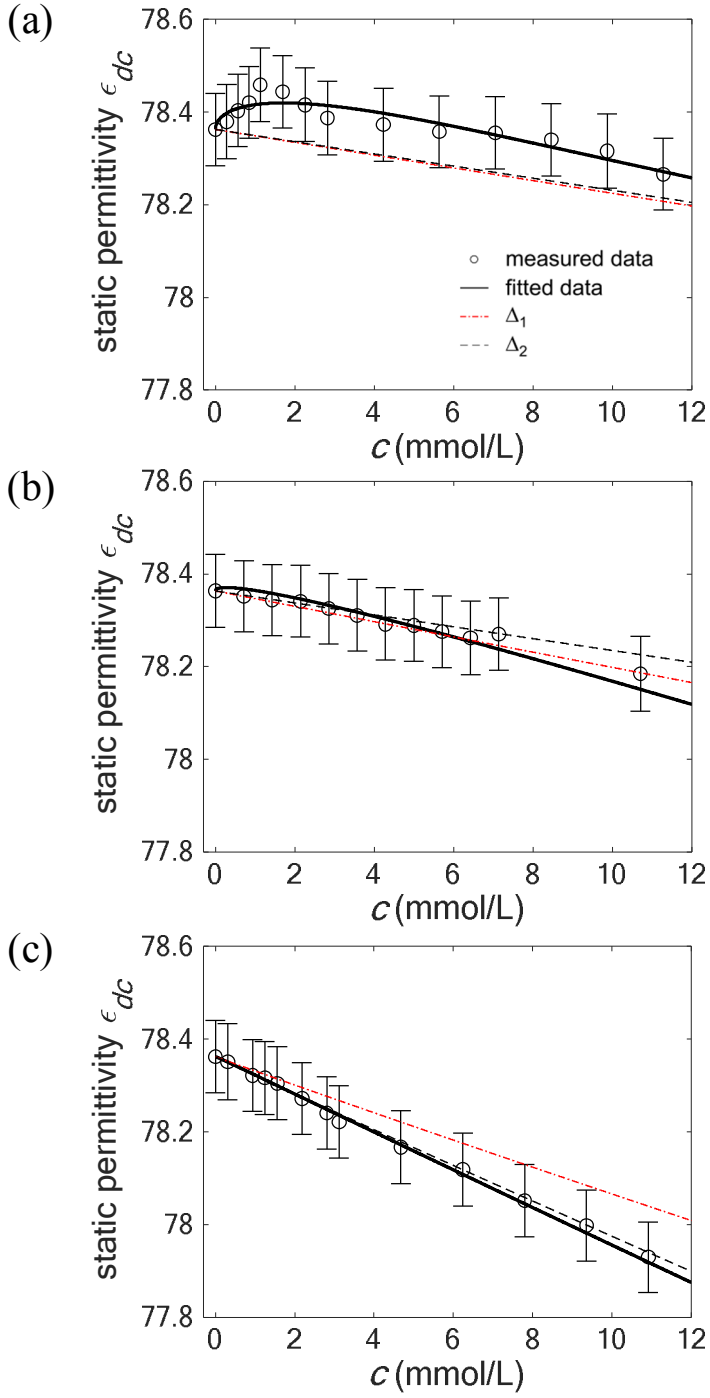

Figure 2.3 Experimental data (open circles) of the static permittivity, ε_{dc}, and fitted semi-empirical model of static permittivity (2.22) (solid line) with parameters listed in Table 2.5, of aqueous solutions of (a) NaCl, (b) $NaNO_3$, and (c) Na_2SO_4 at T = 25 °C. Theoretical discernment term Δ_1 (2.23) accounts for the contributions of dilution and kinetic depolarization (dash-dot line) and Δ_2 (2.24) accounts for the contributions of dilution, kinetic depolarization, and dielectric saturation, where Z_{IB} values are taken from literature [19] and are treated as input variables (dashed line).

Table 2.5 Concentration, ε^0_{dc}, and parameters of semi-empirical static permittivity model (2.22) of aqueous NaCl, $NaNO_3$, and Na_2SO_4 solutions at 25 °C. The sum of squared error (SSE) for each fitted curve is also shown.

	c (mmol/L)	ε^0_{dc}	γ_{DF_1}	γ_{DF_2}	γ_{sat}	SSE
NaCl	0-11.26	78.362	0.64 ± 0.02	122 ± 49	0.003 ± 0.003	0.005
$NaNO_3$	0-17.83	78.358	0.24 ± 0.03	31.3 ± 9.1	9.5 ± 0.4	0.005
Na_2SO_4	0-12.45	78.362	0.008 ± 0.003	27 ± 10	11.8 ± 0.5	0.002

reported in literature for either cation Na^+ or anions Cl^- and NO_3^- are underestimated in the low concentration regime. For Na_2SO_4 (Figure 2.3.c), however, as $\Delta_2 < \Delta_1$ holds, the same, at least comparable, number of Z_{IB} for cation Na^+ and anion SO_4^{2-} can be speculated.

2.6.2. Irrotationally Bound Water Molecules

The number of irrotationally bound water molecules Z_{IB} for each electrolyte solution can be calculated as a function of concentration, through (2.14)-(2.16). An estimate of the Z_{IB} values from (2.15) using $\bar{\varepsilon}_{dc}$, the static permittivitiy corrected for kinetic depolarization, has given unrealistic negative values for NaCl and $NaNO_3$, as depicted in Figure 2.4. These unrealistic values offer support for the veracity of the observed positive contribution of ionic atmosphere and DF effect to the static permittivities at low concentrations. Attempting to obtain realistic non-negative values for Z_{IB} can be achieved by correcting $\bar{\varepsilon}_{dc}$ values in (2.15) for DF effect, i.e., $\bar{\varepsilon}_{dc}(c) = \varepsilon_{dc}(c) + \delta_{KD}(c) - \delta_{DF}(c)$, where $\delta_{DF}(c)$ is calculated from (2.20)-(2.21) and the parameters obtained in Table 2.5. The Z_{IB} values corrected for DF effect are also shown in Figure 2.4.

From the extrapolations of Z_{IB} at $c \rightarrow 0$, and by setting $Z^+_{IB} = 4.5 \pm 0.3$ for Na^+ [12], Z^-_{IB} values for each electrolyte solution are listed in Table 2.6. According to Table 2.6, Z^-_{IB} values corrected only for kinetic depolarization ($Z^-_{IB}{}^{KD}$) result in negative values for NaCl

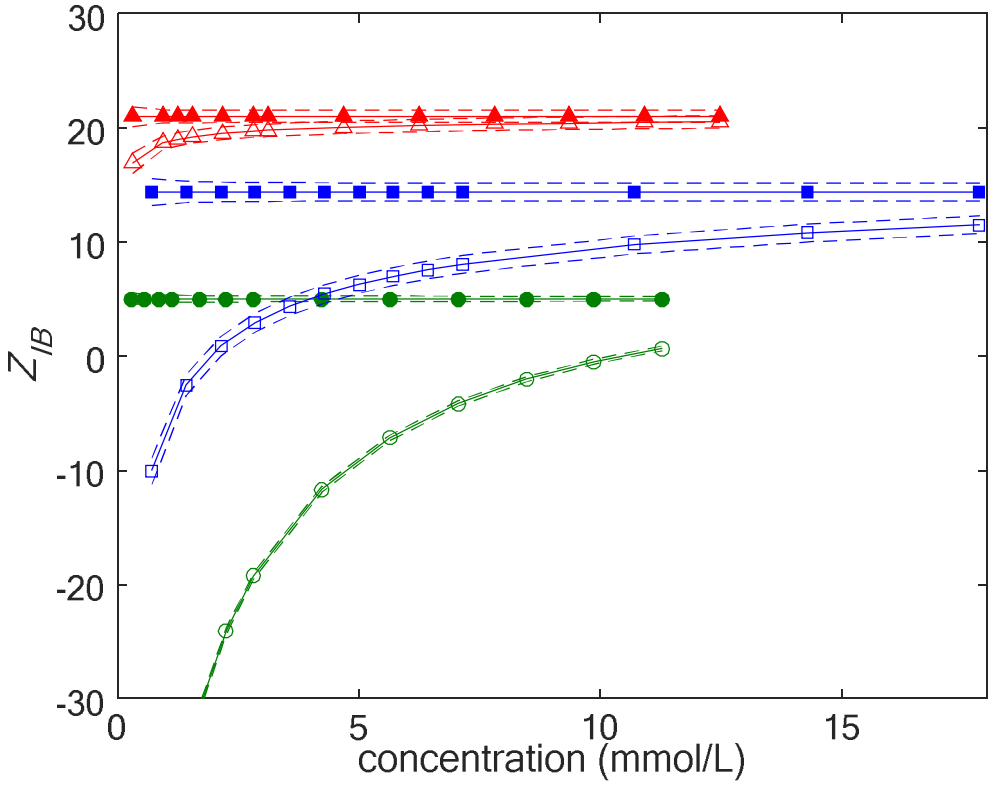

Figure 2.4 Number of irrotationally bound water molecules, Z_{IB}, of NaCl (circle), $NaNO_3$ (square), and Na_2SO_4 (triangle) at 25 °C. Z_{IB} values are corrected for kinetic depolarization (hollow symbols), and corrected for kinetic depolarization and Debye-Falkenhagen effect (filled symbols). The 68% confidence intervals, representing the uncertainties in deriving Z_{IB} values, are also shown (dashed line). Fitted static permittivities (2.22) are used to calculate Z_{IB} through (2.14)-(2.16).

Table 2.6 Number of irrotationally bound water molecules per anion, Z^-_{IB}, corrected for kinetic depolarization ($Z^-_{IB}{}^{KD}$), and corrected for kinetic depolarization and Debye-Falkenhagen effect ($Z^-_{IB}{}^{KD+DF}$). Fitted static permittivities (2.22) are used to calculate Z_{IB} through (2.14)-(2.16). $Z^+_{IB} = 4.2 \pm 0.3$ for Na^+ [12] is assumed for all calculations. The coordination number (CN) and Z^-_{IB} for each anion according to corresponding reference are also given.

	CN (ref)	Z^-_{IB} (ref)[1]	$Z^-_{IB}{}^{KD}$	$Z^-_{IB}{}^{KD+DF}$
Cl^-	6 [19, 57]	0 ± 0.3 [12]	-99.6 ± 0.6	0.5 ± 0.6
NO_3^-	5.9-9 [9, 19]	0 [19]	-14.5 ± 1.2	9.9 ± 1.2
SO_4^{2-}	7-12 [15, 19]	10 ± 0.7 [15]	7.9 ± 1.0	11.9 ± 0.9

[1] Z^-_{IB} values are corrected for kinetic depolarization under slip boundary condition.

and $NaNO_3$ solutions. The Z^-_{IB} values, corrected for both kinetic depolarization and DF effect ($Z^-_{IB}{}^{KD+DF}$), however, result in non-negative and physically realistic values. These values read as 0.5 ± 0.6 for Cl^- and 11.9 ± 0.9 for SO_4^{2-} and are found to be in a good agreement with 0 ± 0.3 for Cl^- reported in [12] and 10 ± 0.7 for SO_4^{2-} reported in [15]. Higher values, however, are calculated for NO_3^- as 9.9 ± 1.2 compared to 0 reported in [19]. Although Z^-_{IB} is not strictly a coordination number (CN) (total number of water molecules in all solvation layers of ion) [7] the level of agreement between coordination number of NO_3^-, i.e., 5.9 to 9 [9, 19], and number of irrotationally bound water molecules around NO_3^-, i.e., 9.9 ± 1.2 (Table 2.6), largely reflects the presence of water molecules with reduced but nonzero rotational mobility in the structural mismatch region. As pointed out by Frank and Wen [30, 58] there must exist a structural mismatch region of water molecules with reduced but non-zero rotational mobility beyond the inner solvation layer. At low concentration of NO_3^- ions (mmol/L), the number of water molecules is much greater than the number of ions ($c_s^0/c \sim$ thousands), thus, those water molecules that could not find an ion to partner with in the inner solvation layer remain in the structural mismatch region. Water molecules with reduced but non-zero rotational mobility in the structural mismatch region, therefore, lead to an increase in the Z^-_{IB} value of NO_3^- ion.

Comparing the coordination number of SO_4^{2-}, i.e., 7 to 12 [15, 19], and the number of irrotationally bound water molecules around SO_4^{2-}, i.e., 11.9 ± 0.9, implies that in the strong Columbic field of bivalent ions more water molecules are irrotationally bound in the first and beyond the first solvation layer [15]. Based on the coordination number of Cl^-, i.e., 6 [19, 57], with a broad distribution from 1 to 8 [12], and the number of irrotationally bound water molecules around Cl^-, i.e., 0.5 ± 0.6, however, no water molecule is found to be bonded

beyond the first solvation layer. Indeed, since $Z^{-}_{IB} \neq 0$ it offers a fraction number of water molecules in the first solvation layer are immobilized within the low concentration range studied. The uncertainty associated with the Z^{-}_{IB} value, however, may not allow one to derive a firm conclusion.

2.6.3. Debye-Falkenhagen Effect

The analysis of DF effect for different electrolyte systems has not been extensively covered in literature. Nevertheless, concentration-independent Debye length $l_{\kappa 0}$ (m) is an available parameter that can be employed to justify the strength of DF effect for different ions. $l_{\kappa 0}$ is calculated as [59]

$$l_{\kappa_0} = \frac{1}{\kappa_0} \tag{2.25}$$

where κ_0 is the concentration-independent inverse Debye length calculated from (2.7). For NaCl and $NaNO_3$ which both have same ionic electron valency $z_1 = 1$, $z_2 = 1$, $l_{\kappa 0} = 9.60$ nm, and for Na_2SO_4 with $z_1 = 1$, $z_2 = 2$, $l_{\kappa 0} = 6.07$ nm at $T = 25$ °C. The Debye length, $l_{\kappa 0}$, can be taken as the corresponding length of the induced dipolar moment created by charge cloud separation of ionic atmosphere. Therefore, the longer the Debye length, the stronger is the induced dipolar moment and thereby the DF effect. As NaCl and $NaNO_3$ possess longer Debye length than Na_2SO_4, according to γ_{DF_1} listed in Table 2.5, the positive contribution of DF effect follows expectedly the trend NaCl > Na_2SO_4 and NaNO3 > Na_2SO_4.

The strength of DF effect, however, should not be solely dependent on Debye length as we should be able to justify the difference in DF effect of NaCl > $NaNO_3$ with the same Debye length. A potential hypothesis can be attributed to “electrophoretic effect” [41] that prevents the formation of complete asymmetric ionic atmosphere. While the asymmetric

ionic atmosphere is forming under the applied electric field, the ions with opposite charges are passing each other. As water molecules (in solvation layers) are pulled along with each ion, each ion (cation and anion), in effect, will see water molecules streaming past itself in the opposite direction, and this will exert a viscous drag on each ion, slowing it down to form a complete (longer) asymmetric ionic atmosphere. As the coordination number of $Cl^- < NO_3^-$ (Table 2.6), and according to the electrophoretic effect, there are less water molecules to create viscous drags in the ionic atmosphere of Na^+ and Cl^-, thus, a longer asymmetric ionic atmosphere will be formed. As a result, the positive contribution of DF effect will follow the trend $NaCl > NaNO_3$.

2.7. Conclusion

The dielectric properties of environmentally-relevant low concentration electrolyte solutions of NaCl, $NaNO_3$, and Na_2SO_4 which are commonly found in water sources have been analyzed through well-controlled laboratory experiments. A semi-empirical parametric model to represent the static permittivity has been represented. The model has efficiently accounted for contributions due to dilution and internal depolarizing fields, kinetic depolarization, dielectric saturation, and the Debye-Falkenhagen effect. The results have shown that the decrements in static permittivity due to aggregation of dilution and internal depolarizing field, kinetic depolarization, and dielectric saturation follows the trend $Na_2SO_4 > NaNO_3 > NaCl$. It has also been demonstrated that, within the low concentration range studied, the static permittivities need to be corrected to incorporate the contributions of both kinetic depolarization and Debye-Falkenhagen effect, to obtain non-negative and physically realistic number of irrotationally bound water molecules per anion. Rather large number of irrotationally bound water molecules for $NaNO_3$, however, suggest the existence of a structural mismatch region of water molecules with reduced but non-zero rotational mobility

that do not contribute to polarization. Moreover, it has been observed that in NaCl and $NaNO_3$ solutions there is significant positive contribution due to the Debye-Falkenhagen effect that increases the static permittivity, particularly at lower concentrations. The concentration-independent Debye screening length has been defined to justify the strength of the DF effect for the electrolyte solutions studied. This parameter has also been discussed to be possibly related to the electrophoretic effect and the coordination number, leading to the DF effect strength to follow $NaCl > NaNO_3 > Na_2SO_4$.

Further measurements and highly accurate experimental data for different electrolyte solutions at various temperatures are desirable to evaluate the semi-empirical parametric model, examine the number of irrotationally bound water molecules, and also extend our knowledge of ionic atmosphere polarization and positive contribution of the DF effect to static permittivities in low concentration regions. Studying the cluster of water molecules hydrating Cl^-, NO_3^-, and SO_4^{2-} ions in understanding the coordination numbers and the physical configuration of ionic atmosphere under an applied electric field will also be of great interest.

Acknowledgment

This work was funded by the USDA-National Institute of Food & Agriculture, Award Number 013025-00001. The authors gratefully acknowledge Amy L. Kaleita for her leadership on this project.

2.8. References

[1] B. A. Zimmerman and A. L. Kaleita, "Dissolved Constituents in Agricultural Drainage Waters," *Transactions of the ASABE,* vol. 60, pp. 847-859, 2017.

[2] R. Buchner, "What can be learnt from dielectric relaxation spectroscopy about ion solvation and association?," *Pure and Applied Chemistry,* vol. 80, pp. 1239-1252, 2008.

[3] U. Kaatze, "Complex permittivity of water as a function of frequency and temperature," *Journal of Chemical and Engineering Data,* vol. 34, pp. 371-374, 1989.

[4] N. Vinh, M. S. Sherwin, S. J. Allen, D. George, A. Rahmani, and K. W. Plaxco, "High-precision gigahertz-to-terahertz spectroscopy of aqueous salt solutions as a probe of the femtosecond-to-picosecond dynamics of liquid water," *The Journal of Chemical Physics,* vol. 142, p. 164502, 2015.

[5] U. Kaatze, V. Lönnecke, and R. Pottel, "Dielectric spectroscopy of aqueous ZnCl 2 solutions. Dependence upon solute concentration and comparison with other electrolytes," *Journal of Molecular Liquids,* vol. 34, pp. 241-255, 1987.

[6] A. Lyashchenko and A. Y. Zasetsky, "Complex dielectric permittivity and relaxation parameters of concentrated aqueous electrolyte solutions in millimeter and centimeter wavelength ranges," *Journal of Molecular Liquids,* vol. 77, pp. 61-75, 1998.

[7] W. Wachter, Š. Fernandez, R. Buchner, and G. Hefter, "Ion association and hydration in aqueous solutions of LiCl and Li2SO4 by dielectric spectroscopy," *The Journal of Physical Chemistry B,* vol. 111, pp. 9010-9017, 2007.

[8] A. Lileev, Z. Filimonova, and A. Lyashchenko, "Dielectric permittivity and relaxation in aqueous solutions of alkali metal sulfates and nitrates in the temperature range 288–313 K," *Journal of Molecular Liquids,* vol. 103, pp. 299-308, 2003.

[9] W. Wachter, W. Kunz, R. Buchner, and G. Hefter, "Is there an anionic Hofmeister effect on water dynamics? Dielectric spectroscopy of aqueous solutions of NaBr, NaI, NaNO3, NaClO4, and NaSCN," *The Journal of Physical Chemistry A,* vol. 109, pp. 8675-8683, 2005.

[10] A. Gorji, A. L. Kaleita, and N. Bowler, "Towards low-cost sensors for real-time monitoring of contaminant ions in water sources," in *Microwave Symposium (IMS), 2017 IEEE MTT-S International*, Honolulu, HI, USA, 2017, pp. 1-4.

[11] K. Nörtemann, J. Hilland, and U. Kaatze, "Dielectric properties of aqueous NaCl solutions at microwave frequencies," *The Journal of Physical Chemistry A,* vol. 101, pp. 6864-6869, 1997.

[12] R. Buchner, G. T. Hefter, and P. M. May, "Dielectric relaxation of aqueous NaCl solutions," *The Journal of Physical Chemistry A,* vol. 103, pp. 1-9, 1999.

[13] E. Levy, A. Puzenko, U. Kaatze, P. B. Ishai, and Y. Feldman, "Dielectric spectra broadening as the signature of dipole-matrix interaction. I. Water in nonionic solutions," *The Journal of Chemical Physics,* vol. 136, p. 114502, 2012.

[14] J. Barthel, H. Hetzenauer, and R. Buchner, "Dielectric Relaxation of Aqueous Electrolyte Solutions II. Ion-Pair Relaxation of 1: 2, 2: 1, and 2: 2 Electrolytes," *Berichte der Bunsengesellschaft für Physikalische Chemie,* vol. 96, pp. 1424-1432, 1992.

[15] R. Buchner, S. G. Capewell, G. Hefter, and P. M. May, "Ion-pair and solvent relaxation processes in aqueous Na2SO4 solutions," *The Journal of Physical Chemistry B,* vol. 103, pp. 1185-1192, 1999.

[16] H. Weingärtner, A. Knocks, W. Schrader, and U. Kaatze, "Dielectric spectroscopy of the room temperature molten salt ethylammonium nitrate," *The Journal of Physical Chemistry A,* vol. 105, pp. 8646-8650, 2001.

[17] T. Fukasawa, T. Sato, J. Watanabe, Y. Hama, W. Kunz, and R. Buchner, "Relation between dielectric and low-frequency Raman spectra of hydrogen-bond liquids," *Physical Review Letters,* vol. 95, p. 197802, 2005.

[18] P. R. Bevington, D. K. Robinson, J. M. Blair, A. J. Mallinckrodt, and S. McKay, "Data reduction and error analysis for the physical sciences," *Computers in Physics,* vol. 7, pp. 415-416, 2003.

[19] R. Buchner and G. Hefter, "Interactions and dynamics in electrolyte solutions by dielectric spectroscopy," *Physical Chemistry Chemical Physics,* vol. 11, pp. 8984-8999, 2009.

[20] R. B. D'Agostino, *Goodness-of-fit-techniques* vol. 68: CRC press, 1986.

[21] I. BIPM, I. IFCC, I. IUPAC, and O. ISO, "Evaluation of measurement data—guide for the expression of uncertainty in measurement. JCGM 100: 2008," *Citado en las,* p. 167, 2008.

[22] C. Gabriel and A. Peyman, "Dielectric measurement: error analysis and assessment of uncertainty," *Physics in Medicine and Biology,* vol. 51, p. 6033, 2006.

[23] A. P. Gregory and R. Clarke, *Tables of the complex permittivity of dielectric reference liquids at frequencies up to 5 GHz*: National Physical Laboratory (NPL), Teddington, 2012.

[24] T. Sato, A. Chiba, and R. Nozaki, "Hydrophobic hydration and molecular association in methanol–water mixtures studied by microwave dielectric analysis," *The Journal of Chemical Physics,* vol. 112, pp. 2924-2932, 2000.

[25] A. Gregory, R. Clarke, and M. Cox, "Traceable measurement of dielectric reference liquids over the temperature interval 10–50 C using coaxial-line methods," *Measurement Science and Technology,* vol. 20, p. 075106, 2009.

[26] R. Buchner, J. Barthel, and J. Stauber, "The dielectric relaxation of water between 0 C and 35 C," *Chemical Physics Letters,* vol. 306, pp. 57-63, 1999.

[27] H. Falkenhagen and W. Fischer, "Dependence of Electrical Conductance and Dielectric Constant upon Frequency in Mixtures of Strong Electrolytes," *Nature,* vol. 130, pp. 928-928, 1932.

[28] J. C. Lestrade, J. P. Badiali, and H. Cachet, "Dielectric relaxation processes in electrolyte solutions," in *Dielectric and Related Molecular Processes*. vol. 2, M. Davies, Ed., ed: The Royal Society of Chemistry, 1975, pp. 106-150.

[29] H. L. Friedman, C. Krishnan, and C. Jolicoeur, "Ionic interactions in water," *Annals of the New York Academy of Sciences,* vol. 204, pp. 79-99, 1973.

[30] R. Pottel, "Dielectric Properties," in *Water, a Comprehensive Treatise: Aqueous solutions of simple electrolytes*. vol. 3, F. Franks, Ed., ed: Springer, 1973, pp. 401-431.

[31] V. H. Sack, "The dielectric constants of solutions of electrolytes at small concentrations," *Phys. Z,* vol. 28, pp. 199-210, 1927.

[32] J. Hasted, D. Ritson, and C. Collie, "Dielectric properties of aqueous ionic solutions. Parts I and II," *The Journal of Chemical Physics,* vol. 16, pp. 1-21, 1948.

[33] E. Glueckauf, "Bulk dielectric constant of aqueous electrolyte solutions," *Transactions of the Faraday Society,* vol. 60, pp. 1637-1645, 1964.

[34] L. Onsager, "Electric moments of molecules in liquids," *Journal of the American Chemical Society,* vol. 58, pp. 1486-1493, 1936.

[35] V. A. Markel, "Introduction to the Maxwell Garnett approximation: tutorial," *JOSA A,* vol. 33, pp. 1244-1256, 2016.

[36] U. Kaatze, "The dielectric properties of water in its different states of interaction," *Journal of solution chemistry,* vol. 26, pp. 1049-1112, 1997.

[37] U. Kaatze, "Bound water: Evidence from and implications for the dielectric properties of aqueous solutions," *Journal of Molecular Liquids,* vol. 162, pp. 105-112, 2011.

[38] J. Hubbard, L. Onsager, W. Van Beek, and M. Mandel, "Kinetic polarization deficiency in electrolyte solutions," *Proceedings of the National Academy of Sciences,* vol. 74, pp. 401-404, 1977.

[39] J. Hubbard, "Kinetic dielectric decrements and conducting liquids," *Biosystems,* vol. 8, pp. 201-205, 1977.

[40] K. Tielrooij, R. Timmer, H. Bakker, and M. Bonn, "Structure dynamics of the proton in liquid water probed with terahertz time-domain spectroscopy," *Physical Review Letters,* vol. 102, p. 198303, 2009.

[41] M. R. Wright, *An introduction to aqueous electrolyte solutions: Ch12*: John Wiley & Sons, 2007.

[42] W. M. Haynes, *CRC handbook of chemistry and physics*: CRC press, 2014.

[43] A. L. Horvath, *Handbook of aqueous electrolyte solutions*: Halsted Press, 1985.

[44] R. Mancinelli, A. Botti, F. Bruni, M. Ricci, and A. Soper, "Perturbation of water structure due to monovalent ions in solution," *Physical Chemistry Chemical Physics,* vol. 9, pp. 2959-2967, 2007.

[45] A. B. Pribil, T. S. Hofer, B. R. Randolf, and B. M. Rode, "Structure and dynamics of phosphate ion in aqueous solution: an ab initio QMCF MD study," *Journal of Computational Chemistry,* vol. 29, pp. 2330-2334, 2008.

[46] E. Cavell, P. Knight, and M. Sheikh, "Dielectric relaxation in non aqueous solutions. Part 2.—Solutions of tri (n-butyl) ammonium picrate and iodide in polar solvents," *Transactions of the Faraday Society,* vol. 67, pp. 2225-2233, 1971.

[47] J. Barthel, H. Hetzenauer, and R. Buchner, "Dielectric relaxation of aqueous electrolyte solutions. I. Solvent relaxation of 1: 2, 2: 1, and 2: 2 electrolyte solutions," *Berichte der Bunsengesellschaft für physikalische Chemie,* vol. 96, pp. 988-997, 1992.

[48] H. Falkenhagen, *Electrolytes (Theorie der Elektrolyte)*: Oxford University Press, Oxford, 1934.

[49] W. M. van Beek and M. Mandel, "Static relative permittivity of some electrolyte solutions in water and methanol," *Journal of the Chemical Society, Faraday Transactions 1: Physical Chemistry in Condensed Phases,* vol. 74, pp. 2339-2351, 1977.

[50] A. Chandra and B. Bagchi, "Frequency dependence of ionic conductivity of electrolyte solutions," *The Journal of Chemical Physics,* vol. 112, pp. 1876-1886, 2000.

[51] T. Yamaguchi, T. Matsuoka, and S. Koda, "A theoretical study on the frequency-dependent electric conductivity of electrolyte solutions," *The Journal of Chemical Physics,* vol. 127, p. 234501, 2007.

[52] J. Anderson, "The Debye-Falkenhagen effect: experimental fact or friction?," *Journal of Non-Crystalline Solids,* vol. 172, pp. 1190-1194, 1994.

[53] C. Collie, J. Hasted, and D. Ritson, "Dielectric properties of aqueous ionic solutions," *J. Chem. PhjBs,* vol. 16, pp. 1-21, 1948.

[54] V. Navarkhele, R. Agrawal, and M. Kurtadikar, "Dielectric properties of electrolytic solutions," *Pramana,* vol. 51, pp. 511-518, 1998.

[55] P. Winsor IV and R. H. Cole, "Dielectric behavior of aqueous sodium chloride solutions," *The Journal of Physical Chemistry,* vol. 89, pp. 3775-3776, 1985.

[56] S. Schrödle, W. W. Rudolph, G. Hefter, and R. Buchner, "Ion association and hydration in 3: 2 electrolyte solutions by dielectric spectroscopy: Aluminum sulfate," *Geochimica et Cosmochimica Acta,* vol. 71, pp. 5287-5300, 2007.

[57] R. Buchner, C. Hölzl, J. Stauber, and J. Barthel, "Dielectric spectroscopy of ion-pairing and hydration in aqueous tetra-n-alkylammonium halide solutions," *Physical Chemistry Chemical Physics,* vol. 4, pp. 2169-2179, 2002.

[58] H. S. Frank and W.-Y. Wen, "Ion-solvent interaction. Structural aspects of ion-solvent interaction in aqueous solutions: a suggested picture of water structure," *Discussions of the Faraday Society,* vol. 24, pp. 133-140, 1957.

[59] K. Ibuki and M. Nakahara, "Effect of relaxation of ionic atmosphere on the short-time dynamics of diffusion-controlled reaction," *The Journal of Chemical Physics,* vol. 92, pp. 7323-7329, 1990.

CHAPTER 3. DIELECTRIC MEASUREMENT OF LOW-CONCENTRATION AQUEOUS SOLUTIONS: ASSESSMENT OF UNCERTAINTY AND ION-SPECIFIC RESPONSES

Submitted to *Measurement Science and Technology*

Amin Gorji[1, 2, a] and Nicola Bowler[1, 2, 3, a]

3.1. Abstract

Excessive amounts of chemicals and ions flowing into water sources cause serious environmental and human-health related concerns. The lack of affordable and real-time monitoring systems for these contaminants limits effective conservation and management strategies. To establish a basis for developing an effective, fast, real-time, and affordable sensing system, dielectric spectroscopy method has been employed to characterize aqueous solutions of sodium chloride (NaCl), sodium nitrate ($NaNO_3$), and sodium sulphate (Na_2SO_4) at environmentally-relevant (low) concentrations. Dielectric spectra were measured over the frequency range from 200 MHz to 20 GHz, at temperature 25 ± 0.01 °C and for concentrations 0 to 20 mmol/L. The measured spectra were fitted with a Debye model using a non-linear, weighted, least-squares analysis. A method of judiciously exploiting the resulting fitting parameters is proposed, that allows the concentration and type of ions to be uniquely determined. Uncertainties due to random and systematic errors that contribute to the measured dielectric spectra and become critical in the context of low concentration aqueous solutions have been assessed. Furthermore, two methods of calculating associated uncertainties of the indicator parameters, viz. covariance matrix and Monte Carlo methods have been performed. The results show the numerical approach taken by the Monte Carlo

[1] Department of Electrical and Computer Engineering, Iowa State University, Ames, Iowa, 50011, USA
[2] Center for Nondestructive Evaluation, Iowa State University, Ames, Iowa, 50011, USA
[3] Department of Materials Science and Engineering, Iowa State University, Ames, Iowa, 50011, USA
[a] Email: amingorji68@gmail.com, nbowler@iastate.edu

method, while yielding the same estimates, reduces the tediousness associated with analytical covariance matrix method.

3.2. Introduction

In November 2014, the nitrate level in the Des Moines River, IA, USA was reported to have reached an unprecedented high [1]. The excessive concentration of nitrates is due to efflux from subsurface tile drainage systems of agricultural lands. Tile drainage is a type of drainage system that allows for removal of the excess amount of water from the soil by using a network of perforated pipes that are typically deployed about 1 m below the soil surface [2]. Transport of unwanted chemicals and ions from artificially drained agricultural land into rivers has caused explosive plant growth, leaving areas unable to support aquatic life, and creating a hypoxic zone in the Gulf of Mexico [3]. Chlorides (Cl^-), which are usually present in the form of common salt (Na^+ and Cl^-) in water, can cause serious corrosion of metals and concretes. Another potential problem caused by Cl^- dissolved in water is in boilers, where it can generate a highly corrosive hydrochloric acid upon heating [4]. The human diet is also subject to elevated chemical levels when exposed to contaminated drinking water and dietary sources. Blue Baby Syndrome, which decreases the blood's ability to transport oxygen, is one severe consequence of nitrate (NO_3^-)-laden drinking water that affects infants below the age of six months [5]. Chronic diarrhea, which is caused by the excess amount of sulphate (SO_4^{2-}) ions in water, can also be threatening to human life. Sulphate ions are also responsible for promoting the biodegradation of organic soils [6].

In order to make significant strides in developing effective conservation and management systems to limit chemical efflux from agricultural lands, it is critical to have a monitoring system that is able to accurately track chemicals' dynamics. Since the concentration of the chemicals is tightly linked to the local hydrology and changes rapidly in

time, space, and temperature, spot and send-to-lab analysis yields incomplete data. All of these issues reinforce the need for effective monitoring that can inform real-time mitigation strategies for unwanted ions in water. In recent years, great efforts have been devoted to the development of effective ion monitoring systems. Among them, the two principal approaches are ion-selective-electrode (ISE) [7] and ultraviolet (UV) absorption [8] technologies. In ISE technology, which is an electrochemical method, the particular ion of interest interacts directly with a specialized electrode membrane. As the specific ion of interest diffuses across the membrane, an electrical potential is developed between the ISE and a reference electrode. In practice, ISEs can experience serious interference from the presence of other ions because no membrane is selective to only one ion. Moreover, there is a need for low solubility of the membrane so that it does not dissolve in the sample solution, which diminishes the suitability of this approach for long continuous periods of deployment. Ultraviolet absorption technology makes use of the ability of a medium (in this case the dissolved ions) to absorb electromagnetic radiation in the UV spectral range, which are then identified according to their spectral fingerprint. This technology, however, requires highly monochromatic UV radiation which is difficult to realize in practice, leading to exorbitant installation and maintenance costs of the sensor. In summary, current ion monitoring systems do not in general meet all criteria for an effective, fast, real-time, and affordable monitoring system to operate in agriculturally relevant conditions.

Dielectric spectroscopy (DS), which monitors the response of a sample, i.e., its complex relative permittivity $\varepsilon_T(f) = \varepsilon'(f) - j\varepsilon''(f)$ to an applied time-varying electric field with frequency f, is a powerful technique for characterizing physical and chemical properties of aqueous solutions [9]. Real relative permittivity $\varepsilon'(f)$ indicates the extent to which

electrical energy is stored by the sample, while imaginary relative permittivity $\varepsilon''(f)$ indicates the extent to which electrical energy is dissipated in the sample. The dielectric properties of an aqueous solution are determined by its molecular structure which means that, by measuring the dielectric properties, we can correlate the influencing parameters including ion concentration, ion type, and temperature to the characteristics of the dielectric spectral response.

The dielectric properties of several important ions have been characterized in the last decade within the RF and microwave frequency range, in particular from 200 MHz to 89 GHz, at different temperatures. The complex relative permittivities of chloride-based aqueous solutions have been reported in [10, 11] for moderate ion concentrations of 0.05 mol/L (moles per liter) to 2 mol/L. Likewise, dielectric properties of nitrate-based aqueous solutions have been reported within the same concentration range in [12] and extended to higher concentrations up to 8.54 mol/L in [13]. Dielectric spectra of sulphate-based ions have also been studied for a moderate concentration range, from 0.05 mol/L to 3 mol/L [13, 14]. The existing studies of dielectric properties of aqueous solutions, however, have been limited by the lack of available data in the literature for very low, agriculturally-relevant concentration levels. For several important ions including sodium chloride (NaCl), sodium nitrate ($NaNO_3$), and sodium sulphate (Na_2SO_4) which are found in excess in agricultural tile drainage waters [15], the dielectric spectroscopy data do not span the relevant concentration levels which are on the order of millimoles per liter (mmol/L). Furthermore, many of the existing data are subject to large uncertainties. This becomes even more problematic by knowing the fact that the data obtained for low concentration levels are more susceptible to random and systematic errors. An increasing need for dielectric data at low concentration

also arises from the necessity for effective, fast, real-time, and affordable ion monitoring system. To the authors' knowledge, no prior investigation has attempted the inverse problem of exploiting the dielectric spectral features to estimate the ion-specific concentration of aqueous solutions.

The first objective of this research is, therefore, to characterize the dielectric properties of rarely-studied agriculturally-relevant low concentration aqueous solutions of NaCl, $NaNO_3$, and Na_2SO_4 in a well-controlled laboratory experiment. In Section 3.3, the details of the improved experimental setup to perform broadband dielectric spectroscopy over the frequency range 200 MHz to 20 GHz and controlled temperature at 25 ± 0.01 °C are presented. Methods of extracting meaningful indicators from the dielectric spectra through fitting procedures are explained in Section 3.4. In Section 3.5, a careful assessment of uncertainty which, to the knowledge of authors, has not been previously applied in the context of dielectric spectroscopy of aqueous solutions in this frequency range is performed. The compilation of uncertainty components that contribute to the measured ε' and ε'' values, along with the analysis to calculate the associated uncertainties of the indicator parameters based on covariance matrix and Monte Carlo methods, are also presented. In Section 3.6, a method of identifying an ion and its concentration based on extracted indicators from the dielectric spectra is proposed. The following work indeed lays a foundation upon which a prototype real-time monitoring system can be built to target the most effective indicators. The chapter is drawn to conclusion in Section 3.7.

3.3. Experimental Setup

The experimental setup developed to measure the dielectric spectra of aqueous solutions is shown in Figure 3.1. Dielectric experiments were performed using a Speag open-ended coaxial DAK3.5 Dielectric Probe Kit (200 MHz to 20 GHz recommended bandwidth)

and Anritsu 37347C Vector Network Analyzer (VNA) (40 MHz to 20 GHz nominal bandwidth). Open-ended coaxial probes are fairly broadband and are well suited for measuring properties of semi-liquid and liquid materials that allow perfect contact with the face of the sensor without any air gaps [16]. The optimal probe size and sensitivity of the sensor is related to the frequency range and the complex permittivity of the sample. As shown in Figure 3.1, the probe was mounted on a rigid stand and tilted at an angle of about 30° to the vertical for these measurements. After calibration, described below, disturbance of the probe and cable connecting it to the VNA was avoided by moving the sample beaker to encompass the probe instead of moving the probe and cable. The DAK software was used to calculate the relative permittivity, i.e., ε' and ε'' of the sample from the complex reflection coefficient (S_{11}) measured at the interface between the immersed coaxial probe and the liquid sample (the calibration reference plane).

A one-port calibration using three standards each having different but known complex reflection coefficient was conducted prior to measurement. This technique, which is based on bilinear transform corrections [17], is the most common and reliable method used for calibrating VNAs for open-ended coaxial probe measurements. The reference plane for the calibration of open-ended coaxial probes is normally defined to be at the face of the sensor. In this work, the system was calibrated using three standards: a shorting block, air (open-circuited), and a reference liquid which was, in this case, deionized water at 25 °C. For measuring electrolyte solutions in which water is the solvent, calibration with deionized water often gives the lowest uncertainties [16]. Another, different, reference liquid should be used for checking the calibration uncertainty. As reported in [18, 19], mercury (liquid phase metal) was alternatively used as a short circuit standard to improve the overall performance

and reproducibility of their measurements. Due to possible risks and health effects of exposure to mercury vapor, however, it is commonly not recommended as a calibration standard. For each sample, the frequency was swept and recorded ten times at 100 frequency points between 200 MHz and 20 GHz with equal logarithmic frequency steps. Instead of obtaining the conductivity κ as an adjustable parameter in the fitting procedure, it was measured separately using a Seven2Go^{TM} Conductivity meter with InLab720 probe (operating range 0.1 to 500 μS/cm ± 0.5 %), to reduce uncertainty in obtaining corresponding dielectric parameters by spectral fitting (discussed in Section 3.4). The conductivity probe was calibrated using a Mettler Toledo 84 μS/cm standard potassium chloride solution at 25 °C.

The sample beaker was placed in a temperature-controlled Anova R10 Refrigerated and Heating Circulator (± 0.01 °C) and the temperature held at 25 ± 0.01 °C during this experiment. Dowtherm SR-1 Ethylene Glycol oil (18.1 Vol. %) was used as the bath fluid in order to minimize the influence of ambient temperature fluctuations. It was observed that the temperature variation throughout the sample can significantly increase the uncertainty associated with the measured dielectric spectra, potentially masking concentration- or ion-dependent responses particularly when the ion concentration is very low. To mitigate against the uncertainty generated by temperature variability, an electric stirrer was immersed in the sample beaker and the sample liquid stirred continuously but gently, avoiding turbulence, promote a uniform temperature throughout the sample.

Three sets of environmentally-relevant electrolyte solutions were prepared and 14 concentrations c of each (including de-ionized water as zero concentration) were tested: (i) sodium chloride (NaCl) solutions with concentration ranging from c = 0 to 11.26 mmol/L,

(ii) sodium nitrate ($NaNO_3$) solutions with c = 0 to 17.83 mmol/L, and (iii) sodium sulphate (Na_2SO_4) solutions with c = 0 to 12.45 mmol/L. Measurements were made on samples of increasing concentration, by successive titration of a pre-calculated volume of each stock electrolyte into a specified volume of deionized water. At each titration step, uncertainty ± 0.05 ml in volume was introduced.

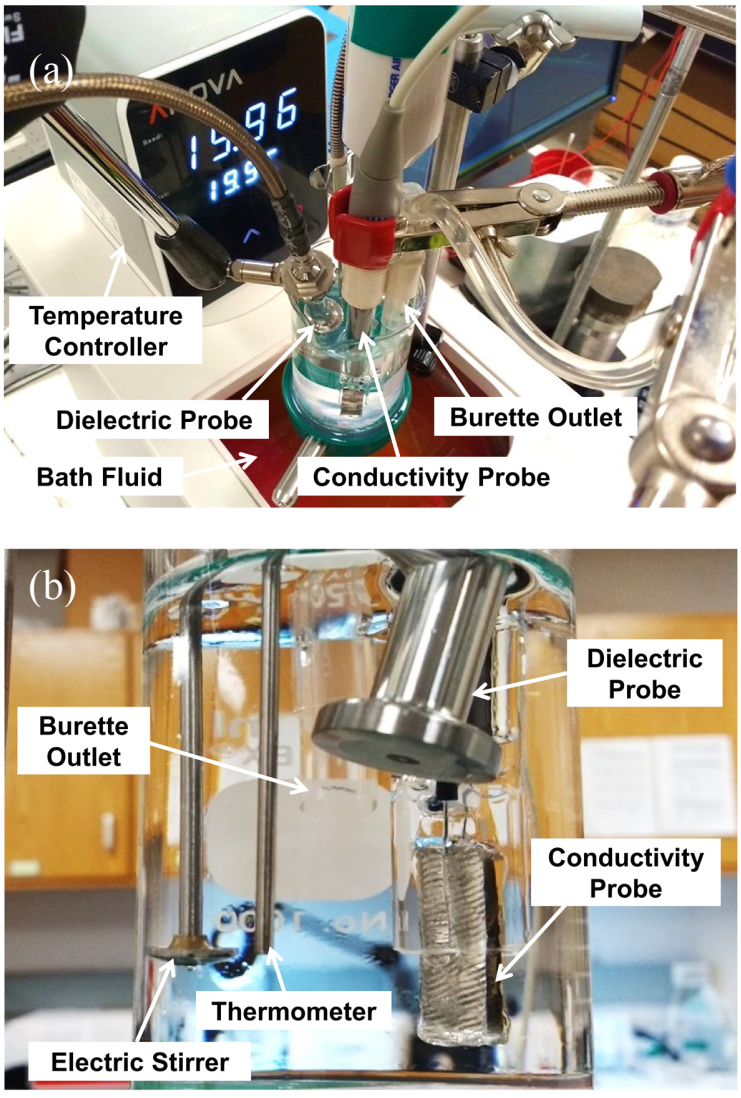

Figure 3.1 Experimental setup for measuring the dielectric spectrum and conductivity of an aqueous ionic solution at controlled temperature. The vector network analyzer is not shown in the picture.

3.4. Fitting Procedure

Assuming that each individual measured pair of (x_i, y_i) $i = 1, 2, \ldots, n$, where n is the total number of data points, is drawn from a normal (Gaussian) distribution with mean (actual value) $\hat{y}(x_i)$ and standard deviation σ_i, the probability distribution P for establishing the observed set of measurements of the n values of y_i about the actual value $\hat{y}(x_i)$ is the product of the probability distribution for each observation [20]:

$$P = \prod_{i=1}^{n} \left(\frac{1}{\sigma_i \sqrt{2\pi}} \right) \exp\left\{ -\frac{1}{2} \sum_{i=1}^{n} \left[\frac{y_i - \hat{y}(x_i)}{\sigma_i} \right]^2 \right\} \tag{3.1}$$

Maximizing the probability P is equivalent to minimizing the sum in the exponential term in (3.1). This sum, which is also known as the least-squares fitting function or the weighted sum of squares χ^2, can be defined

$$\chi^2 = \sum_{i=1}^{n} \frac{1}{\sigma_i^2} \left[y_i - \hat{y}(x_i) \right]^2 \tag{3.2}$$

In measuring dielectric spectra of aqueous solutions, the measured pair values of (f, ε_T) where f is the frequency of measurement and ε_T is the total complex relative permittivity can be obtained by combining the measured frequency-dependent polarization $\varepsilon'(f)$ and energy dissipation $\varepsilon''(f)$ parameters. The total complex relative permittivity ε_T which is composed of real and imaginary components can be written as:

$$\begin{aligned} \varepsilon_T(f) &= \varepsilon'(f) - j\varepsilon''(f) \\ &= \varepsilon'(f) - j\left[\varepsilon_d''(f) + \frac{\kappa}{2\pi\varepsilon_0 f} \right] \end{aligned} \tag{3.3}$$

where $j = \sqrt{-1}$ and the energy dissipation component $\varepsilon''(f)$ is composed of dipolar loss $\varepsilon_d''(f)$ and specific conductivity κ (dc conductivity) terms. The fitting of dielectric spectra requires care especially, in this study, for samples with low concentration for which the dielectric

spectra differ only slightly from that of deionized water. By subtracting the specific conductivity contribution from $\varepsilon''(f)$ to take into account the dipolar loss $\varepsilon_d''(f)$ only, and within the frequency range under consideration, the corrected complex relative permittivity $\varepsilon_c(f) = \varepsilon'(f) - j\varepsilon_d''(f)$ can be approximated by single-term Debye relaxation model $\hat{\varepsilon}(f)$ as

$$\begin{aligned} \hat{\varepsilon}(f) &= \hat{\varepsilon}'(f) - j\hat{\varepsilon}''(f) \\ &= \varepsilon_\infty + \frac{\varepsilon_{dc} - \varepsilon_\infty}{1 + j2\pi f\tau} \end{aligned} \tag{3.4}$$

where ε_{dc} is the static permittivity, ε_∞ is the permittivity at a frequency well above that of the relaxation frequency f_r, and $\tau = 1/(2\pi f_r)$ is the relaxation time. To obtain the best fit to the measured data we need to find values of ε_{dc}, ε_∞, and τ that minimize (3.2). By incorporating (3.3) and (3.4) into (3.2), the weighted sum of squares can be formulated as:

$$\chi^2 = \sum_{i=1}^{n} \left(\left\{ \frac{1}{\sigma_i'^2} \left[\varepsilon'(f_i) - \hat{\varepsilon}'(f_i, \varepsilon_{dc}, \varepsilon_\infty, \tau) \right] \right\}^2 + \left\{ \frac{1}{\sigma_i''^2} \left[\varepsilon_d''(f_i) - \hat{\varepsilon}''(f_i, \varepsilon_{dc}, \varepsilon_\infty, \tau) \right] \right\}^2 \right) \tag{3.5}$$

where σ_i' and σ_i'' are the standard deviations of ten recorded spectra of ε' and ε_d'', respectively. Because analytic methods of least-squares fitting cannot be used for nonlinear problems, it is necessary to search the parameter space in the following way. A simultaneous, non-linear, weighted, unconstrained, least-squares analysis to minimize the residuals χ^2 based on Levenberg-Marquardt searching algorithm [21] was performed. The Levenberg-Marquardt algorithm is a combination of a gradient search, which uses the slope "*steepest descent*" of the function to rapidly approach the minimum from far away, and the method of linearly approximating the fitting function as the search converges near the minimum leading to increased accuracy. The Levenberg-Marquardt algorithm, therefore, guarantees finding the minimum most directly and efficiently.

3.5. Uncertainty Analysis

3.5.1. Compilation of Uncertainty Elements

The measurement uncertainty [22, 23], which may limit the precision and accuracy of the measurement result, derives from random fluctuations of replicate measurements and from systematic errors that influence each result in a similar way. Careful assessment of the measurement uncertainties is necessary for reliable interpretation of measurement data in general and is particularly important in this case concerning the dielectric properties of electrolyte solutions at low concentrations. Instrument uncertainty of between 1 and 3 % in ε' and between 2 and 4 % in ε'' is common at frequencies below 100 GHz and may easily reach ~10 % for both quantities in the THz region [9]. The ability to resolve the variations in ε' and ε'' that arise for small changes in concentration is governed by the requirement that they must exceed the experimental uncertainties for ε' and ε'', i.e., $u'(f_i)$ and $u''(f_i)$, respectively, where f_i is the frequency of measurement. In addition, as the number of parameters in the fitting equation increases (which is equivalent to reducing the degrees of freedom = $n - m$ where n is the number of data points and m is the number of fitting parameters) the associated uncertainty for each fitting parameter increases [24]. In this work, the latter difficulty is mitigated by measuring the d.c. conductivity κ independently using a high-precision instrument, and then subtracting that contribution $\kappa/2\pi f$ from the experimentally accessible $\varepsilon''(f)$, to obtain $\varepsilon''_d(f)$. By fitting $\varepsilon''_d(f)$ rather than $\varepsilon''(f)$, the number of fitting parameters is reduced and hence the associated uncertainty for each fitting parameter is decreased.

In this work, the combined standard uncertainties $u'_c(f_i)$ and $u''_c(f_i)$ of the measured dielectric spectra were calculated in accordance with established NIST [25] and GUM [26]

guidelines. The extent of random errors that, in this work, are mainly due to VNA noise, temperature fluctuations, thermoelectric effects, and electromagnetic interference, can be calculated from repeated measurements. Systematic errors due to non-ideal probe dimensions, imperfect instrument (VNA) calibration, calibration of the probe (short-air-load method), and cable phase instability can be estimated from the deviation of values measured on a reference material [27] from *a priori* known values measured independently on the same material. A reference standard is defined as a material with well-characterized properties. Since, in this work, deionized water is used as a calibration standard, it cannot be employed as a reference material for the purpose of calculating the systematic errors in the measurement system. Instead, methanol is used as a reference standard in this work. Random errors and systematic errors are combined to calculate the total uncertainty in the measurement of the dielectric properties.

The budget for the calculation of measurement uncertainties in this work is shown in Table 3.1. The individual standard uncertainties include contributions from the sources described in following sections.

3.5.1.1. Random errors

Random errors are obtained from 10 recorded spectra of repeated measurements on the test sample and are conducted under strict temperature control at 25.00 ± 0.01 °C. At each measurement frequency, the mean value of $\varepsilon'(f_i)$ and $\varepsilon''(f_i)$ and the corresponding standard deviations $\sigma_{\varepsilon'}(f_i)$ and $\sigma_{\varepsilon''}(f_i)$ were calculated in order to be used in the fitting procedure, (3.5). The standard deviation of the mean (SDM), $\sigma_{\varepsilon'}(f_i)/\sqrt{N}$ and $\sigma_{\varepsilon''}(f_i)/\sqrt{N}$, where N is the number of recorded spectra, were calculated at each frequency. The relative (%) SDM values with respect to mean $\varepsilon'(f_i)$ and $\varepsilon''(f_i)$ were calculated as relative uncertainty

components $a'_{rand}(f_i)$ and $a''_{rand}(f_i)$. As random errors are best described by a normal (Gaussian) distribution, the relative standard uncertainties $u'_{rand}(f_i)$ and $u''_{rand}(f_i)$ can be calculated by dividing the relative uncertainty components $a'_{rand}(f_i)$ and $a''_{rand}(f_i)$ by factor 1.

3.5.1.2. Systematic errors

Systematic errors are obtained through comparison of the measured and reference data for methanol CH_3OH at 25 °C. A hybrid set of reference methanol data was created by combining the permittivity data reported by NPL [28] for frequency range 200 MHz to 10 GHz with that presented by Sato *et al*. [29] for higher frequencies from 10 GHz up to 20 GHz, at 25 °C. The former data set captures the first relaxation of methanol, which occurs at 3 GHz, and the latter covers the second relaxation which occurs at around 20 GHz. The single-term and double-term Debye model parameters for the methanol reference data are listed in Table 3.2. Comparing the relaxation parameters of the hybrid model with those obtained in this work shows that the main discrepancy lies around the frequency range of the second relaxation process (denoted by II). That frequency range contributes more to the systematic errors, therefore. Moreover, the observed differences in relaxation parameters can be attributed to limited data at frequencies well above the second relaxation frequency (~ 22 GHz), which causes inadequacy of information in fitting ε_∞. Treating the systematic error to be relative [30], the recovery components $R'(f_i)$ and $R''(f_i)$ at each frequency can be calculated as

$$R'(f_i) = \frac{\varepsilon'_{meth}(f_i)}{\varepsilon'_{ref}(f_i)}$$
$$R''(f_i) = \frac{\varepsilon''_{meth}(f_i)}{\varepsilon''_{ref}(f_i)} \quad (3.6)$$

where $\varepsilon'_{meth}(f_i)$ and $\varepsilon''_{meth}(f_i)$ are the mean values of measured methanol data, and $\varepsilon'_{ref}(f_i)$ and $\varepsilon''_{ref}(f_i)$ are the reference hybrid methanol data with parameters listed in Table 3.2. Note that, the bias term approach holds if the systematic error is assumed to be absolute [31]. In this work, the individual permittivity results are not corrected for the recognized significant recovery. Correction may be unsafe to apply as it fundamentally changes the original permittivity values obtained from direct measurements. As the extracted fitting parameters, which are of great interest, depend on the permittivity values in the whole frequency range, unnecessary correction of permittivity values at each frequency may have an effect on the final extracted fitting parameters and thus hinder the possibility to track any potential trends in data with respect to changes in concentration. It accordingly becomes important to consider how uncorrected permittivity results can be treated in terms of uncertainty estimation. The best practice, which has been widely discussed in the literature [31, 32], is to enlarge the uncertainty intervals via recovery terms to account for known or suspected systematic errors. The enlarged combined standard uncertainty will be formulated later in this section.

The uncertainties associated with the recovery terms at each measured frequency, $u_{R'}(f_i)$ and $u_{R''}(f_i)$ are estimated through the law of propagation of uncertainty [26] performed on (3.6) as

$$\begin{aligned} u_{R'}(f_i) &= R'(f_i)\sqrt{u'_{meth}(f_i)^2 + u'_{ref}(f_i)^2} \\ u_{R''}(f_i) &= R''(f_i)\sqrt{u''_{meth}(f_i)^2 + u''_{ref}(f_i)^2} \end{aligned} \tag{3.7}$$

where $u'_{meth}(f_i)$ and $u''_{meth}(f_i)$ are the relative standard uncertainties of measured methanol data, and $u'_{ref}(f_i)$ and $u''_{ref}(f_i)$ are the relative standard uncertainties associated with the

reference hybrid methanol data. The $u'_{meth}(f_i)$ and $u''_{meth}(f_i)$ were calculated as relative SDM of 10 recorded methanol data with respect to $\varepsilon'_{meth}(f_i)$ and $\varepsilon''_{meth}(f_i)$, respectively.

3.5.1.3. Reference data uncertainty

Uncertainties of the reference data $u'_{ref}(f_i)$ and $u''_{ref}(f_i)$ should be considered. These uncertainty values can be found in the literature where the data are taken. The relative uncertainty components associated with reference methanol data $a'_{BF}(f_i)$ and $a''_{BF}(f_i)$, obtained by NPL at 25 °C, corresponding to uncertainties of "Best-fit" (BF) [28] values of ε' and ε'' that include contributions of NPL's random and systematic errors. The corresponding BF relative standard uncertainties $u'_{BF}(f_i)$ and $u''_{BF}(f_i)$ can be calculated by dividing the relative uncertainty components by factor 1 under the normal distribution. The BF uncertainty values do not, however, include uncertainty contributions associated with the temperature measurements [28]. As reported by NPL guidelines, the standard uncertainty associated with the temperature measurement of the reference data is ± 0.05 °C. By combining the temperature uncertainty of our work, i.e., 0.01 °C (Section 3.3) with that of NPL to get $u(T)$ = $\sqrt{(0.05^2 + 0.01^2)}$, and through the law of propagation of uncertainty, one can evaluate the relative standard uncertainties $u'_T(f_i)$ and $u''_T(f_i)$ associated with overall temperature contribution, as in (3.8)

$$u'_T(f_i) = \frac{\frac{\partial \varepsilon'_{ref}(f_i)}{\partial T} u(T)}{\varepsilon'_{ref}(f_i)}$$
$$u''_T(f_i) = \frac{\frac{\partial \varepsilon''_{ref}(f_i)}{\partial T} u(T)}{\varepsilon''_{ref}(f_i)} \qquad (3.8)$$

where the partial derivatives are calculated numerically between the BF permittivity values of two nearest temperatures which are available in NPL guidelines. For the reference data

presented by Sato *et al*., however, no uncertainty values were reported. The overall relative standard uncertainties associated with reference methanol data $u'_{\text{ref}}(f_i)$ and $u''_{\text{ref}}(f_i)$ can be calculated as (3.9) by combining the relative standard uncertainties of BF and temperature measurement:

$$u'_{\text{ref}}(f_i) = \sqrt{u'_{BF}(f_i)^2 + u'_T(f_i)^2}$$
$$u''_{\text{ref}}(f_i) = \sqrt{u''_{BF}(f_i)^2 + u''_T(f_i)^2} \tag{3.9}$$

The uncertainties of reference data (3.9) are used to calculate the uncertainties of recovery terms (3.7), which are incorporated in calculating the overall uncertainties discussed next.

3.5.1.4. Combined standards uncertainties

As mentioned earlier, the combined standard uncertainties should be enlarged to account for possible systematic errors. The combined relative standard uncertainties $u'_c(f_i)$ and $u''_c(f_i)$ can be calculated as the root sum of squares (RSSu) of individual relative standard uncertainties and the recovery term [31] as

$$u'_c(f_i) = \sqrt{u'_{\text{rand}}(f_i)^2 + \left[R'(f_i) - 1\right]^2 + u_{R'}(f_i)^2}$$
$$u''_c(f_i) = \sqrt{u''_{\text{rand}}(f_i)^2 + \left[R''(f_i) - 1\right]^2 + u_{R''}(f_i)^2} \tag{3.10}$$

where the recovery terms $R'(f_i)$ and $R''(f_i)$, and the corresponding recovery uncertainty terms $u_{R'}(f_i)$ and $u_{R''}(f_i)$, can be calculated through (3.6)-(3.9). The standard uncertainties provide a level of confidence of approximately 68 %.

By way of demonstration of this uncertainty analysis as applied in this work, each contribution of individual relative standard uncertainty is plotted in Figure 3.2 for a sample 7.139 mmol/L sodium nitrate ($NaNO_3$) solution. As can be seen, the systematic error

Table 3.1 Compilation of relative standard uncertainties over the frequency range 200 MHz to 20 GHz for measuring the permittivity of aqueous ionic solutions. The nomenclature and methodology are taken from NIST [25] and GUM [26]. Type A evaluation of uncertainty is based on statistical analysis of a series of observations whereas Type B evaluation of uncertainty relies upon scientific assessment of information other than Type A. Each source of uncertainty is composed of a real and an imaginary part.

Source of uncertainty	Type of uncertainty	Probability distribution	Standard uncertainty (%)
Repeatability (test sample) [a]	A	Normal	$u_{\text{rand}}(f_i)$
Recovery (deviation from reference data) [b]	-	-	$R(f_i)$-1
Repeatability (reference sample) [a]	A	Normal	$u_{\text{meth}}(f_i)$
Uncertainty of reference data (*Best-fit* values) [c, d]	B	Normal	$u_{BF}(f_i)$
Uncertainty of reference data (Temperature) [d, e]	B	Propagation	$u_T(f_i)$
Combined standard uncertainty [f]	$u_c(f_i) = [u_{\text{rand}}(f_i)^2 + (R(f_i)\text{-}1)^2 + u_R(f_i)^2]^{1/2}$		

[a] Standard deviation of the mean (SDM) calculated from 10 recorded spectra.
[b] A hybrid methanol data created from Gregory *et al*. [28] and Sato *et al*. [29].
[c] Gregory *et al*. [28]: uncertainties of best-fit permittivity values which are provided only up to 5 GHz.
[d] Sato *et al*. [29]: no associated uncertainty was reported.
[e] Temperature uncertainty: ± 0.05 °C Gregory *et al*. [28] and ± 0.01 °C this work.
[f] Refer to (3.6)-(3.9).

Table 3.2 Debye model parameters for methanol data at 25 °C, various authors.

Reference	Model	$\varepsilon_{dc}^{\text{I}}$	τ^{I}(ps)	$\varepsilon_{dc}^{\text{II}}$	τ^{II}(ps)	ε_∞
Gregory *et al*. [28] (0.05-10 GHz) [a]	Debye 1D	32.66 ± 0.03	50.670 ± 0.266	-	-	5.563 ± 0.088
Sato *et al*. [29] (0.5-25 GHz) [b]	Debye 2D	32.52	51.168	6.07	7.24	4.8
Hybrid model (0.2-20 GHz) [c]	Debye 2D	32.64	51.431	5.93	7.33	4.621
This work (0.2-20 GHz)	Debye 2D	32.34	51.168	5.84	5.11	3.985

[a] The measured frequency in their work is 0.05-5 GHz, but good accuracy is claimed up to 10 GHz [28].
[b] No associated uncertainty was reported.
[c] Created by combining permittivity data of Gregory *et al*. [28] (200 MHz to 10 GHz) and Sato *et al*. [29] (10 to 20 GHz)

represented by recovery term $|R(f_i)\text{-}1|$ provides the main contribution to the uncertainty in both real and imaginary parts, and is far larger than the random errors $u_{\text{rand}}(f_i)$.

In addition, there is a sweet spot in the frequency range between 1 and 10 GHz in which all uncertainty contributions are around or below 1 %. Increased uncertainty below 1 GHz, particularly in the imaginary part of the permittivity, can be attributed to the minimum

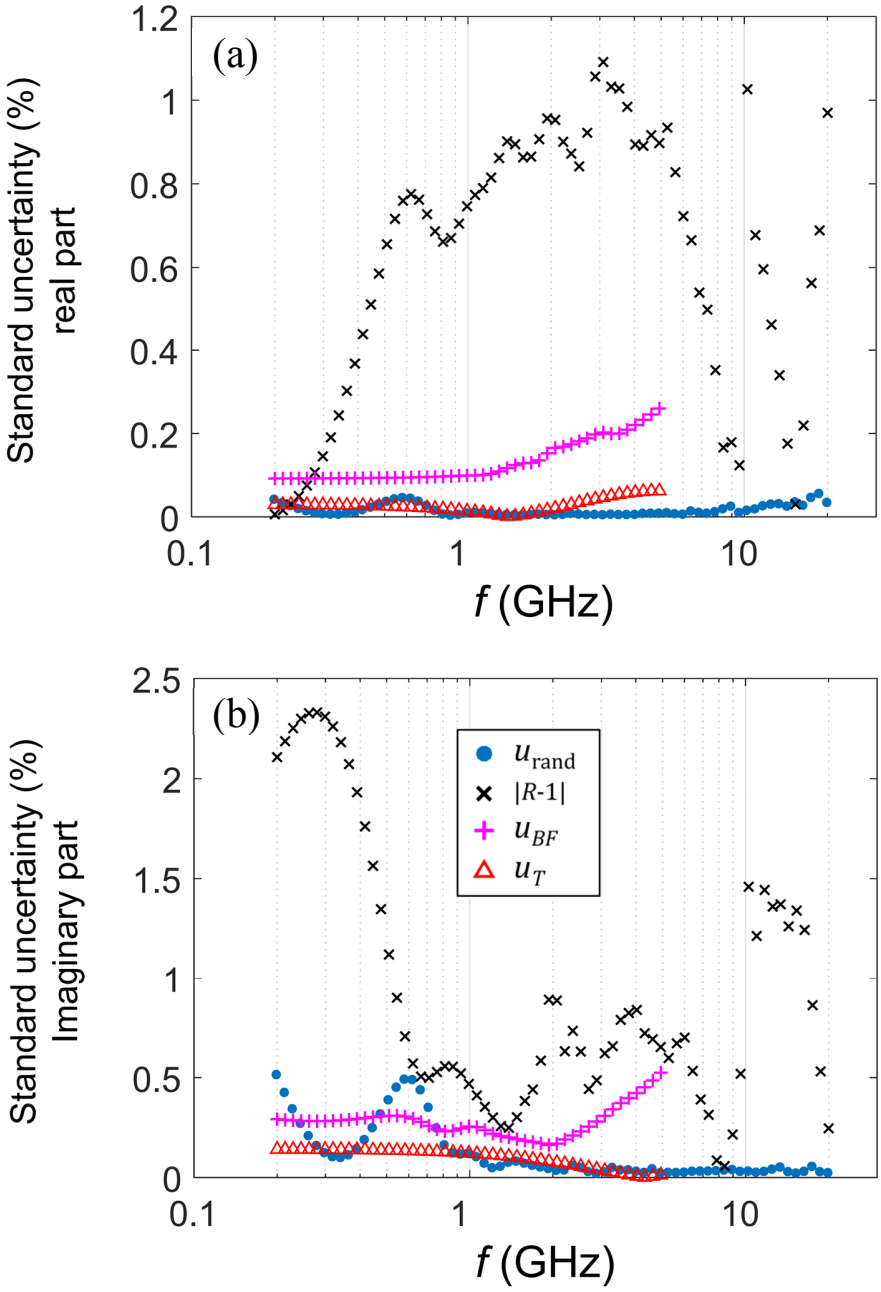

Figure 3.2 Calculated individual relative (%) standard uncertainties in permittivity measured over the frequency range 200 MHz to 20 GHz for a sample $NaNO_3$ solution with concentration c = 7.139 mmol/L at 25 °C. (a) Real, and (b) imaginary parts. Random and systematic sources of uncertainty are due to repeatability u'_{rand} (u'_{meth}) and u''_{rand} (u''_{meth}), deviation from reference data represented by recovery terms $|R'\text{-}1|$ and $|R''\text{-}1|$, uncertainty in best-fit values of reference data u'_{BF} and u''_{BF}, and temperature uncertainty of reference data u'_T and u''_T. The uncertainties of reference data are provided only up to 5 GHz; refer to Table 3.1 for further details.

recommended operating frequency of the DAK3.5 open-ended coaxial probe, i.e., 200 MHz. As the measurement frequency approaches the minimum recommended frequency, the systematic errors (which are partly related to the errors in probe dimensions) become significant.

3.5.2. Covariance Matrix Method

After finding the best fitting parameters ε_{dc}, ε_{∞}, and τ that minimize (3.5), it is necessary to obtain the uncertainties $u(\varepsilon_{dc})$, $u(\varepsilon_{\infty})$, and $u(\tau)$ associated with the fitting parameters. In general, these can be calculated by extending the propagation of uncertainties method which is a common method used in linear regression analysis [33]. As the number of terms in the fitting equation increases and particularly in the case of non-linear regression, however, the algebra becomes more tedious and the propagation method fails. Therefore, the customary method for obtaining the uncertainties of the fitting parameters for non-linear regressions involves calculating the covariance matrix $C_{m\times m}$ where m is the number of fitting parameters [34, 35], as in

$$C = (J^T J)^{-1} s^2 \tag{3.11}$$

where $J_{n\times m}$ is the Jacobian matrix, n is the total number of data points, $J^T_{m\times n}$ is the transpose matrix of J, and s^2 is the mean squared error (MSE) of the regression. The Jacobian matrix comprises the first-order partial derivatives of the fitting equation $\hat{y}(x_i, a_1, ..., a_m)$ with respect to the fitting parameters $a_1, ..., a_m$. In order to include the uncertainties associated with the measured data $u_c(x_i)$ in obtaining the uncertainties of the fitting parameters, the Jacobian matrix and the mean squared error are weighted as in (3.12) and (3.13), respectively,

$$J=\begin{pmatrix} \frac{1}{u_c(x_1)}\frac{\partial\hat{y}(x_1,a_1,\ldots,a_m)}{\partial a_1} & \cdots & \frac{1}{u_c(x_1)}\frac{\partial\hat{y}(x_1,a_1,\ldots,a_m)}{\partial a_m} \\ \vdots & \ddots & \vdots \\ \frac{1}{u_c(x_n)}\frac{\partial\hat{y}(x_n,a_1,\ldots,a_m)}{\partial a_1} & \cdots & \frac{1}{u_c(x_n)}\frac{\partial\hat{y}(x_n,a_1,\ldots,a_m)}{\partial a_m} \end{pmatrix}_{n\times m} \tag{3.12}$$

$$s^2=\frac{\sum_{i=1}^{n}\frac{1}{u_c{}^2(x_i)}\left[y(x_i)-\hat{y}(x_i,a_1,\ldots,a_m)\right]^2}{n-m} \tag{3.13}$$

where $y(x_i)$ is a set of measured data points, as already noted. Replacing $y(x_i)$ by the measured $\varepsilon'(f_i)$ and $\varepsilon''_d(f_i)$, the fitting equation $\hat{y}(x_i, a_1, ..., a_m)$ by Debye relaxation model $\hat{\varepsilon}'(f_i, \varepsilon_{dc}, \varepsilon_\infty, \tau)$ and $\hat{\varepsilon}''(f_i, \varepsilon_{dc}, \varepsilon_\infty, \tau)$, and $u_c(x_i)$ by $u'_c(f_i)$ and $u''_c(f_i)$, (3.12) and (3.13) become

$$J=\begin{pmatrix} \frac{1}{u'_c(f_1)}\frac{\partial\hat{\varepsilon}'(f_1,\varepsilon_{dc},\varepsilon_\infty,\tau)}{\partial\varepsilon_{dc}} & \frac{1}{u'_c(f_1)}\frac{\partial\hat{\varepsilon}'(f_1,\varepsilon_{dc},\varepsilon_\infty,\tau)}{\partial\varepsilon_\infty} & \frac{1}{u'_c(f_1)}\frac{\partial\hat{\varepsilon}'(f_1,\varepsilon_{dc},\varepsilon_\infty,\tau)}{\partial\tau} \\ \vdots & \vdots & \vdots \\ \frac{1}{u'_c(f_n)}\frac{\partial\hat{\varepsilon}'(f_n,\varepsilon_{dc},\varepsilon_\infty,\tau)}{\partial\varepsilon_{dc}} & \frac{1}{u'_c(f_n)}\frac{\partial\hat{\varepsilon}'(f_n,\varepsilon_{dc},\varepsilon_\infty,\tau)}{\partial\varepsilon_\infty} & \frac{1}{u'_c(f_n)}\frac{\partial\hat{\varepsilon}'(f_n,\varepsilon_{dc},\varepsilon_\infty,\tau)}{\partial\tau} \\ \frac{1}{u''_c(f_1)}\frac{\partial\hat{\varepsilon}''(f_1,\varepsilon_{dc},\varepsilon_\infty,\tau)}{\partial\varepsilon_{dc}} & \frac{1}{u''_c(f_1)}\frac{\partial\hat{\varepsilon}''(f_1,\varepsilon_{dc},\varepsilon_\infty,\tau)}{\partial\varepsilon_\infty} & \frac{1}{u''_c(f_1)}\frac{\partial\hat{\varepsilon}''(f_1,\varepsilon_{dc},\varepsilon_\infty,\tau)}{\partial\tau} \\ \vdots & \vdots & \vdots \\ \frac{1}{u''_c(f_n)}\frac{\partial\hat{\varepsilon}''(f_n,\varepsilon_{dc},\varepsilon_\infty,\tau)}{\partial\varepsilon_{dc}} & \frac{1}{u''_c(f_n)}\frac{\partial\hat{\varepsilon}''(f_n,\varepsilon_{dc},\varepsilon_\infty,\tau)}{\partial\varepsilon_\infty} & \frac{1}{u''_c(f_n)}\frac{\partial\hat{\varepsilon}''(f_n,\varepsilon_{dc},\varepsilon_\infty,\tau)}{\partial\tau} \end{pmatrix}_{2n\times 3} \tag{3.14}$$

$$s^2=\frac{\sum_{i=1}^{n}\left\{\left[\frac{1}{u'^2_c(f_i)}\left(\varepsilon'(f_i)-\hat{\varepsilon}'(f_i,\varepsilon_{dc},\varepsilon_\infty,\tau)\right)\right]^2+\left[\frac{1}{u''^2_c(f_i)}\left(\varepsilon''_d(f_i)-\hat{\varepsilon}''(f_i,\varepsilon_{dc},\varepsilon_\infty,\tau)\right)\right]^2\right\}}{2n-m} \tag{3.15}$$

where the number of rows in the Jacobian matrix is $2n$, including both the real and the imaginary parts in the calculation. In addition, the partial derivatives can be calculated numerically at each frequency through finite difference methods (FDM). By employing (3.14) and (3.15) in (3.11), the covariance matrix can then be calculated as

$$C = \begin{pmatrix} C_{11} & C_{12} & C_{13} \\ C_{21} & C_{22} & C_{23} \\ C_{31} & C_{32} & C_{33} \end{pmatrix}_{3\times 3} \tag{3.16}$$

where C_{jk} (j, k = 1, 2, 3) are the resulting matrix elements, and C_{jj} are the diagonal elements of the covariance matrix. In this work, the partial derivatives were calculated and the matrix inversion performed using available routines in Matlab ™. The expanded uncertainties associated with the fitting parameters $U(\varepsilon_{dc})$, $U(\varepsilon_{\infty})$, and $U(\tau)$ that return (1 - α)100 % confidence interval are evaluated as

$$\begin{aligned} U(\varepsilon_{dc}) &= t_{\frac{\alpha}{2},2n-m}\sqrt{C_{11}} \\ U(\varepsilon_{\infty}) &= t_{\frac{\alpha}{2},2n-m}\sqrt{C_{22}} \\ U(\tau) &= t_{\frac{\alpha}{2},2n-m}\sqrt{C_{33}} \end{aligned} \tag{3.17}$$

where $t_{\alpha/2,(2n\text{-}m)}$ is computed using the inverse of Student's t cumulative distribution function [36]. For the standard uncertainties $u(\varepsilon_{dc})$, $u(\varepsilon_{\infty})$, and $u(\tau)$ that return ~ 68 % confidence interval, $t_{0.32/(200\text{-}4)}$ = 0.996 which can be approximated to unity.

3.5.3. Monte Carlo Method

A Monte Carlo (MC) calculation [37, 38] is a statistical method of studying problems that contain a combination of many different distributions, based on the use of artificially generating random numbers. With Monte Carlo techniques, very complicated scientific and mathematical problems can be solved with neither a deep theoretical understanding of

statistical analysis nor sophisticated programming techniques [20]. In order to calculate the standard uncertainties $u(\varepsilon_{dc})$, $u(\varepsilon_{\infty})$, and $u(\tau)$ associated with the fitting parameters, the Monte Carlo modeling technique presented by Gregory *et al*. [39] has been applied. In this method, an approximation to the distribution function of each individual source of uncertainty (Table 3.1) is established numerically by making random draws from the associated probability distributions. The Monte Carlo modeling, as shown in Figure 3.3, is performed with consideration of the following factors.

3.5.3.1. Generating random errors

At each frequency, M random errors $\Delta\varepsilon'$ and $\Delta\varepsilon''$ are drawn from the probability distribution of each individual source of uncertainty. The random errors are taken from the corresponding populations with zero mean ($\mu = 0$) and variances (σ) equal to relative standard uncertainties listed in Table 3.1, in order to generate $\Delta\varepsilon_i'$ and $\Delta\varepsilon_i''$ (i = 1,…,5) at each draw. These values are also generated independently at every measured frequency to simulate random noise [39].

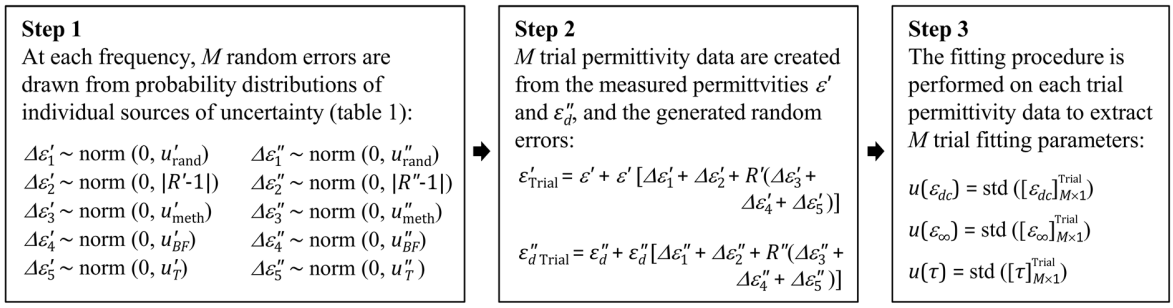

Figure 3.3 The procedure followed for computing each trial permittivity data set for evaluation of the standard uncertainties associated with the Debye fitting parameters, (3.4). In the Monte Carlo modeling in this work, 10^4 trials are generated. The relative standard uncertainties and recovery (Table 3.1) can be best described by a normal (Gaussian) distribution, norm(μ,σ), where μ is the mean and σ is the variance of the population. The standard deviation of a set of samples is denoted 'std'.

3.5.3.2. Generating trial permittivity data

The MC modeling requires a large number of trial data to be constructed which are representative of the expected statistical variations of the measured data. Therefore, 10^4 trial permittivity data sets (M =10^4) are created by superposing the generated random errors to the measured permittivity data ε' and ε''_d at each frequency point to obtain trial permittivity data, $\varepsilon'_{\text{Trial}}$ and $\varepsilon''_{d\ \text{Trial}}$. The residual discrepancies between each trial permittivity data and the measured data are plotted in Figure 3.4.

3.5.3.3. Generating trial fitting parameters

The Debye fitting procedure, according to (3.5), is performed on each trial permittivity data set to extract the trial fitting parameters, i.e., $[\varepsilon_{dc}]_{M\times1}$, $[\varepsilon_{\infty}]_{M\times1}$, and $[\tau]_{M\times1}$. The standard deviations of 10^4 trial fitting parameters are taken to be their associated standard uncertainties, $u(\varepsilon_{dc})$, $u(\varepsilon_{\infty})$, and $u(\tau)$. The reported uncertainty is based on a standard uncertainty multiplied by a coverage factor k = 1, providing a level of confidence of approximately 68 %.

3.5.4. Results

The extracted Debye relaxation parameters along with the associated uncertainties and the mean squared error (s^2) for each of NaCl, $NaNO_3$, and Na_2SO_4 aqueous solutions at T = 25 °C are listed in Tables 3.3 to 3.5. The specific conductivity κ, as mentioned in Section 3.3, was measured directly using a conductivity meter. There were, however, concentrations where κ was higher than the operating range of the conductivity meter, i.e., greater than 500 µS/cm. In such cases, the specific conductivity κ was treated as an additional fitting parameter, meaning that the sum of a single-term Debye relaxation model and a conductivity

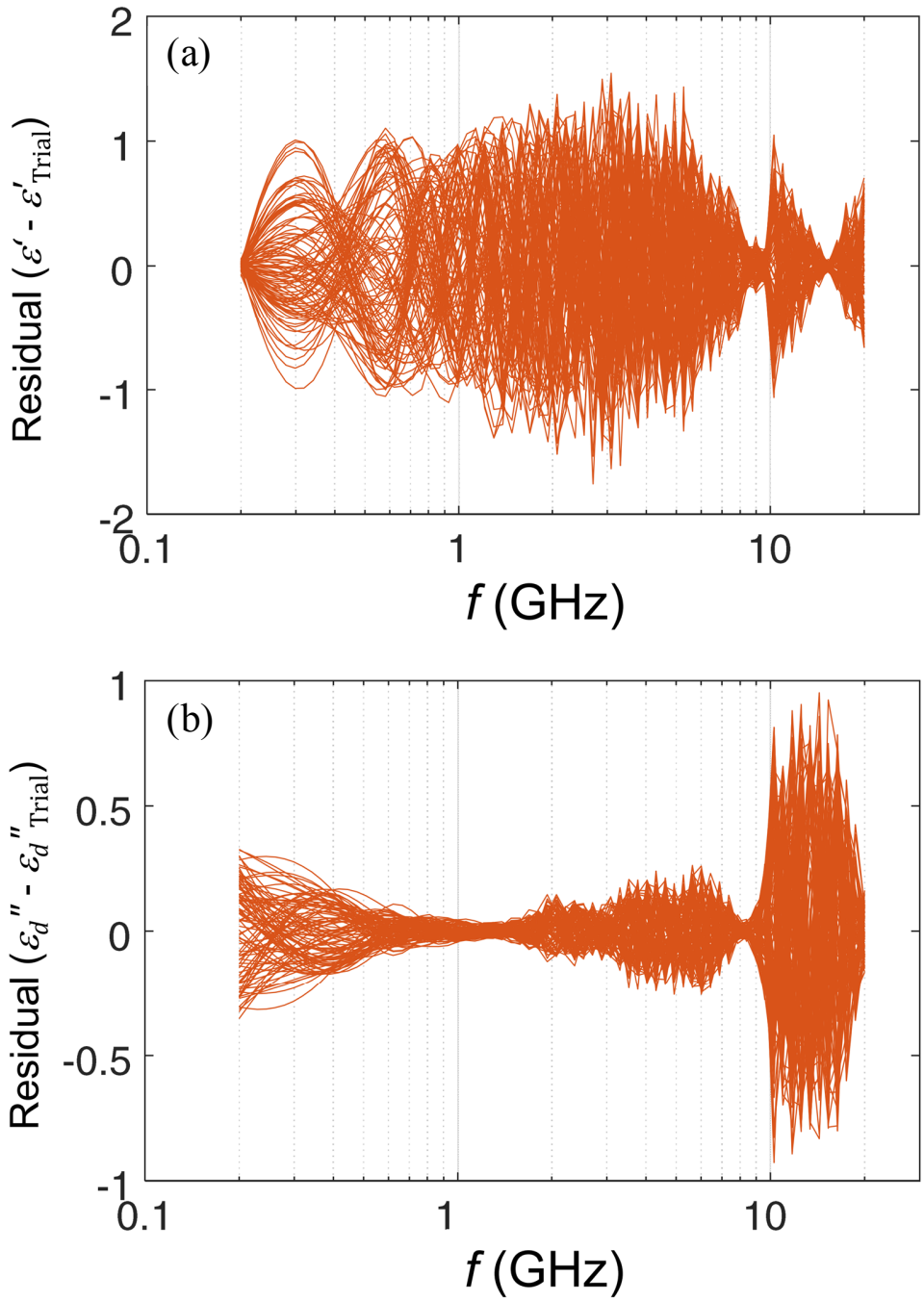

Figure 3.4 Residual discrepancies between Monte Carlo trial permittivity data and measured permittivity data (a) real part ($\varepsilon' - \varepsilon'_{\text{Trial}}$) (b) imaginary part ($\varepsilon''_d - \varepsilon''_{d\,\text{Trial}}$), over the measured frequency range 200 MHz to 20 GHz for a sample $NaNO_3$ solution with c = 7.139 mmol/L at 25 °C. For clarity, only 100 trials are plotted in this figure.

contribution ($\kappa/2\pi\varepsilon_0 f$) was used to analytically represent the measured permittivity spectrum, i.e., (3.3).

According to Tables 3.3 to 3.5, good agreement between the uncertainty values of the fitting parameters evaluated through the covariance matrix method and the Monte Carlo method is obtained. In general, the uncertainty values evaluated through the Monte Carlo method are slightly larger than those evaluated through the covariance matrix method. This is likely due to the approximation nature of the Monte Carlo method, which takes advantage of artificially generating random numbers to construct the population of individual sources of uncertainty and eliminates the need to perform analytical calculations as required by the covariance matrix method. It is also worth mentioning that the uncertainty values calculated through the covariance matrix method slightly increase with concentration. According to (3.11), there is a direct proportion between the covariance matrix $C_{m\times m}$ and the MSE (s^2). As the MSE increases with concentration, likewise, the covariance matrix becomes larger and the corresponding uncertainty elements associated with the fitting parameters increase.

The fitting parameters presented in Tables 3.3 to 3.5 provide a set of benchmark data for environmentally-relevant aqueous solutions of NaCl, $NaNO_3$, and Na_2SO_4 at 25 °C. The fitted model is a single-term Debye relaxation function and provides the corresponding static permittivity ε_{dc}, infinite-frequency permittivity ε_∞, relaxation time τ, and specific conductivity κ. In the next section, a method of identifying an ion and its concentration based on indicators extracted from the permittivity spectra is discussed.

Table 3.3 Parameters of the single-term Debye model (ε_{dc}, τ, and ε_∞), the associated standard uncertainties ($u(\varepsilon_{dc})$, $u(\tau)$, and $u(\varepsilon_\infty)$) calculated from Monte Carlo and covariance matrix methods, and mean squared error (s^2) of aqueous NaCl solutions at T = 25 °C. The standard uncertainties provide a level of confidence of approximately 68 %. The specific conductivity was measured independently up to 500 µS/cm with ± 0.5 % instrument uncertainty. For concentrations corresponding to specific conductivity greater than 500 µS/cm, κ was treated as an additional fitting parameter, and the covariance matrix and Monte Carlo methods give similar uncertainty values within reported significant figures.

c (mmol/L)	κ (µS/cm)	ε_{dc}	$u(\varepsilon_{dc})$		τ (ps)	$u(\tau)$		ε_∞	$u(\varepsilon_\infty)$		s^2
			Monte Carlo	covar. matrix		Monte Carlo	covar. matrix		Monte Carlo	covar. matrix	
0	8.184 ± 0.040	78.362	0.078	0.073	8.275	0.047	0.044	5.237	0.16	0.093	0.002
0.294 ± 0.016	35.13 ± 0.18	78.380	0.080	0.073	8.260	0.047	0.044	5.066	0.17	0.093	0.002
0.585 ± 0.024	69.91 ± 0.35	78.403	0.078	0.073	8.254	0.047	0.044	4.868	0.16	0.096	0.004
0.873 ± 0.029	105.44 ± 0.52	78.421	0.078	0.075	8.192	0.046	0.044	4.255	0.15	0.11	0.016
1.159 ± 0.033	138.18 ± 0.70	78.459	0.080	0.077	8.175	0.047	0.045	3.998	0.16	0.14	0.041
1.722 ± 0.040	207.8 ± 1.0	78.444	0.078	0.076	8.181	0.046	0.045	3.996	0.16	0.13	0.044
2.276 ± 0.045	273.1 ± 1.4	78.415	0.079	0.076	8.172	0.046	0.045	3.894	0.16	0.13	0.047
2.820 ± 0.049	345.1 ± 1.7	78.387	0.079	0.078	8.126	0.046	0.045	3.527	0.16	0.14	0.049
4.244 ± 0.049	517.0 ± 7.6	78.373	0.079	0.078	8.129	0.046	0.046	3.462	0.16	0.15	0.065
5.653 ± 0.049	675.5 ± 8.4	78.357	0.078	0.079	8.081	0.045	0.046	3.067	0.15	0.16	0.075
7.045 ± 0.049	838.2 ± 9.1	78.355	0.078	0.081	8.104	0.046	0.047	3.092	0.15	0.18	0.120
8.462 ± 0.048	977.0 ± 9.4	78.340	0.078	0.083	8.080	0.046	0.048	2.849	0.15	0.20	0.131
9.853 ± 0.047	1167 ± 10	78.316	0.081	0.089	8.061	0.046	0.050	2.693	0.17	0.24	0.153
11.259 ± 0.047	1297 ± 10	78.266	0.078	0.083	8.058	0.045	0.048	2.658	0.15	0.21	0.144

Table 3.4 As for Table 3.3 but for aqueous $NaNO_3$ solutions.

c (mmol/L)	κ (µS/cm)	ε_{dc}	$u(\varepsilon_{dc})$		τ (ps)	$u(\tau)$		ε_∞	$u(\varepsilon_\infty)$		s^2
			Monte Carlo	covar. matrix		Monte Carlo	covar. matrix		Monte Carlo	covar. matrix	
0	8.331 ± 0.042	78.363	0.079	0.073	8.268	0.047	0.044	5.187	0.17	0.095	0.001
0.743 ± 0.043	84.77 ± 0.42	78.352	0.077	0.073	8.258	0.046	0.044	5.096	0.15	0.093	0.002
1.479 ± 0.060	168.50 ± 0.84	78.344	0.076	0.073	8.242	0.046	0.044	4.962	0.15	0.090	0.003
2.209 ± 0.073	250.5± 1.3	78.341	0.078	0.073	8.235	0.047	0.044	4.873	0.16	0.090	0.005
2.932 ± 0.083	333.3 ± 1.7	78.325	0.076	0.073	8.226	0.046	0.044	4.732	0.15	0.087	0.005
3.649 ± 0.092	414.6 ± 2.1	78.310	0.077	0.073	8.209	0.046	0.044	4.605	0.15	0.089	0.006
4.36 ± 0.10	491.2 ± 2.5	78.292	0.078	0.073	8.213	0.047	0.044	4.659	0.16	0.089	0.007
5.06 ± 0.11	566.9 ± 8.0	78.289	0.078	0.073	8.196	0.046	0.044	4.480	0.16	0.094	0.011
5.76 ± 0.11	648.0 ± 8.1	78.275	0.078	0.073	8.188	0.046	0.044	4.386	0.16	0.098	0.014
6.45 ± 0.12	728.8 ± 8.7	78.263	0.079	0.074	8.177	0.047	0.044	4.291	0.17	0.11	0.018
7.14 ± 0.13	809.0 ± 9.0	78.270	0.079	0.074	8.166	0.046	0.044	4.155	0.16	0.10	0.023
10.74 ± 0.13	1200± 10	78.185	0.081	0.075	8.162	0.047	0.044	4.132	0.17	0.11	0.025
14.31 ± 0.13	1540 ± 13	78.014	0.081	0.074	8.163	0.047	0.044	4.308	0.18	0.10	0.016
17.83 ± 0.12	1946 ± 13	77.975	0.078	0.073	8.156	0.046	0.044	4.273	0.16	0.095	0.014

Table 3.5 As for Table 3.3 but for aqueous Na_2SO_4 solutions.

c (mmol/L)	κ (μS/cm)	ε_{dc}	$u(\varepsilon_{dc})$		τ (ps)	$u(\tau)$		ε_∞	$u(\varepsilon_\infty)$		s^2
			Monte Carlo	covar. matrix		Monte Carlo	covar. matrix		Monte Carlo	covar. matrix	
0	8.218 ± 0.041	78.362	0.078	0.073	8.277	0.047	0.044	5.255	0.16	0.099	0.002
0.325 ± 0.019	78.44 ± 0.39	78.351	0.082	0.073	8.271	0.048	0.044	5.173	0.19	0.10	0.002
0.965 ± 0.032	225.0 ± 1.1	78.322	0.077	0.073	8.277	0.046	0.044	5.246	0.16	0.097	0.003
1.281 ± 0.036	297.0 ± 1.5	78.316	0.079	0.073	8.270	0.047	0.044	5.147	0.17	0.10	0.002
1.594 ± 0.040	366.9 ± 1.8	78.305	0.079	0.073	8.267	0.047	0.044	5.145	0.17	0.10	0.003
2.212 ± 0.047	496.7 ± 7.8	78.272	0.078	0.073	8.273	0.047	0.044	5.221	0.16	0.10	0.003
2.819 ± 0.052	638.1 ± 8.5	78.240	0.078	0.073	8.267	0.047	0.044	5.214	0.16	0.098	0.003
3.119 ± 0.054	703.0 ± 8.6	78.221	0.078	0.073	8.280	0.047	0.044	5.303	0.16	0.11	0.003
4.693 ± 0.054	1038 ± 10	78.167	0.079	0.074	8.266	0.047	0.044	5.178	0.17	0.11	0.003
6.250 ± 0.054	1320 ± 11	78.119	0.079	0.075	8.265	0.047	0.045	5.163	0.17	0.12	0.005
7.789 ± 0.054	1596 ± 12	78.052	0.078	0.075	8.252	0.047	0.045	5.077	0.16	0.12	0.005
9.356 ± 0.053	1904 ± 13	77.998	0.077	0.075	8.245	0.047	0.046	4.945	0.15	0.13	0.007
10.895 ± 0.052	2163 ± 14	77.930	0.076	0.076	8.238	0.046	0.046	4.914	0.15	0.14	0.010
12.449 ± 0.051	2394 ± 16	77.832	0.077	0.079	8.221	0.046	0.048	4.857	0.15	0.17	0.022

3.6. Ion-Specific Indicators

Extracted Debye parameters ε_{dc}, τ, and κ given in Tables 3.3 to 3.5 for NaCl, $NaNO_3$, and Na_2SO_4 samples respectively are plotted against concentration in Figures 3.5 to 3.7. In addition, the parameters are fitted using appropriate chemical-physical models. A semi-empirical model of static permittivity $\hat{\varepsilon}_{dc}$ within the defined range of concentration has been proposed in previous work [40] as

$$\hat{\varepsilon}_{dc}(c,\gamma_1,\gamma_2,\gamma_3) = \varepsilon_{dc}^0 + \underbrace{\gamma_1 c^{0.5}\exp(-\gamma_2 c)}_{1} - \underbrace{\left[\frac{3v(c)\varepsilon_{dc}^0\left(\varepsilon_e-\varepsilon_{dc}^0\right)}{2\varepsilon_{dc}^0+\varepsilon_e-v(c)\left(\varepsilon_e-\varepsilon_{dc}^0\right)}\right]}_{2} - \underbrace{\left[\frac{2}{3}\frac{\varepsilon_{dc}^0-\varepsilon_\infty^0}{\varepsilon_0\varepsilon_{dc}^0}\tau^0\kappa_t(c)\right]}_{3} - \underbrace{\gamma_3 c}_{4} \tag{3.18}$$

where ε^0_{dc}, ε^0_∞, and τ^0 correspond to the values for deionized water (solvent), ε_e = 2 is approximated for nonpolar solutes [41], $v(c) = cM/\rho$ is volume fraction of the solute where c (mol/L), ρ (g/L), and M (g/mol) are concentration of solute, water density, and solute molecular weight, respectively, $\kappa_t(c)$ (S/m) is the theoretical conductivity, and γ_1, γ_2, and γ_3 are adjustable parameters extracted through the fitting procedure. Each term in (3.18)

expresses a polarization mechanism that is present in these electrolyte solutions. The model presented in (3.18) efficiently accounts for contributions due to the Debye-Falkenhagen effect (term 1) [42], dilution and internal depolarizing fields (term 2) [41], kinetic depolarization (term 3) [43], and dielectric saturation (term 4) [44]. An empirical model of relaxation time $\hat{\tau}$ can also be represented as follows [11]

$$\hat{\tau}(c,\alpha_1,\alpha_2) = \alpha_1 \exp(-\alpha_2 c) + (\tau^0 - \alpha_1) \tag{3.19}$$

where α_1 and α_2 are adjustable parameters extracted through the fitting procedure. The theoretical conductivity $\kappa_t(c)$ can be calculated as [45]

$$\kappa_t(c) = c\left[\Lambda^{\infty} - B\sqrt{10^3 c}\right] \tag{3.20}$$

where c (mol/L) is the solute concentration, Λ^{∞} (m^2S/mol) is the infinite molar conductivity of the solution at infinite dilution, and B ($m^{3.5}S/mol^{1.5}$) is the coefficient combining the non-idealities of electrophoretic and relaxation effects [45]. The input quantities required to calculate the volume fraction and conductivity of each electrolyte solution are listed in Table 3.6. The corresponding fitting parameters resulting from (3.18) for static permittivity $\hat{\varepsilon}_{dc}$ and from (3.19) for relaxation time $\hat{\tau}$ are given in Table 3.7.

The static permittivity ε_{dc} of NaCl [43, 46], $NaNO_3$ [12], Na_2SO_4 [47, 48] and indeed most other strong electrolytes [11, 14] in water has already been shown to be a decreasing non-linear function of concentration for c in the range 0.5 to 5 mol/L. In the concentration range of the present work, which is on the order of mmol/L, the static permittivity so obtained shows a slight initial increase with concentration for both NaCl and $NaNO_3$, while it shows an almost linear decrease with concentration for Na_2SO_4. The positive contribution to static permittivity at very low concentrations is represented by γ_1. The eventual decline in

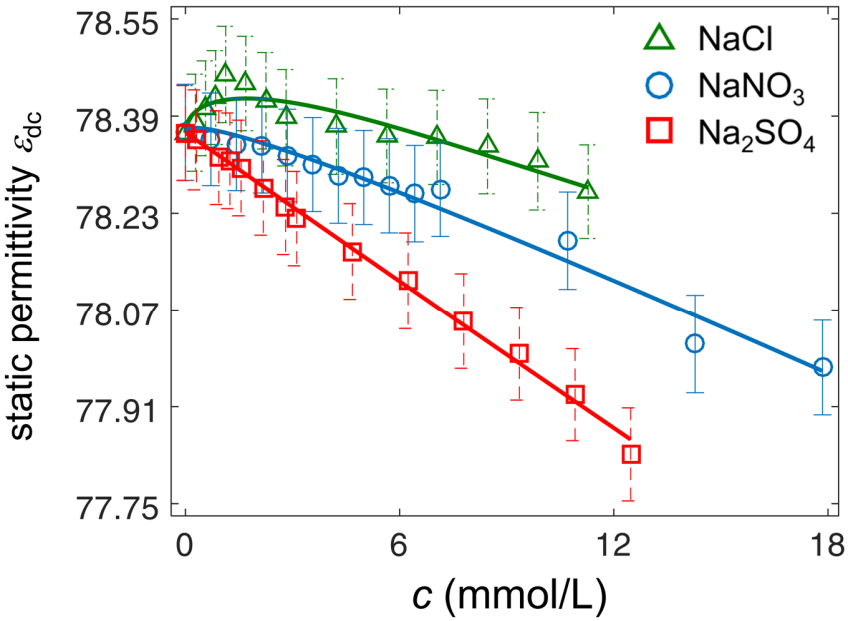

Figure 3.5 Experimental data (symbols) and fitted (solid lines) semi-empirical model, (3.18), of static permittivity ε_{dc} with parameters listed in Table 3.7 for aqueous solutions of NaCl, $NaNO_3$ and Na_2SO_4 at T = 25 °C. The error bars represent the calculated standard uncertainty based on the Monte Carlo method (Tables 3.3 to 3.5) and reflect a level of confidence of approximately 68 %.

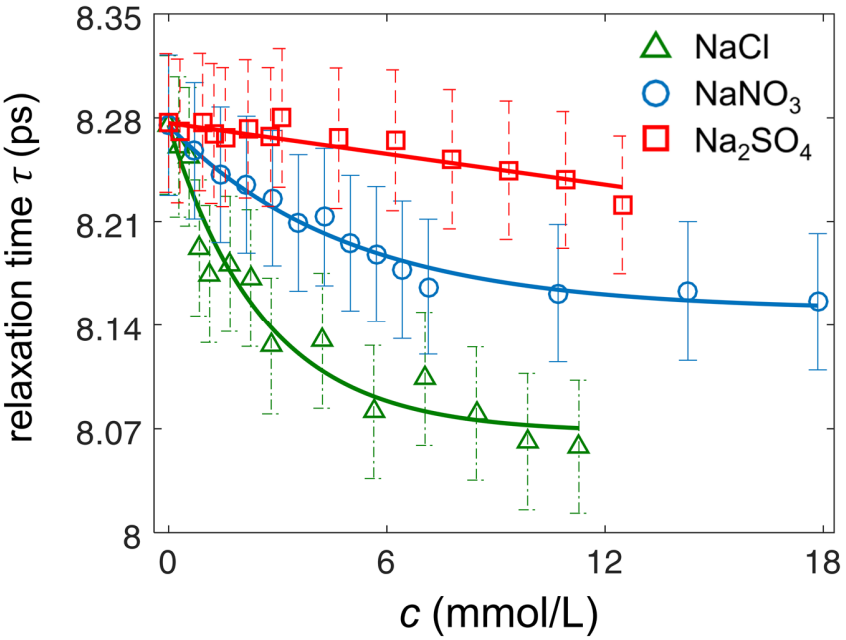

Figure 3.6 As for Figure 3.5 but for relaxation time, (3.19).

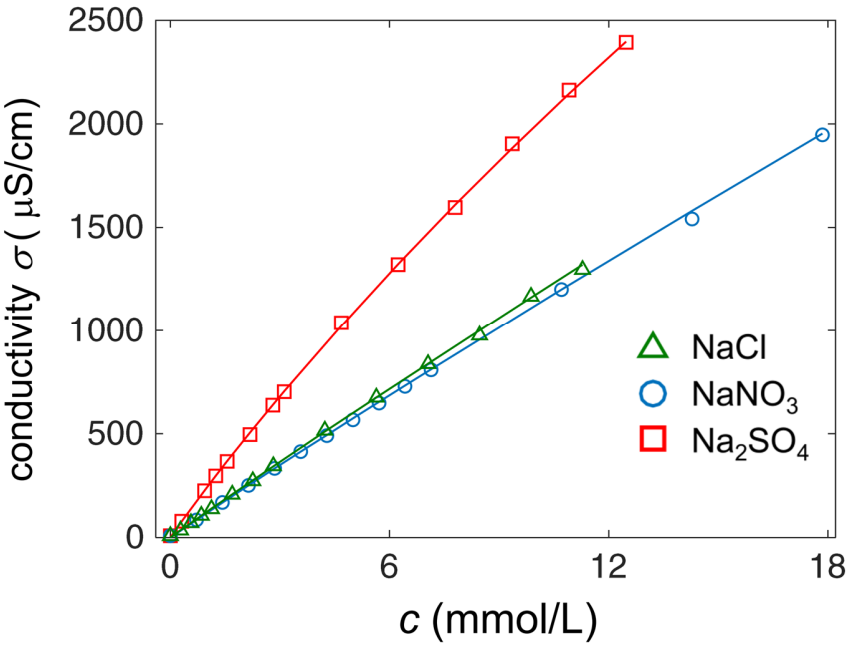

Figure 3.7 As for Figure 3.5 but for conductivity κ, (3.20), employing parameters listed in Table 3.6. The error bars that represent the calculated standard uncertainty (Tables 3.3 to 3.5) are too small to be visible in the figure.

Table 3.6 Input quantities for calculation of the volume fraction and conductivity (3.20), of NaCl, $NaNO_3$, and Na_2SO_4 solutions at 25 °C. Water density is ρ = 997.06 (g/L) at 25 °C [49]. The infinite molar conductivity values Λ^∞ are taken from [50], and the values of non-ideality coefficient B are calculated through the steps stated in [40].

ion	M (g/mol)	Λ^∞ (m^2S/mol)	B ($m^{3.5}S/mol^{1.5}$)
NaCl	58.4428	126.5×10^{-4}	2.83×10^{-4}
$NaNO_3$	84.9947	121.5×10^{-4}	2.79×10^{-4}
Na_2SO_4	142.0421	260.2×10^{-4}	19.2×10^{-4}

Table 3.7 Concentration, parameters of semi-empirical static permittivity model (3.18), and parameters of empirical relaxation time model (3.19) for aqueous NaCl, $NaNO_3$, and Na_2SO_4 solutions at 25 °C. The standard uncertainties of the fitting parameters are calculated based on the covariance matrix method and provide a level of confidence of approximately 68 %.

ion	c (mmol/L)	γ_1 ($L^{0.5}/mol^{0.5}$)	γ_2 (L/mol)	γ_3 (L/mol)	α_1 (ps)	$\alpha_2\times10^{-3}$ (L/mol)
NaCl	0-11.26	2.39 ± 0.40	122 ± 49	0.003 ± 0.003	0.21 ± 0.02	0.38 ± 0.11
$NaNO_3$	0-17.83	0.96 ± 0.49	31.3 ± 9.1	9.5 ± 4.1	0.125 ± 0.003	0.20 ± 0.08
Na_2SO_4	0-12.45	0.101 ± 0.042	27 ± 10	11.8 ± 4.2	-	0.003 ± 0.001[a]

[a] For sodium sulphate data, linear fitting, i.e., $\hat{\tau}(c) = \tau^0 - \alpha_2 c$ is used.

static permittivity as concentration increases is represented by γ_3. Likewise, the relaxation time τ of medium-sized ions (radii between 1.5 to 3 Å) of electrolyte NaCl, $NaNO_3$, and Na_2SO_4 systems - the *negative hydration* effect - has been shown to decrease as concentration increases [51]. The resulting decrement in the relaxation time is characterized by α_1. In addition, as concentration increases the slope of variation of the relaxation time which is described by $\exp(-\alpha_2)$ becomes smaller. For electrolyte solutions with water as solvent, conductivity κ is an increasing function of concentration [45]. According to (3.20), as concentration increases moderately, on the orders of a few mol/L, the conductivity variation becomes highly non-linear. Within the concentration range of this work the conductivity follows a linear relationship with concentration for NaCl, $NaNO_3$, and Na_2SO_4 solutions.

The results shown in Figures 3.5 to 3.7 demonstrate useful trends in static permittivity ε_{dc}, relaxation time τ, and conductivity κ as potential indicators of ion concentration and type. In a real system, multiple ion types and other contaminant species may be present [15]. To identify an ion and measure its concentration uniquely, therefore, requires judicious employment of the indicators. One possibility is to consider, simultaneously, three dimensions of data. Figure 3.8 shows a 3D trajectory plot of measured and fitted static permittivity ε_{dc}, relaxation time τ, and conductivity κ data for NaCl, $NaNO_3$, and Na_2SO_4 solutions. In addition, 2D contour plots of each pair of fitting parameters τ- ε_{dc}, τ-κ, and ε_{dc}-κ are projected onto the corresponding planes. According to Figure 3.8, the 3D trajectory for each solution type is a unique curve in ε_{dc}-τ-κ space. The 3D trajectory plot shown in Figure 3.8 suggests that the ion type and concentration of an unknown electrolyte solution can be found by measuring its dielectric spectrum, extracting ε_{dc}, τ, and κ parameters, and mapping

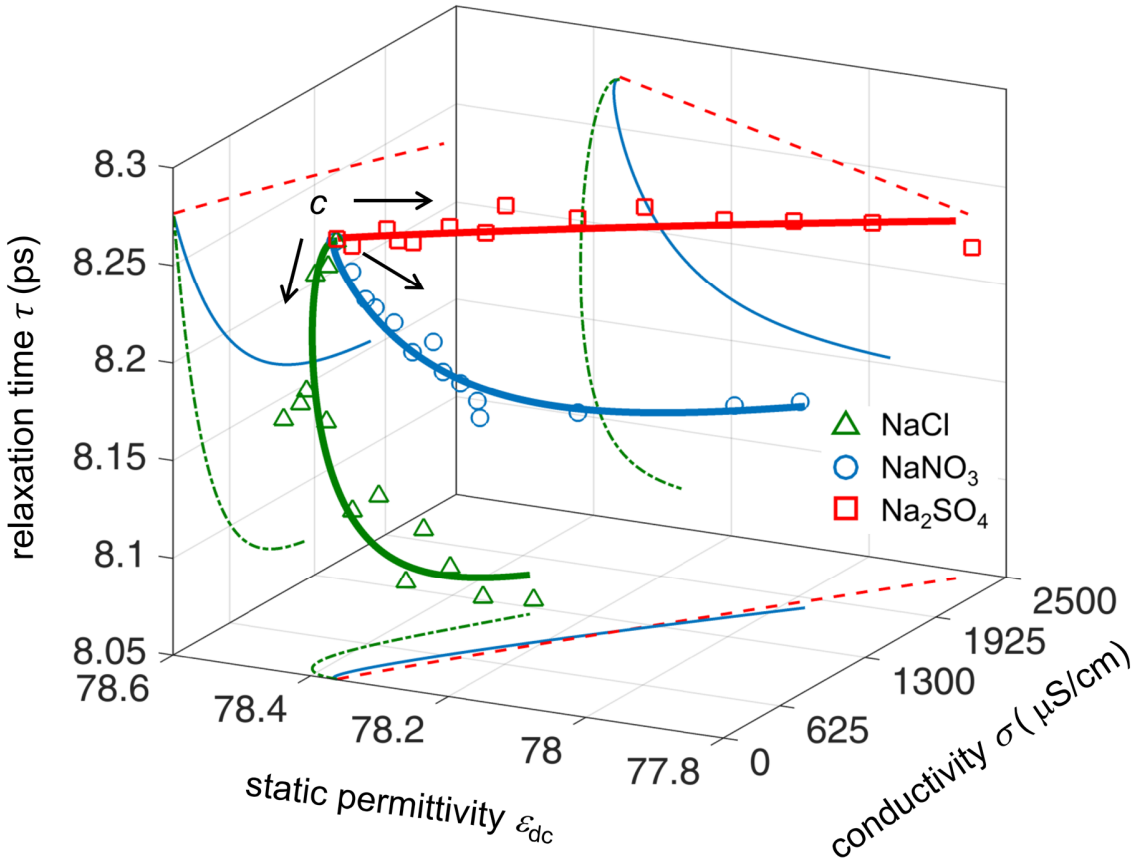

Figure 3.8 3D trajectory plot mapped from extracted measured (symbols) and fitted (solid lines) static permittivity ε_{dc}, relaxation time τ, and conductivity κ of NaCl, $NaNO_3$ and Na_2SO_4 solutions at T = 25 °C. The 2D contour plots of each pair of fitted parameters are projected onto the corresponding planes for NaCl (dashed-dotted line), $NaNO_3$ (solid line) and Na_2SO_4 (dashed line). For clarity, error bars that represent the standard uncertainty of the data (Tables 3.3 to 3.5) are not shown in this figure.

these indicators to a benchmark data set from which the ion type and concentration can be inferred. A sensing system capable of identifying these and, potentially, other ions can be designed on the basis of measuring these fundamental indicators.

3.7. Conclusion

The dielectric spectra of agriculturally-relevant aqueous solutions of sodium chloride (NaCl), sodium nitrate ($NaNO_3$), and sodium sulphate (Na_2SO_4) that are commonly found in water run-off were analyzed through well-controlled laboratory experiments. The extracted

static permittivity ε_{dc}, relaxation time τ, and conductivity κ parameters were fitted within the defined low range of concentration, which is on the order of mmol/L, by using appropriate chemical-physical models. These parameters demonstrate useful trends as potential indicators of ion concentration and type. A method of judiciously exploiting the indicators, by means of 3D trajectory plot, was proposed to uniquely identify an ion and infer its concentration. Assessment of measurement uncertainties, which comprise random and systematic errors and are particularly important in the context of low concentration aqueous solutions, was also conducted. The individual standard uncertainties include contributions from repeated measurements, deviation from a reference data (calibration uncertainty), and uncertainties associated with the reference data. It was shown that systematic errors, with relative standard uncertainties around or below 1 %, are the main contributor to the measurement uncertainty in both real ε' and imaginary ε'' permittivity values, and are far larger than the random errors whose relative standard uncertainties are around 0.1 %. Furthermore, covariance matrix and Monte Carlo methods were conducted to calculate the associated uncertainties of the extracted indicator parameters. The uncertainty values evaluated through the Monte Carlo method were found to be slightly higher than those evaluated through the covariance matrix method. The approximation nature of the Monte Carlo method in constructing the distribution function of individual sources of uncertainty by artificially generating random numbers, nevertheless, reduces the tediousness of analytical calculations associated with the covariance matrix method.

This work lays a foundation upon which an electrical sensor can be designed for the efficient analysis of agricultural run-off. A method based upon dielectric spectroscopy can potentially address the need for a fast, real-time, field-deployable, and economically feasible

sensor, improving upon existing high-cost or non-durable monitoring systems. In ongoing research, the effect of temperature-dependence is being analyzed and the further development of the method for distinguishing between multiple ions present in a sample is being examined.

Acknowledgment

This work was funded by the USDA-National Institute of Food & Agriculture, Award Number 013025-00001. The authors gratefully acknowledge Amy L. Kaleita for her leadership on this project.

3.8. References

[1] D. Eller, "Raccoon River nitrate level peaked Saturday," ed: The Des Moines Register, , 24 Nov. 2014.

[2] J. Wright and G. Sands, "Planning an agricultural subsurface drainage system," *College of Agricultural, Food and Environmental Sciences, University of Minnesota. BU-07685,* pp. 1-10, 2001.

[3] G. Randall and M. Goss, "Nitrate losses to surface water through subsurface, tile drainage," *Nitrogen in the environment: sources, problems, and management, 2nd edn. Elsevier, New York,* pp. 145-175, 2008.

[4] G. Venkatesan and G. Swaminathan, "Review of chloride and sulphate attenuation in ground water nearby solid-waste landfill sites," *Journal of Environmental Engineering and Landscape Management,* vol. 17, pp. 1-7, 2009.

[5] M. H. Ward, B. A. Kilfoy, P. J. Weyer, K. E. Anderson, A. R. Folsom, and J. R. Cerhan, "Nitrate intake and the risk of thyroid cancer and thyroid disease," *Epidemiology (Cambridge, Mass.),* vol. 21, p. 389, 2010.

[6] W. Orem, C. Gilmour, D. Axelrad, D. Krabbenhoft, D. Scheidt, P. Kalla*, et al.*, "Sulfur in the South Florida ecosystem: distribution, sources, biogeochemistry, impacts, and management for restoration," *Critical Reviews in Environmental Science and Technology,* vol. 41, pp. 249-288, 2011.

[7] W. E. Morf, *The principles of ion-selective electrodes and of membrane transport* vol. 2: Elsevier, 2012.

[8] B. A. Pellerin, B. A. Bergamaschi, B. D. Downing, J. F. Saraceno, J. D. Garrett, and L. D. Olsen, "Optical techniques for the determination of nitrate in environmental waters," *Quality Assurance, and Data Reporting. In: Techniques and Methods,* pp. 1-D5, 2013.

[9] R. Buchner and G. Hefter, "Interactions and dynamics in electrolyte solutions by dielectric spectroscopy," *Physical Chemistry Chemical Physics,* vol. 11, pp. 8984-8999, 2009.

[10] K. Nörtemann, J. Hilland, and U. Kaatze, "Dielectric properties of aqueous NaCl solutions at microwave frequencies," *The Journal of Physical Chemistry A,* vol. 101, pp. 6864-6869, 1997.

[11] T. Chen, G. Hefter, and R. Buchner, "Dielectric spectroscopy of aqueous solutions of KCl and CsCl," *The Journal of Physical Chemistry A,* vol. 107, pp. 4025-4031, 2003.

[12] W. Wachter, W. Kunz, R. Buchner, and G. Hefter, "Is there an anionic Hofmeister effect on water dynamics? Dielectric spectroscopy of aqueous solutions of NaBr, NaI, NaNO3, NaClO4, and NaSCN," *The Journal of Physical Chemistry A,* vol. 109, pp. 8675-8683, 2005.

[13] A. Lileev, Z. Filimonova, and A. Lyashchenko, "Dielectric permittivity and relaxation in aqueous solutions of alkali metal sulfates and nitrates in the temperature range 288–313 K," *Journal of Molecular Liquids,* vol. 103, pp. 299-308, 2003.

[14] W. Wachter, Š. Fernandez, R. Buchner, and G. Hefter, "Ion association and hydration in aqueous solutions of LiCl and Li2SO4 by dielectric spectroscopy," *The Journal of Physical Chemistry B,* vol. 111, pp. 9010-9017, 2007.

[15] B. A. Zimmerman and A. L. Kaleita, "Dissolved Constituents in Agricultural Drainage Waters," *Transactions of the ASABE,* vol. 60, pp. 847-859, 2017.

[16] A. P. Gregory and R. N. Clarke, "A review of RF and microwave techniques for dielectric measurements on polar liquids," *IEEE Transactions on Dielectrics and Electrical Insulation,* vol. 13, pp. 727-743, 2006.

[17] J. Fitzpatrick, "Error models for systems measurement," *Microwave Journal,* vol. 21, pp. 63-66, 1978.

[18] R. Buchner, T. Chen, and G. Hefter, "Complexity in “simple” electrolyte solutions: ion pairing in MgSO4 (aq)," *The Journal of Physical Chemistry B,* vol. 108, pp. 2365-2375, 2004.

[19] S. Schrödle, W. Wachter, R. Buchner, and G. Hefter, "Scandium sulfate complexation in aqueous solution by dielectric relaxation spectroscopy," *Inorganic Chemistry,* vol. 47, pp. 8619-8628, 2008.

[20] P. R. Bevington, D. K. Robinson, J. M. Blair, A. J. Mallinckrodt, and S. McKay, "Data reduction and error analysis for the physical sciences," *Computers in Physics,* vol. 7, pp. 415-416, 1993.

[21] A. George, F. Seber, and C. Wild, "Nonlinear regression," ed: Wiley-Interscience, 2003.

[22] F. Attivissimo, A. Cataldo, N. Giaquinto, and M. Savino, "Assessment of the uncertainty associated with systematic errors in digital instruments: an experimental study on offset errors," *Measurement Science and Technology,* vol. 23, p. 035004, 2012.

[23] D. Barker, T. Jackson, P. Suherman, M. Gashinova, and M. Lancaster, "Uncertainties in the permittivity of thin films extracted from measurements with near field microwave microscopy calibrated by an image charge model," *Measurement Science and Technology,* vol. 25, p. 105601, 2014.

[24] R. B. D'Agostino, *Goodness-of-fit-techniques* vol. 68: CRC press, 1986.

[25] B. N. Taylor and C. E. Kuyatt, *Guidelines for evaluating and expressing the uncertainty of NIST measurement results*: US Department of Commerce, Technology Administration, National Institute of Standards and Technology Gaithersburg, MD, 1994.

[26] I. BIPM, I. IFCC, I. IUPAC, and O. ISO, "Evaluation of measurement data—guide for the expression of uncertainty in measurement. JCGM 100: 2008," p. 167, 2008.

[27] U. Kaatze, "Reference liquids for the calibration of dielectric sensors and measurement instruments," *Measurement Science and Technology,* vol. 18, p. 967, 2007.

[28] A. P. Gregory and R. Clarke, *Tables of the complex permittivity of dielectric reference liquids at frequencies up to 5 GHz*: National Physical Laboratory (NPL), Teddington, 2012.

[29] T. Sato, A. Chiba, and R. Nozaki, "Hydrophobic hydration and molecular association in methanol–water mixtures studied by microwave dielectric analysis," *The Journal of Chemical Physics,* vol. 112, pp. 2924-2932, 2000.

[30] V. Barwick and S. R. Ellison, "Measurement uncertainty: approaches to the evaluation of uncertainties associated with recovery," *Analyst,* vol. 124, pp. 981-990, 1999.

[31] B. Magnusson and S. L. Ellison, "Treatment of uncorrected measurement bias in uncertainty estimation for chemical measurements," *Analytical and Bioanalytical Chemistry,* vol. 390, pp. 201-213, 2008.

[32] V. Synek, "Attempts to include uncorrected bias in the measurement uncertainty," *Talanta,* vol. 65, pp. 829-837, 2005.

[33] J. Taylor, *Introduction to error analysis, the study of uncertainties in physical measurements*, 1997.

[34] J. S. Alper and R. I. Gelb, "Standard errors and confidence intervals in nonlinear regression: comparison of Monte Carlo and parametric statistics," *Journal of Physical Chemistry,* vol. 94, pp. 4747-4751, 1990.

[35] A. Ruckstuhl, "*Introduction to Nonlinear Regression*," 2010.

[36] I. Miller and M. Miller, *John E. Freund's mathematical statistics with applications*: Pearson, 2015.

[37] G. Wübbeler, M. Krystek, and C. Elster, "Evaluation of measurement uncertainty and its numerical calculation by a Monte Carlo method," *Measurement Science and Technology,* vol. 19, p. 084009, 2008.

[38] J. Yao and S. Yeo, "Using the Monte Carlo approach to study effects of power measurement uncertainties on six-port reflectometer performance," *Measurement Science and Technology,* vol. 21, p. 025103, 2010.

[39] A. Gregory, R. Clarke, and M. Cox, "Traceable measurement of dielectric reference liquids over the temperature interval 10–50 C using coaxial-line methods," *Measurement Science and Technology,* vol. 20, p. 075106, 2009.

[40] A. Gorji and N. Bowler, "Static Permittivity of Environmentally-Relevant Low-Concentration Aqueous Solutions of NaCl, NaNO3, and Na2SO4," *The Journal of chemical physics,* (in progress).

[41] U. Kaatze, "The dielectric properties of water in its different states of interaction," *Journal of Solution Chemistry,* vol. 26, pp. 1049-1112, 1997.

[42] H. Falkenhagen and W. Fischer, "Dependence of Electrical Conductance and Dielectric Constant upon Frequency in Mixtures of Strong Electrolytes," *Nature,* vol. 130, pp. 928-928, 1932.

[43] R. Buchner, G. T. Hefter, and P. M. May, "Dielectric relaxation of aqueous NaCl solutions," *The Journal of Physical Chemistry A,* vol. 103, pp. 1-9, 1999.

[44] R. Buchner, C. Hölzl, J. Stauber, and J. Barthel, "Dielectric spectroscopy of ion-pairing and hydration in aqueous tetra-n-alkylammonium halide solutions," *Physical Chemistry Chemical Physics,* vol. 4, pp. 2169-2179, 2002.

[45] M. R. Wright, *An introduction to aqueous electrolyte solutions: Ch12*: John Wiley & Sons, 2007.

[46] E. Levy, A. Puzenko, U. Kaatze, P. B. Ishai, and Y. Feldman, "Dielectric spectra broadening as the signature of dipole-matrix interaction. I. Water in nonionic solutions," *The Journal of Chemical Physics,* vol. 136, p. 114502, 2012.

[47] J. Barthel, H. Hetzenauer, and R. Buchner, "Dielectric Relaxation of Aqueous Electrolyte Solutions II. Ion-Pair Relaxation of 1: 2, 2: 1, and 2: 2 Electrolytes," *Berichte der Bunsengesellschaft für physikalische Chemie,* vol. 96, pp. 1424-1432, 1992.

[48] R. Buchner, S. G. Capewell, G. Hefter, and P. M. May, "Ion-pair and solvent relaxation processes in aqueous Na2SO4 solutions," *The Journal of Physical Chemistry B,* vol. 103, pp. 1185-1192, 1999.

[49] W. M. Haynes, *CRC handbook of chemistry and physics*: CRC press, 2014.

[50] A. L. Horvath, *Handbook of aqueous electrolyte solutions*: Halsted Press, 1985.

[51] U. Kaatze, R. Behrends, and R. Pottel, "Hydrogen network fluctuations and dielectric spectrometry of liquids," *Journal of Non-Crystalline Solids,* vol. 305, pp. 19-28, 2002.

CHAPTER 4. CONCENTRATION AND TEMPERATURE DEPENDENT MODELS OF DIELECTRIC SPECTRAL PARAMETERS FOR LOW-CONCENTRATION IONIC AQUEOUS SOLUTIONS

Manuscript in preparation

Amin Gorji[1, 2, a] and Nicola Bowler[1, 2, 3, a]

4.1. Abstract

In this work, the complex relative permittivity of sodium chloride (NaCl), sodium nitrate ($NaNO_3$), and sodium sulphate (Na_2SO_4) ionic aqueous solutions has been measured over frequency range from 200 MHz to 20 GHz for agriculturally-relevant low concentrations of 0 to 15 mmol/L at various temperatures between 5 °C and 30 °C. The measured spectra were fitted with a Debye relaxation model and conductivity was measured independently, to reduce uncertainty in obtaining other parameters by spectral fitting. The extracted fitting parameters including specific conductivity σ, static permittivity ε_{dc}, and relaxation time τ have been fully parametrized as a function of concentration and temperature, based on comprehensive studies on physical chemistry and molecular dynamics present in low-concentration ionic aqueous systems. These models can be employed for a reasonable estimate of dielectric spectral features for any combination of agriculturally-relevant concentration and temperature within the radio-frequency and microwave ranges.

4.2. Introduction

High levels of contaminant ions, including sodium Na^+, chloride Cl^-, nitrate NO_3^-, and sulphate SO_4^{2-} which are mainly due to efflux from agricultural land, cause serious environmental and human-health related concerns. These ions are a major contributor to

[1] Department of Electrical and Computer Engineering, Iowa State University, Ames, Iowa, 50011, USA
[2] Center for Nondestructive Evaluation, Iowa State University, Ames, Iowa, 50011, USA
[3] Department of Materials Science and Engineering, Iowa State University, Ames, Iowa, 50011, USA
[a] Email: amingorji68@gmail.com, nbowler@iastate.edu

hypoxic conditions in receiving waters, and are expensive to remove from drinking water [1]. Precise knowledge of dielectric properties of these ions dissolved in water is of considerable interest. In available studies of NaCl aqueous solution, Nörtemann *et al*. [2] determined complex relative permittivities for moderate concentrations $c \sim 0.05$ to 0.6 mol/L over combined frequency range $f = 0.02$ to 40 GHz by using multiple apparatus at temperature $T =$ 20 °C. Buchner *et al*. [3] studied solutions up to higher concentrations $c \sim 0.1$ to 5 mol/L over single-swept frequency range 0.2 to 20 GHz at more various temperatures of 5, 20, 25, 35 °C. Levy *et al*. [4] extended the frequency range to 50 GHz for concentrations $c \sim 0.1$ to 1 mol/L at room temperature $T = 25$ °C. Likewise the dielectric properties of $NaNO_3$ aqueous solution have been reported by Lileev *et al*. [5] and Wachter *et al*. [6]. The former measured the permittivity of very high concentration samples $c \sim 0.52$ to 8.54 mol/L over five discrete frequencies between 7 to 25 GHz at different temperatures from 10 °C to 40 °C. The latter, however, covered a broad frequency range up to 89 GHz within concentration range $c \sim 0.05$ to 1.5 mol/L at $T = 25$ °C. The dielectric spectroscopy measurements of Na_2SO_4 aqueous solution have been obtained by Barthel *et al*. [7] for concentrations $c \sim 0.1$ to 1 mol/L over a wide frequency range 0.95 to 89 GHz at $T = 25$ °C. In addition, Buchner *et al*. [8] studied the solutions within the same temperature and the frequency range for concentrations $c \sim 0.025$ to 1.6 mol/L.

Many of the previous studies, however, did not consider agriculturally-relevant concentration levels of NaCl, $NaNO_3$, and Na_2SO_4 ionic aqueous solutions which are on the order of millimoles per liter in tile drainage waters [9]. In addition, concentration- and temperature-dependent parametric models of dielectric spectra and the associated fitting parameters have not been thoroughly investigated. In a recent study by Peyman *et al*. [10],

polynomial equations were derived for Debye (c < 0.5 mol/L) and Cole-Cole (c > 0.5 mol/L) fitting parameters relating each of the static permittivity ε_{dc}, relaxation time τ (s), specific conductivity σ (S/m), and distribution parameter α to the concentration and temperature of NaCl solutions in water. The measured results of their work at T = 20 °C for concentrations c ~ 0.001 to 5 mol/L over frequency range f = 0.13 to 20 GHz were combined with literature data [2, 3, 11-14] to cover the same concentrations between 5 °C to 35 °C. In another study by Gulich *et al*. [15], they provided a set of 13 parameters which describe the frequency, temperature and concentration dependence of Cole-Davidson fitting parameters for aqueous solutions of NaCl and KCl. Their measurements were conducted for concentrations c ~ 0.001 to 1 mol/L (0.001, 0.01, 0.1, 0.5, and 1 mol/L) over frequency range f = 0.1 to 40 GHz GHz at various temperatures from T = 10 °C to 60 °C.

In this work, detailed analytical and semi-empirical concentration- and temperature-dependent parametric models of Debye fitting parameters including specific conductivity σ, static permittivity ε_{dc}, and relaxation time τ, accounting for physical chemistry and molecular dynamics for aqueous solutions of NaCl, $NaNO_3$, and Na_2SO_4 have been developed. In Section 4.3 the details of the experimental setup to perform broadband dielectric spectroscopy over the frequency range 200 MHz to 20 GHz at well-controlled temperatures from 5 °C to 30 °C for concentrations 0 to 15 mmol/L are presented. The data fitting procedure for extracting Debye parameters from the measured dielectric spectra is also explained in Section 4.3. Results of extracted fitting parameters and their associated uncertainties are presented in Section 4.4. Complete concentration- and temperature-dependent models of specific conductivity σ, relaxation time τ, and static permittivity ε_{dc} are given in Sections 4.5, 4.6, and 4.7, respectively. In Section 4.8, the 3D trajectory plots, as

proposed in Chapter 3 (Section 3.6), as a method of identifying an ion and its concentration based on extracted indicators from the dielectric spectra are given at each temperature. The chapter is drawn to conclusion in Section 4.9.

4.3. Measurement and Analysis

4.3.1. Experimental Setup

The experimental setup developed to measure the dielectric spectra of ionic aqueous solutions at various temperatures is shown in Figure 4.1. The details of the measurement instruments and the procedure are already explained in Chapter 3 (Section 3.3). In summary, dielectric experiments were performed using a Speag open-ended coaxial DAK3.5 Dielectric Probe Kit (200 MHz to 20 GHz recommended bandwidth) and Anritsu 37347C Vector Network Analyzer (VNA) (40 MHz to 20 GHz nominal bandwidth). In addition, the specific conductivity σ was measured separately using a Seven2Go^{TM} Conductivity meter with InLab720 probe (operating range 0.1 to 500 μS/cm ± 0.5 %). For concentrations of ionic solutions corresponding to specific conductivity greater than 500 μS/cm, however, σ was treated as an additional fitting parameter. The sample beaker was placed in a temperature-controlled Anova R10 Refrigerated and Heating Circulator (± 0.01 °C) and the temperature held at various temperatures from 5 °C to 30 °C (5 °C interval) during this experiment. Dowtherm SR-1 Ethylene Glycol oil (18.1 Vol. %) was used as the bath fluid in order to minimize the influence of ambient temperature fluctuations. Three sets of agriculturally-relevant ionic aqueous solutions were prepared and 8 concentrations c of each (including de-ionized water as zero concentration) were tested: (i) sodium chloride (NaCl) solutions with concentration ranging from c = 0 to 10.28 mmol/L, (ii) sodium nitrate ($NaNO_3$) solutions with c = 0 to 14.31 mmol/L, and (iii) sodium sulphate (Na_2SO_4) solutions with c = 0 to 11.36

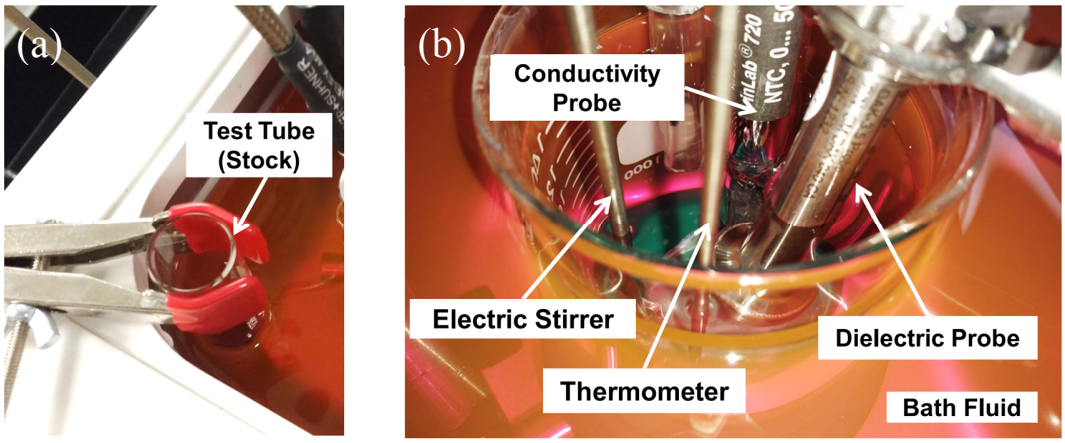

Figure 4.1 Experimental setup for measuring the dielectric spectra and conductivity of an aqueous ionic solution at a controlled temperature. (a) Test tube containing high-concentrated stock solution, (b) Sample beaker containing diluted solutions.

mmol/L. The samples were tested from lower to higher concentrations by successive titration (± 0.1 ml graduated pipette) of a pre-calculated volume of each stock ionic solution into a specified starting volume of deionized water. To reduce temperature perturbation in the sample beaker in every step stock solution was added, the stock solution was kept in a test tube located in the temperature bath to retain the same temperature as the sample beaker.

4.3.2. Data Fitting

The data fitting procedure of the measured dielectric spectra, i.e., polarization $\varepsilon'(f)$ and energy dissipation $\varepsilon''(f)$, by means of single-term Debye relaxation model was extensively addressed in Chapters 2 (Section 2.3.2) and 3 (Section 3.4). The extracted fitting parameters including specific conductivity σ, static permittivity ε_{dc}, relaxation time τ, and infinite permittivity ε_∞ are given in the next section for a various range of concentrations and temperatures for NaCl, $NaNO_3$, and Na_2SO_4 ionic aqueous solutions.

The compilation of uncertainty components of $\varepsilon'(f)$ and $\varepsilon''(f)$ which comprise random and systematic errors was given in Chapter 3 (Section 3.5). The uncertainty of the fitting

parameters $u(\sigma)$, $u(\varepsilon_{dc})$, $u(\tau)$, and $u(\varepsilon_{\infty})$, which return 68% confidence interval, was also calculated via Monte Carlo (MC) modeling described therein.

4.4. Results

The extracted Debye relaxation parameters along with the associated uncertainties for each of NaCl, $NaNO_3$, and Na_2SO_4 aqueous solutions from 5 °C to 30 °C and different concentrations are listed in Tables 4.1 to 4.3. The fitting parameters presented in here provide a set of benchmark data for agriculturally-relevant aqueous solutions of NaCl, $NaNO_3$, and Na_2SO_4. The fitted model is a single-term Debye relaxation function and provides the corresponding specific conductivity σ, static permittivity ε_{dc}, relaxation time τ, and infinite-frequency permittivity ε_{∞}. In the next three sections, concentration- and temperature-dependent parametric models of Debye fitting parameters accounting for corresponding physical chemistry and molecular dynamics for aqueous solutions of NaCl, $NaNO_3$, and Na_2SO_4 are constructed.

4.5. Conductivity Modeling

The procedure to calculate the specific conductivity σ of general multivalent electrolyte system composed of ion species with electron valency $z_1 = y$ and $z_2 = -x$ for cation A^{y+} and anion B^{x-}, respectively, has been conducted in Chapter 2 for dilute range of concentrations (~ mmol/L) and at a constant temperature based on Debye, Huckel, and Onsager (DHO) theory [16]. In this section, the theory is extended to include the temperature-dependence of specific conductivity. The analysis starts by defining temperature-dependent inverse Debye length $\kappa_0(T)$ (m^{-1}) as

$$\kappa_0(T) = \sqrt{\frac{e^2 N_A}{\varepsilon_0 \varepsilon_{dc}^0(T) k_B T}\left(|z_2| z_1^2 + |z_1| z_2^2\right)} \tag{4.1}$$

Table 4.1 Specific conductivity (σ) and parameters of single-term Debye model (ε_{dc}, τ, and ε_∞) for various concentrations (c) and temperatures (T) of aqueous NaCl solutions. The specific conductivity was measured directly up to 500 μS/cm with ± 0.5 % instrument uncertainty. For concentrations corresponding to specific conductivity greater than 500 μS/cm, σ was treated as an additional fitting parameter. The standard uncertainties were calculated from Monte Carlo method and correspond to approximately 68 % confidence interval.

σ (μS/cm)						
c (mmol/L)	T = 5 °C	T = 10 °C	T = 15 °C	T = 20 °C	T = 25 °C	T = 30 °C
0	4.999 ± 0.025	5.787 ± 0.029	6.613 ± 0.033	7.420 ± 0.037	8.212 ± 0.041	9.025 ± 0.045
0.294 ± 0.017	22.75 ± 0.11	25.91 ± 0.13	29.77 ± 0.15	33.22 ± 0.16	36.74 ± 0.18	40.04 ± 0.20
0.585 ± 0.024	45.14 ± 0.23	51.70 ± 0.26	58.91 ± 0.29	66.10 ± 0.33	72.91 ± 0.36	79.92 ± 0.39
0.988 ± 0.029	75.86 ± 0.38	86.63 ± 0.44	98.48 ± 0.49	110.57 ± 0.55	121.29 ± 0.61	134.38 ± 0.66
1.834 ± 0.032	138.26 ± 0.70	160.44 ± 0.80	181.20 ± 0.91	205.9 ± 1.0	223.7 ± 1.1	246.4 ± 1.2
3.514 ± 0.034	264.6 ± 1.3	305.3 ± 1.5	341.9 ± 1.7	390.7 ± 1.9	427.9 ± 2.1	466.7 ± 2.3
5.653 ± 0.035	419.4 ± 2.1	487.9 ± 2.4	545.1 ± 8.4	614.0 ± 8.4	675.9 ± 8.4	746.0 ± 8.3
8.595 ± 0.034	623.3 ± 8.9	744.1 ± 9.5	813.6 ± 9.5	901.8 ± 9.5	1020.9 ± 9.5	1097.4 ± 9.5
10.275 ± 0.034	741.9 ± 9.4	862 ± 10	985 ± 10	1088 ± 10	1196 ± 10	1313 ± 10
ε_{dc}						
0	85.830 ± 0.091	83.921 ± 0.089	82.053 ± 0.098	80.214 ± 0.088	78.362 ± 0.078	76.565 ± 0.085
0.294 ± 0.017	85.84 ± 0.11	83.94 ± 0.11	82.065 ± 0.089	80.245 ± 0.098	78.380 ± 0.080	76.586 ± 0.085
0.585 ± 0.024	85.81 ± 0.10	83.91 ± 0.10	82.081 ± 0.089	80.254 ± 0.085	78.404± 0.078	76.572 ± 0.085
0.988 ± 0.029	85.821 ± 0.098	83.913 ± 0.095	82.071 ± 0.096	80.256 ± 0.079	78.443 ± 0.079	76.640 ± 0.091
1.834 ± 0.032	85.808 ± 0.081	83.916 ± 0.079	82.064 ± 0.079	80.238 ± 0.083	78.437 ± 0.078	76.615 ± 0.091
3.514 ± 0.034	85.781 ± 0.082	83.897 ± 0.081	82.040 ± 0.096	80.266 ± 0.093	78.378 ± 0.079	76.572 ± 0.079
5.653 ± 0.035	85.715 ± 0.083	83.815 ± 0.081	81.995 ± 0.083	80.179 ± 0.091	78.357 ± 0.078	76.553 ± 0.086
8.595 ± 0.034	85.66 ± 0.11	83.78 ± 0.10	81.922 ± 0.095	80.151 ± 0.088	78.339 ± 0.078	76.496 ± 0.092
10.275 ± 0.034	85.62 ± 0.10	83.73 ± 0.10	81.906 ± 0.094	80.112 ± 0.087	78.305 ± 0.080	76.487 ± 0.094
τ (ps)						
0	14.910 ± 0.076	12.681 ± 0.064	10.833 ± 0.061	9.365 ± 0.046	8.275 ± 0.047	7.284 ± 0.048
0.294 ± 0.017	14.902 ± 0.086	12.670 ± 0.073	10.821 ± 0.067	9.355 ± 0.050	8.260 ± 0.047	7.267 ± 0.046
0.585 ± 0.024	14.902 ± 0.081	12.655 ± 0.069	10.818 ± 0.064	9.333 ± 0.040	8.252 ± 0.047	7.262 ± 0.051
0.988 ± 0.029	14.900 ± 0.091	12.643 ± 0.077	10.798 ± 0.054	9.338 ± 0.048	8.182 ± 0.046	7.245 ± 0.048
1.834 ± 0.032	14.871 ± 0.082	12.644 ± 0.070	10.790 ± 0.059	9.311 ± 0.043	8.176 ± 0.046	7.220 ± 0.050
3.514 ± 0.034	14.834 ± 0.075	12.619 ± 0.063	10.745 ± 0.056	9.287 ± 0.039	8.129 ± 0.046	7.176 ± 0.045
5.653 ± 0.035	14.783 ± 0.087	12.596 ± 0.074	10.730 ± 0.055	9.270 ± 0.042	8.085 ± 0.045	7.145 ± 0.044
8.595 ± 0.034	14.754 ± 0.076	12.567 ± 0.065	10.682 ± 0.067	9.228 ± 0.043	8.084 ± 0.046	7.121 ± 0.046
10.275 ± 0.034	14.752 ± 0.097	12.528 ± 0.082	10.674 ± 0.065	9.210 ± 0.047	8.066 ± 0.046	7.098 ± 0.044
ε_∞						
0	5.70 ± 0.20	5.53 ± 0.19	6.03 ± 0.27	5.63 ± 0.25	5.24 ± 0.16	5.22 ± 0.23
0.294 ± 0.017	5.70 ± 0.39	5.49 ± 0.38	5.99 ± 0.40	5.55 ± 0.25	5.06 ± 0.17	5.03 ± 0.28
0.585 ± 0.024	5.67 ± 0.26	5.46 ± 0.25	5.95 ± 0.25	5.43 ± 0.20	4.84 ± 0.16	4.98 ± 0.26
0.988 ± 0.029	5.63 ± 0.38	5.42 ± 0.37	5.92 ± 0.32	5.44 ± 0.30	4.11 ± 0.16	4.80 ± 0.26
1.834 ± 0.032	5.59 ± 0.39	5.42 ± 0.38	5.94 ± 0.46	5.29 ± 0.34	3.96 ± 0.16	4.52 ± 0.30
3.514 ± 0.034	5.55 ± 0.38	5.36 ± 0.37	5.88 ± 0.53	5.22 ± 0.36	3.49 ± 0.16	3.97 ± 0.33
5.653 ± 0.035	5.47 ± 0.43	5.44 ± 0.42	5.97 ± 0.38	5.37 ± 0.28	3.07 ± 0.15	3.53 ± 0.24
8.595 ± 0.034	5.36 ± 0.34	5.34 ± 0.34	5.95 ± 0.54	5.04 ± 0.32	2.83 ± 0.15	3.15 ± 0.19
10.275 ± 0.034	5.34 ± 0.50	5.30 ± 0.50	5.95 ± 0.50	5.02 ± 0.42	2.68 ± 0.17	2.65 ± 0.29

Table 4.2 As for Table 4.1 but for aqueous $NaNO_3$ solutions.

σ (μS/cm)						
c (mmol/L)	T = 5 °C	T = 10 °C	T = 15 °C	T = 20 °C	T = 25 °C	T = 30 °C
0	4.940 ± 0.025	5.787 ± 0.029	6.639 ± 0.033	7.490 ± 0.037	8.338 ± 0.042	9.118 ± 0.046
0.743 ± 0.043	55.83 ± 0.28	64.06 ± 0.32	71.77 ± 0.36	79.71 ± 0.40	88.01 ± 0.44	96.79 ± 0.48
1.479 ± 0.060	109.45 ± 0.55	125.57 ± 0.63	141.54 ± 0.71	158.35 ± 0.80	173.98 ± 0.87	190.86 ± 0.95
2.788 ± 0.072	204.0 ± 1.0	235.6 ± 1.2	266.2 ± 1.3	298.3 ± 1.5	327.8 ± 1.6	358.6 ± 1.8
3.934 ± 0.082	285.3 ± 1.4	329.3 ± 1.7	370.9 ± 1.9	411.9 ± 2.1	457.0 ± 2.3	496.8 ± 2.5
5.483 ± 0.090	403.6 ± 2.0	456.5 ± 2.3	516.8 ± 8.0	569.1 ± 8.1	628.2 ± 8.1	668.3 ± 8.1
8.895 ± 0.095	645.2 ± 8.8	726.7 ± 9.5	817.7 ± 9.5	924 ± 10	1016.5 ± 9.7	1111.0 ± 9.7
11.521 ± 0.099	819.0 ± 8.7	933 ± 11	1056 ± 11	1184 ± 11	1275 ± 11	14.17 ± 11
14.31 ± 0.10	995 ± 11	1137 ± 13	1262 ± 13	1446 ± 13	1578 ± 13	1718 ± 13
ε_{dc}						
0	85.830 ± 0.099	83.921 ± 0.097	82.053 ± 0.081	80.214 ± 0.080	78.363 ± 0.079	76.565 ± 0.081
0.743 ± 0.043	85.840 ± 0.083	83.910 ± 0.081	82.041 ± 0.079	80.202 ± 0.079	78.351 ± 0.077	76.572 ± 0.079
1.479 ± 0.060	85.803 ± 0.098	83.899 ± 0.096	82.021 ± 0.087	80.193 ± 0.077	78.343 ± 0.076	76.557 ± 0.083
2.788 ± 0.072	85.757 ± 0.099	83.851 ± 0.097	81.998 ± 0.079	80.175 ± 0.087	78.327 ± 0.076	76.514 ± 0.084
3.934 ± 0.082	85.72 ± 0.10	83.841 ± 0.097	81.979 ± 0.093	80.157 ± 0.082	78.299 ± 0.078	76.512 ± 0.091
5.483 ± 0.090	85.683 ± 0.088	83.772 ± 0.086	81.926 ± 0.079	80.091 ± 0.087	78.280 ± 0.078	76.469 ± 0.088
8.895 ± 0.095	85.562 ± 0.085	83.671 ± 0.083	81.833 ± 0.080	80.00 ± 0.10	78.242 ± 0.080	76.376 ± 0.096
11.521 ± 0.099	85.48 ± 0.11	83.60 ± 0.11	81.765 ± 0.091	79.916 ± 0.097	78.149 ± 0.081	76.281 ± 0.099
14.31 ± 0.10	85.39 ± 0.11	83.51 ± 0.11	81.690 ± 0.092	79.857 ± 0.090	78.013 ± 0.080	76.228 ± 0.086
τ (ps)						
0	14.910 ± 0.089	12.681 ± 0.076	10.833 ± 0.056	9.365 ± 0.041	8.268 ± 0.047	7.284 ± 0.048
0.743 ± 0.043	14.901 ± 0.092	12.669 ± 0.078	10.819 ± 0.066	9.354 ± 0.044	8.257 ± 0.046	7.266 ± 0.044
1.479 ± 0.060	14.888 ± 0.072	12.651 ± 0.061	10.798 ± 0.055	9.357 ± 0.036	8.241 ± 0.046	7.246 ± 0.046
2.788 ± 0.072	14.875 ± 0.075	12.647 ± 0.064	10.790 ± 0.057	9.330 ± 0.040	8.227 ± 0.046	7.211 ± 0.046
3.934 ± 0.082	14.858 ± 0.098	12.632 ± 0.083	10.770 ± 0.062	9.319 ± 0.038	8.211 ± 0.046	7.201 ± 0.050
5.483 ± 0.090	14.837 ± 0.082	12.612 ± 0.069	10.759 ± 0.061	9.295 ± 0.044	8.190 ± 0.046	7.197 ± 0.048
8.895 ± 0.095	14.802 ± 0.088	12.581 ± 0.074	10.738 ± 0.069	9.283 ± 0.039	8.163 ± 0.047	7.165 ± 0.045
11.521 ± 0.099	14.786 ± 0.093	12.573 ± 0.079	10.717 ± 0.066	9.269 ± 0.052	8.162 ± 0.047	7.151 ± 0.049
14.31 ± 0.10	14.785 ± 0.082	12.564 ± 0.070	10.713 ± 0.057	9.266 ± 0.042	8.163 ± 0.047	7.152 ± 0.045
ε_∞						
0	5.70 ± 0.30	5.53 ± 0.29	6.03 ± 0.37	5.63 ± 0.22	5.19 ± 0.17	5.22 ± 0.19
0.743 ± 0.043	5.66 ± 0.18	5.49 ± 0.18	5.99 ± 0.34	5.59 ± 0.21	5.09 ± 0.15	5.14 ± 0.18
1.479 ± 0.060	5.62 ± 0.19	5.45 ± 0.19	6.02 ± 0.25	5.42 ± 0.25	4.95 ± 0.15	4.97 ± 0.17
2.788 ± 0.072	5.62 ± 0.37	5.43 ± 0.35	5.98 ± 0.33	5.52 ± 0.22	4.75 ± 0.15	4.98 ± 0.12
3.934 ± 0.082	5.58 ± 0.32	5.41 ± 0.31	6.02 ± 0.22	5.49 ± 0.25	4.63 ± 0.16	5.01 ± 0.12
5.483 ± 0.090	5.53 ± 0.42	5.37 ± 0.40	5.94 ± 0.28	5.59 ± 0.31	4.41 ± 0.16	4.78 ± 0.10
8.895 ± 0.095	5.53 ± 0.42	5.38 ± 040	5.95 ± 0.37	5.47 ± 0.39	4.14 ± 0.17	4.75 ± 0.10
11.521 ± 0.099	5.54 ± 0.25	5.36 ± 0.24	5.98 ± 0.25	5.40 ± 0.24	4.16 ± 0.17	4.69 ± 0.11
14.31 ± 0.10	5.00 ± 0.51	5.33 ± 0.49	6.00 ± 0.39	5.38 ± 0.24	4.31 ± 0.18	4.71 ± 0.10

Table 4.3 As for Table 4.1 but for aqueous Na_2SO_4 solutions.

σ (μS/cm)						
c (mmol/L)	T = 5 °C	T = 10 °C	T = 15 °C	T = 20 °C	T = 25 °C	T = 30 °C
0	4.962 ± 0.025	5.777 ± 0.029	6.688 ± 0.033	7.445 ± 0.037	8.264 ± 0.041	9.139 ± 0.046
0.325 ± 0.019	49.11 ± 0.25	57.14 ± 0.29	65.29 ± 0.33	73.03 ± 0.37	80.69 ± 0.40	88.97 ± 0.44
0.647 ± 0.026	95.50 ± 0.48	111.60 ± 0.56	128.76 ± 0.64	142.86 ± 0.71	157.44 ± 0.79	174.16 ± 0.87
1.092 ± 0.032	158.49 ± 0.80	185.38 ± 0.93	209.4 ± 1.1	236.6 ± 1.1	260.7 ± 1.3	287.4 ± 1.4
2.028 ± 0.036	286.7 ± 1.4	339.4 ± 1.7	380.2 ± 1.9	424.4 ± 2.1	470.8 ± 2.4	517.3 ± 7.5
3.886 ± 0.038	524.2 ± 7.3	610.0 ± 9.3	682.5 ± 9.3	787.3 ± 9.3	853.0 ± 9.3	947.1 ± 9.3
6.250 ± 0.038	800.0 ± 9.2	922 ± 11	1084 ± 11	1214 ± 11	1343 ± 11	1442 ± 11
9.504 ± 0.037	1168 ± 11	1381 ± 13	1561 ± 13	1719 ± 13	1893 ± 13	2107 ± 13
11.360 ± 0.038	1372 ± 12	1585 ± 15	1770 ± 15	2036 ± 15	2250 ± 15	2426 ± 15
ε_{dc}						
0	85.83 ± 0.10	83.921 ± 0.098	82.053 ± 0.083	80.214 ± 0.081	78.362 ± 0.078	76.565 ± 0.082
0.325 ± 0.019	85.81 ± 0.11	83.90 ± 0.11	82.022 ± 0.083	80.189 ± 0.087	78.351 ± 0.082	76.556 ± 0.088
0.647 ± 0.026	85.805 ± 0.094	83.890 ± 0.092	82.047 ± 0.096	80.150 ± 0.090	78.344 ± 0.078	76.547 ± 0.082
1.092 ± 0.032	85.796 ± 0.082	83.876 ± 0.080	82.001 ± 0.079	80.151 ± 0.089	78.319 ± 0.078	76.523 ± 0.090
2.028 ± 0.036	85.745 ± 0.083	83.830 ± 0.081	82.019 ± 0.084	80.135 ± 0.080	78.275 ± 0.078	76.482 ± 0.079
3.886 ± 0.038	85.65 ± 0.10	83.75 ± 0.10	82.146 ± 0.092	80.029 ± 0.082	78.192 ± 0.078	76.424 ± 0.085
6.250 ± 0.038	85.54 ± 0.11	83.64 ± 0.10	81.764 ± 0.080	79.957 ± 0.097	78.118 ± 0.079	76.348 ± 0.099
9.504 ± 0.037	85.380 ± 0.096	83.519 ± 0.094	81.577 ± 0.087	79.836 ± 0.089	77.992 ± 0.077	76.228 ± 0.089
11.360 ± 0.038	85.296 ± 0.090	83.461 ± 0.088	81.534 ± 0.077	79.756 ± 0.078	77.905 ± 0.076	76.166 ± 0.089
τ (ps)						
0	14.910 ± 0.075	12.681 ± 0.064	10.833 ± 0.055	9.365 ± 0.045	8.276 ± 0.047	7.284 ± 0.047
0.325 ± 0.019	14.918 ± 0.096	12.679 ± 0.081	10.833 ± 0.066	9.352 ± 0.048	8.272 ± 0.048	7.277 ± 0.055
0.647 ± 0.026	14.898 ± 0.079	12.667 ± 0.067	10.833 ± 0.057	9.356 ± 0.046	8.272 ± 0.047	7.277 ± 0.048
1.092 ± 0.032	14.899 ± 0.081	12.683 ± 0.069	10.829 ± 0.061	9.337 ± 0.040	8.272 ± 0.047	7.270 ± 0.047
2.028 ± 0.036	14.890 ± 0.088	12.665 ± 0.075	10.825 ± 0.057	9.345 ± 0.043	8.266 ± 0.047	7.266 ± 0.045
3.886 ± 0.038	14.887 ± 0.081	12.663 ± 0.069	10.815 ± 0.059	9.364 ± 0.052	8.266 ± 0.047	7.256 ± 0.045
6.250 ± 0.038	14.886 ± 0.095	12.630 ± 0.081	10.817 ± 0.055	9.331 ± 0.041	8.245 ± 0.047	7.243 ± 0.050
9.504 ± 0.037	14.853 ± 0.087	12.635 ± 0.074	10.800 ± 0.057	9.322 ± 0.045	8.248 ± 0.047	7.238 ± 0.045
11.360 ± 0.038	14.860 ± 0.085	12.646 ± 0.073	10.806 ± 0.060	9.314 ± 0.042	8.243 ± 0.046	7.233 ± 0.049
ε_∞						
0	5.70 ± 0.19	5.53 ± 0.19	6.03 ± 0.23	5.63 ± 0.18	5.26 ± 0.16	5.22 ± 0.19
0.325 ± 0.019	5.68 ± 0.41	5.49 ± 0.40	6.01 ± 0.37	5.66 ± 0.29	5.17 ± 0.19	5.11 ± 0.27
0.647 ± 0.026	5.66 ± 0.25	5.44 ± 0.24	5.99 ± 0.28	5.76 ± 0.27	5.18 ± 0.17	5.03 ± 0.23
1.092 ± 0.032	5.61 ± 0.32	5.45 ± 0.31	5.95 ± 0.35	5.69 ± 0.27	5.20 ± 0.16	4.88 ± 0.24
2.028 ± 0.036	5.59 ± 0.27	5.40 ± 0.26	5.93 ± 0.23	5.63 ± 0.21	5.21 ± 0.16	4.81 ± 0.25
3.886 ± 0.038	5.57 ± 0.25	5.39 ± 0.24	5.84 ± 0.26	6.29 ± 0.32	5.25 ± 0.16	4.55 ± 0.20
6.250 ± 0.038	5.56 ± 0.32	5.35 ± 031	5.98 ± 0.38	6.70 ± 0.23	5.16 ± 0.17	4.45 ± 0.20
9.504 ± 0.037	5.74 ± 0.31	5.39 ± 0.29	5.96 ± 0.29	6.50 ± 0.20	4.94 ± 0.15	4.43 ± 0.18
11.360 ± 0.038	5.96 ± 0.31	5.36 ± 0.28	5.92 ± 0.23	6.21 ± 0.31	4.90 ± 0.15	4.27 ± 0.18

where temperature T is in kelvin, e = 1.60×10^{-19} C is the elementary charge, N_A = 6.02×10^{23} mol^{-1} is Avogadro's number, k_B = 1.38×10^{-23} J/K is the Boltzmann constant, ε_0 = 8.85×10^{-12} F/m is the free space permittivity, and $\varepsilon^0_{dc}(T)$ is the temperature-dependent static permittivity of deionized water (zero concentration) which will be later modeled in Section 4.6.1. Next, the electrophoretic coefficient, $a(T)$ (m$^{3.5}$S/mol$^{1.5}$), and the asymmetric relaxation coefficient, $b(T)$ (m$^{3.5}$S/mol$^{1.5}$) can be written as a function of temperature

$$a(T) = |z_2| \frac{z_1^2 Fe\kappa_0(T)}{6\pi\eta(T)} + |z_1| \frac{z_2^2 Fe\kappa_0(T)}{6\pi\eta(T)} \tag{4.2}$$

$$b(T) = |z_2| \frac{z_1^2 e^2 \kappa_0(T)}{24\pi\varepsilon_0 \varepsilon^0_{dc}(T) k_B T} \frac{1}{1+\sqrt{0.5}} \lambda_1(T) + |z_1| \frac{z_2^2 e^2 \kappa_0(T)}{24\pi\varepsilon_0 \varepsilon^0_{dc}(T) k_B T} \frac{1}{1+\sqrt{0.5}} \lambda_2(T) \tag{4.3}$$

where F = 96,485.33 C/mol is the Faraday constant. The temperature-dependent dynamic viscosity of water $\eta(T)$ (kg m^{-1}s^{-1}), within the temperature range 273 K < T < 373 K, can be modeled by Vogel's equation [17] as

$$\eta(T) = 2.426\times10^{-5} \exp\left(\frac{578.919}{-137.546+T}\right) \tag{4.4}$$

and the temperature-dependent ionic conductivities at infinite dilution of cation $\lambda_1(T)$ (m^{2}S/mol) and anion $\lambda_2(T)$ (m^{2}S/mol) can be modeled as a linear function from the data provided for discrete temperatures in [18]. The linear functions of ion constituents for NaCl

Table 4.4 Linear model of cation $\lambda_1(T)$ and anion $\lambda_2(T)$ conductivities at infinite dilution for NaCl and $NaNO_3$ aqueous solutions with z_1 = 1 and z_2 = -1, and Na_2SO_4 aqueous solution with z_1 = 1 and z_2 = -2. Ionic conductivity values are taken from [18].

	$\lambda_1(T)\times10^4$ (m^{2}S/mol)	$\lambda_2(T)\times10^4$ (m^{2}S/mol)
NaCl	(1.001 ± 0.018)(T - 273) + (25.06 ± 0.35)	(1.411 ± 0.008)(T - 273) + (41.11 ± 0.16)
$NaNO_3$	(1.001 ± 0.018)(T - 273) + (25.06 ± 0.35)	(1.230 ± 0.004)(T - 273) + (40.345 ± 0.079)
Na_2SO_4	(1.001 ± 0.018)(T - 273) + (25.06 ± 0.35)	(3.123 ± 0.003)(T - 273) + (81.940 ± 0.068)

(Na^+ and Cl^-), $NaNO_3$ (Na^+ and NO_3^-), and Na_2SO_4 (Na^+ and SO_4^{2-}) electrolyte systems are shown in Table 4.4.

The temperature-dependent infinite molar conductivity of the whole system at infinite dilution, $\Lambda^{\infty}(T)$ (m^2S/mol), is then calculated as

$$\Lambda^{\infty}(T) = |z_2|\lambda_1(T) + |z_1|\lambda_2(T) \tag{4.5}$$

The temperature- and concentration-d-ependent molar conductivity of the whole system, $\Lambda(T, c)$ (m^2S/mol), can be calculated from (4.1) to (4.5) as

$$\Lambda(T,c) = \Lambda^{\infty}(T) - [a(T) + b(T)]\sqrt{10^3 c} \tag{4.6}$$

where c (mol/L) is the concentration of the whole solute. The temperature- and concentration-dependent specific conductivity $\sigma(T, c)$ (S/m) of the solution can be readily expressed by multiplying the solute concentration c and the molar conductivity Λ for each electrolyte system, as

$$\sigma(T,c) = (10^3 c)\Lambda(T,c) \tag{4.7}$$

The measured specific conductivities σ and the analytical values calculated from (4.7) at different temperatures and concentrations for NaCl, $NaNO_3$, and Na_2SO_4 aqueous solutions are shown in Figure 4.2.

According to Figure 4.2, the specific conductivity increases with increasing the temperature. This is because ions which are responsible for the flowing capability of the electrical current become more agile with rising the temperature, therefore, their mobility in the solution increases. As the electrical current is carried by the ions in aqueous solutions solution, it would be expected that the specific conductivity is strictly proportional to the number of ions, i.e., concentration. Within the range of dilute concentrations (< 0.01 mol/L)

the conductivity follows nearly a linear relationship with concentration, as observed for all solutions in Figure 4.2. As concentration increases moderately, on the orders of a few mol/L, the interaction between ions, represented through the electrophoretic and asymmetric relaxation effects [16], is more pronounced. As a result, the variation of specific conductivity with concentration becomes highly non-linear and decreases considerably.

The surface plots demonstrating the specific conductivity (4.7) as a function of concentration and temperature, along with the measured data (Tables 4.1 to 4.3) for NaCl, $NaNO_3$ and Na_2SO_4 aqueous solutions are shown in Figure 4.3.

4.6. Relaxation Time Modeling

4.6.1. Temperature Dependence of Deionized Water

To develop a model for the relaxation time of ionic aqueous solutions as a function of temperature and concentration, it is first needed to understand the physical chemistry mechanisms behind the temperature dependence of the relaxation time of deionized water (i.e. zero concentration solution). In water system, water molecules form an almost tetrahedrally structured hydrogen-bond (H-bond) network with neighboring molecules. The dominant relaxation process in water centered on ~ 11 to 22 GHz at temperatures 5 to 30 °C [19] is generally attributed to the reorientation of hydrogen-bonded water molecules.

Reorientation of a water molecule is possible only when a sufficient amount of hydrogen bonds is broken [20, 21]. The threshold energy required for a complete separation of a water molecule from neighboring H-bonds and thus making it to reorient, commonly known as Arrhenius activation energy E_a, can be obtained from the empirical Arrhenius equation as

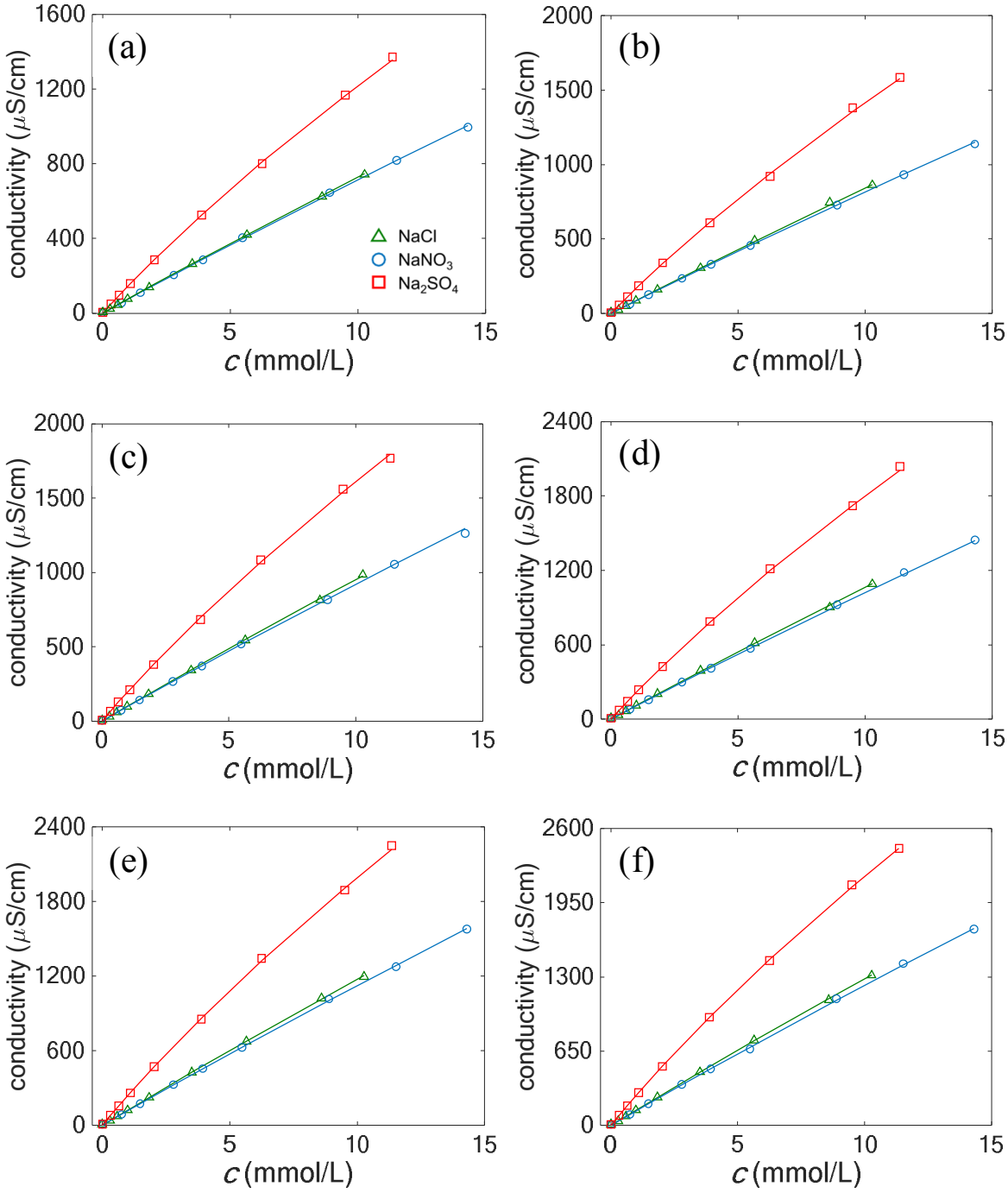

Figure 4.2 Experimental data (symbols), Tables 4.1 to 4.3, and analytical model (solid lines), (4.7), of specific conductivity σ for aqueous solutions of NaCl, $NaNO_3$, and Na_2SO_4 at (a) 5 °C, (b) 10 °C, (c) 15 °C, (d) 20 °C, (e) 25 °C, and (f) 30 °C. The error bars that represent the calculated standard uncertainty (Tables 4.1 to 4.3) are too small to be visible in the figures.

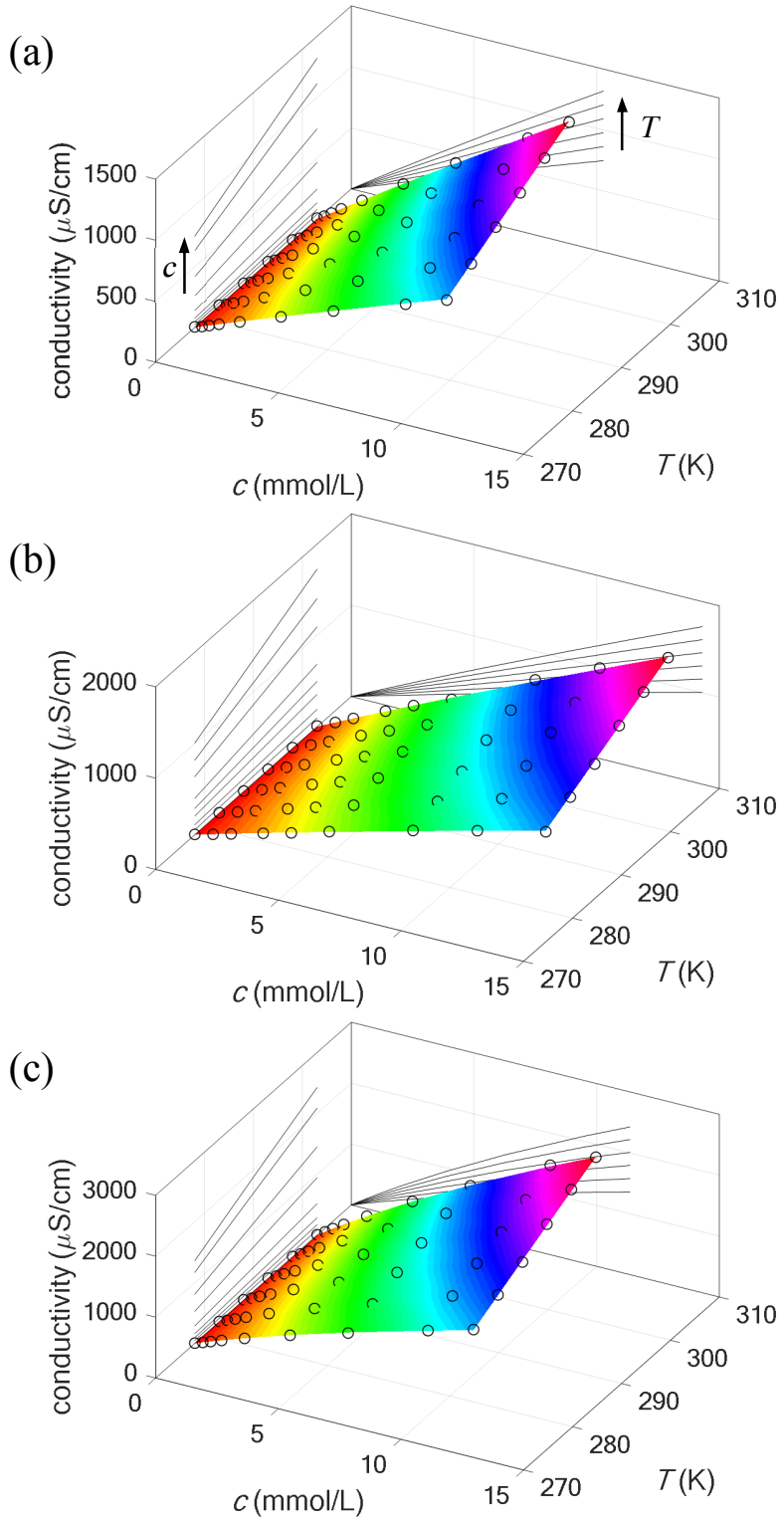

Figure 4.3 Surface plot of specific conductivity (4.7) and experimental data (Tables 4.1 to 4.3) for aqueous solutions of (a) NaCl, (b) $NaNO_3$, and (c) Na_2SO_4. The 2D contour plots of σ-vs-c and σ-vs-T are also projected onto the corresponding planes.

$$\tau^{0}(T) = A\exp\left(\frac{E_a}{RT}\right) \tag{4.8}$$

where $\tau^0(T)$ (s) is the relaxation time of deionized water (zero concentration), A is the pre-exponential factor, R = 8.3145 J mol^{-1} K^{-1} is the universal gas constant, and temperature T is in kelvin. The number of H-bonds connected to a water molecule that needs to be broken for the reorientation of water, however, vary from single bond at high temperature to four bonds in deeply super-cooled water [22]. This implies that the activation energy E_a is expected to be temperature-dependent for water system as such the energy required to break the H-bonds increases with lowering the temperature. The activation energy E_a calculated from the slope of logarithmic-Arrhenius equation $E_a = (R/A)\ \mathrm{dln}(\tau^0)/\mathrm{d}(1/T)$ increases roughly from 18.4 kJ/mol at ~ 30 °C (303 K) to 21.8 kJ/mol at ~ 5 °C (278 K) [22]. As a result the relaxation time cannot be adequately fitted by an Arrhenius equation with temperature-independent parameters.

Taking the fact that the number of H-bonds which must be broken to obtain mobile water molecules which are capable to reorient with the applied electric field depends on

Table 4.5 Eyring fitting parameters for the temperature-dependent model of relaxation time $\tau^0(T)$, (4.9), of deionized water, various authors. The uncertainties represent the standard uncertainty and reflect a level of confidence of approximately 68 %. The sum of squared errors (sse) of the fit corresponding to values calculated by each author is shown. Also see Figure 4.4 for plots representing Arrhenius, (4.8), and Eyring, (4.9), equations as a function of temperature.

	T (°C)	$\Delta H^{\#}_{298}$ (kJ mol^{-1})	$\Delta S^{\#}_{298}$ (J K^{-1} mol^{-1})	$\Delta c^{\#}_{p}$ (J K^{-1} mol^{-1})	sse
Buchner *et al.* [19]	0.35-35.15	15.9 ± 0.2	20.4 ± 0.7	-160 ± 22	0.011
Loginova *et al.* [23]	10-40	17.1	24.8	-	-
This work	5-30	16.27 ± 0.41	21.9 ± 1.4	-172.6 ± 40	0.004

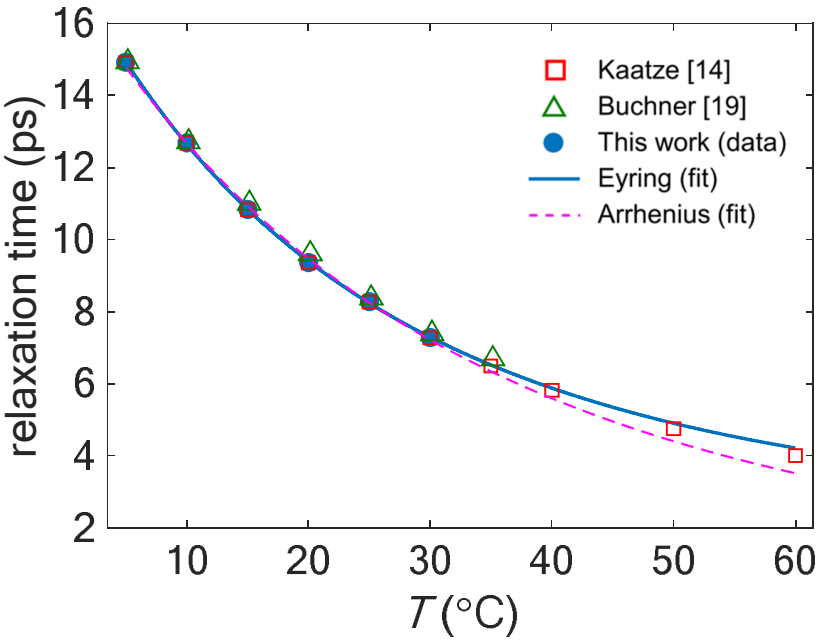

Figure 4.4 Relaxation time τ^0, data (symbols), Arrhenius (4.8), and Eyring (4.9) fitting equations of deionized water as a function of temperature T. The Eyring equation can better predict the relaxation time at higher temperatures than the Arrhenius equation.

temperature, Barthel *et al.* [24] proposed that the relaxation time can be modeled by Eyring's approach originating from the transition state theory [25] as

$$\tau^0(T) = \frac{h}{k_B T} \exp\left[\frac{\Delta G^{\#}(T)}{RT}\right] \tag{4.9}$$

with temperature-dependent modified Gibbs free energy of activation, $\Delta G^{\#}$ (J mol^{-1}), as

$$\Delta G^{\#}(T) = \Delta H^{\#}_{298} + \Delta c^{\#}_p (T - 298) - T\left(\Delta S^{\#}_{298} + \Delta c^{\#}_p \ln\frac{T}{298}\right) \tag{4.10}$$

where $\Delta H^{\#}_{298}$ (J mol^{-1}), $\Delta S^{\#}_{298}$ (J K^{-1} mol^{-1}), and $\Delta c^{\#}_p$ (J K^{-1} mol^{-1}) are the standard enthalpy of activation, standard entropy of activation, and the standard heat capacity of water, h = 6.26×10^{-34} m^{2}kg/s is the Planck constant, and k_B = 1.38×10^{-23} J/K is the Boltzmann constant.

The experimental relaxation times of deionized water (c = 0) as listed in Table 4.1 for temperature range from 5 °C to 30 °C are fitted using the Eyring equation (4.9). The Eyring fitting parameters are shown in Table 4.5. The resulting plot is also depicted in Figure 4.4.

4.6.2. Temperature Dependence of Ionic Aqueous Solutions

The concentration-dependent empirical model of relaxation time at a constant temperature was proposed by Chen *et al*. [26] (Also see Chapter 1). In this section the model is developed to include the temperature dependence of the relaxation time for NaCl, $NaNO_3$ and Na_2SO_4 aqueous solutions within the range of concentrations and temperatures studied in this work. The concentration-dependent relaxation time $\tau(c)$ (s) at each temperature can be modeled as

$$\tau(c) = \alpha_1 \exp(-\alpha_2 c) + (\tau^0 - \alpha_1) \tag{4.11}$$

where α_1 (s) and α_2 (L/mol) are adjustable fitting parameters extracted through the fitting procedure at each temperature. The experimental relaxation times of NaCl, $NaNO_3$ and Na_2SO_4 aqueous solutions as listed in Tables 4.1 to 4.3 were fitted using (4.11) at each temperature (5 °C to 30 °C) and the fitting parameters α_1 and α_2 were calculated as in Table 4.6. The resulting plots are also depicted in Figure 4.5.

The relaxation time of medium-sized ions (radii between 1.5 to 3 Å) of NaCl, $NaNO_3$, and Na_2SO_4 aqueous solutions - the *negative hydration* effect – has been shown to decrease as concentration increases [27]. In general, this is equivalent to an increase in the percentage of bonds broken when ions are added to water. Therefore, the freedom of orientation of water molecules under the applied electric field increases which results in faster reorientations (i.e. smaller relaxation times). The resulting decrement in the relaxation time, characterized by α_1, follows the trend NaCl > $NaNO_3$ > Na_2SO_4 at various temperatures. The difference in

relaxation times due to ions has been attributed under structure maker and structure breaker effects [6, 27]. The structure-maker ions are small or highly charged ions, e.g. SO_4^{2-} with electron valency $z_2 = 2$, which can force water molecules beyond the hydration layer to all orient toward the ion. These ions exhibit stronger forces with water molecules than the neighboring H-bond forces so the reorientation of water molecules becomes slower (i.e. less decrease in relaxation time). On the other hand, the structure-breaker ions are large ions which do not have a strong enough force to orient water molecules beyond the hydration layer. This effect which is more pronounced for larger ions exhibits weaker interactions with water molecules than the neighboring H-bond forces so the water molecules can reorient faster (i.e. more decrease in relaxation time). The ionic radius of Cl^-, i.e., 184 pm, is greater than the ionic radius of NO_3^-, i.e., 179pm [28], thus, the decrement in relaxation time for Cl^- system is larger than NO_3^- system.

As temperature increases, the weaker drop in relaxation time with concentration is observed (i.e. α_1 decreases) for NaCl, $NaNO_3$, and Na_2SO_4 aqueous solutions. This is because the hydrogen bonds needed to be broken for the reorientation of water molecule has been already ruptured by the elevated temperature [23]. Likewise, as temperature increases the slope of variation of the relaxation time which is described by $\exp(-\alpha_2)$ becomes smaller.

Considering the range of uncertainties associated with α_1 and α_2 (Table 4.6) for various temperatures, the temperature dependence of these parameters can be best modeled by a linear behavior. By employing (4.9) and (4.10) in (4.11), the complete temperature- and concentration-dependent model of the relaxation time $\tau(c, T)$ for NaCl, $NaNO_3$, and Na_2SO_4 aqueous solutions can be obtained as

$$\tau(T,c) = \hat{\alpha}_1(T)\exp\left[-\hat{\alpha}_2(T)c\right] + \left\{\frac{h}{k_B T}\exp\left[\frac{\Delta H^{\#}_{298} + \Delta c^{\#}_p (T-298) - T\left(\Delta S^{\#}_{298} + \Delta c^{\#}_p \ln\frac{T}{298}\right)}{RT}\right] - \hat{\alpha}_1(T)\right\} \quad (4.12)$$

where $\hat{\alpha}_1(T)$ and $\hat{\alpha}_2(T)$ are the temperature-dependent linear functions calculated for α_1 and α_2 (Table 4.6), respectively, and are given in Table 4.7. Eyring fitting parameters $\Delta H^{\#}_{298}$ (J mol^{-1}), $\Delta S^{\#}_{298}$ (J K^{-1} mol^{-1}), and $\Delta c^{\#}_p$ (J K^{-1} mol^{-1}) are also listed in the table (taken from Table 4.5).

The surface plots demonstrating the relaxation time (4.12) as a function of concentration and temperature, along with the measured data (Tables 4.1 to 4.3) for NaCl, $NaNO_3$ and Na_2SO_4 aqueous solutions are shown in Figure 4.6. The required parameters to fully describe the model for each ionic aqueous solution are listed in Table 4.7. The sum of squared errors (sse) of the surface-plot fits (4.12) and the measured data are also given in Table 4.7.

Table 4.6 Parameters of empirical relaxation time model, (4.11), of aqueous NaCl (c = 0 to 10.275 mmol/L), $NaNO_3$ (c = 0 to 14.31 mmol/L), and Na_2SO_4 (c = 0 to 11.36 mmol/L) solutions for discrete temperatures from 5 °C to 30 °C. The relaxation time of deionized water τ^0 at each temperature is taken from Table 4.1. The standard uncertainties of the fitting parameters were calculated based on Monte Carlo method and provide a level of confidence of approximately 68 %.

NaCl						
T (°C)	5	10	15	20	25	30
α_1 (ps)	0.263 ± 0.093	0.221 ± 0.073	0.208 ± 0.063	0.187 ± 0.063	0.208 ± 0.025	0.206 ± 0.047
α_2 (L/mol)	100 ± 44	95 ± 40	140 ± 55	152 ± 71	382 ± 110	204 ± 89
$NaNO_3$						
α_1 (ps)	0.178 ± 0.062	0.150 ± 0.049	0.136 ± 0.042	0.127 ± 0.041	0.122 ± 0.035	0.139 ± 0.036
α_2 (L/mol)	95 ± 43	111 ± 47	152 ± 71	116 ± 52	170 ± 79	222 ± 93
Na_2SO_4						
α_1 (ps)	0.082 ± 0.039	0.049 ± 0.020	0.043 ± 0.022	0.061 ± 0.024	0.042 ± 0.021	0.056 ± 0.021
α_2 (L/mol)	90 ± 51	187 ± 94	107 ± 57	131 ± 60	131 ± 58	197 ± 89

Table 4.7 Parameters of temperature- and concentration-dependent relaxation time model, (4.12), for aqueous NaCl (c = 0 to 10.275 mmol/L), $NaNO_3$ (c = 0 to 14.31 mmol/L), and Na_2SO_4 (c = 0 to 11.36 mmol/L) solutions. The standard uncertainties of the fitting parameters were calculated based on Monte Carlo method and provide a level of confidence of approximately 68 %. The sum of squared errors (sse) of the surface-plot fits and the measured data are also shown.

	$\hat{\alpha}_1(T)$ (ps)	$\hat{\alpha}_2(T)$ (L/mol)	$\Delta H^{\#}_{298}$	$\Delta S^{\#}_{298}$	$\Delta c^{\#}_p$	sse
NaCl	$(-0.0012 \pm 0.0010)(T - 273) + (0.237 \pm 0.023)$	$(6.5 \pm 3.2)(T - 273) + (49 \pm 47)$	16.27 ± 0.41 (kJ mol^{-1})	20.4 ± 0.7 (J K^{-1} mol^{-1})	-172.6 ± 40 (J K^{-1} mol^{-1})	0.069
$NaNO_3$	$(-0.0012 \pm 0.0008)(T - 273) + (0.160 \pm 0.017)$	$(3.7 \pm 1.4)(T - 273) + (73 \pm 21)$				0.066
Na_2SO_4	$(-0.0002 \pm 0.0007)(T - 273) + (0.056 \pm 0.015)$	$(2.5 \pm 1.8)(T - 273) + (85 \pm 32)$				0.079

4.7. Static Permittivity Modeling

4.7.1. Temperature Dependence of Deionized Water

Similar to Section 4.5, the first step needed to develop a temperature- and concentration- dependent model for the static permittivity of ionic aqueous solutions is to understand the mechanisms behind the temperature dependence of the static permittivity of deionized water (i.e. zero concentration solution). The analysis here starts with the Kirkwood-Frohlich equation [3], which relates the macroscopic permittivity parameters to microscopic dipolar mechanisms, as

$$\frac{\left(\varepsilon_{dc}^{0}-\varepsilon_{\infty}\right)\left(2\varepsilon_{dc}^{0}+\varepsilon_{\infty}\right)}{\varepsilon_{dc}^{0}\left(\varepsilon_{\infty}+2\right)^{2}}=\frac{N_{A}g\mu^{2}c_{d}}{9k_{B}\varepsilon_{0}T} \tag{4.13}$$

where ε^0_{dc} is the static permittivity of deionized water (zero concentration), ε_∞ (infinite permittivity) is the permittivity at a frequency well above that of the dominant relaxation frequency, ε_0 = 8.85×10^{-12} F/m is the free space permittivity, N_A = 6.02×10^{23} mol^{-1} is Avogadro's number, k_B = 1.38×10^{-23} J/K is the Boltzmann constant, μ is the dipolar moment of water molecule, c_d (mol/m^3) is the concentration of dipolar moments (water

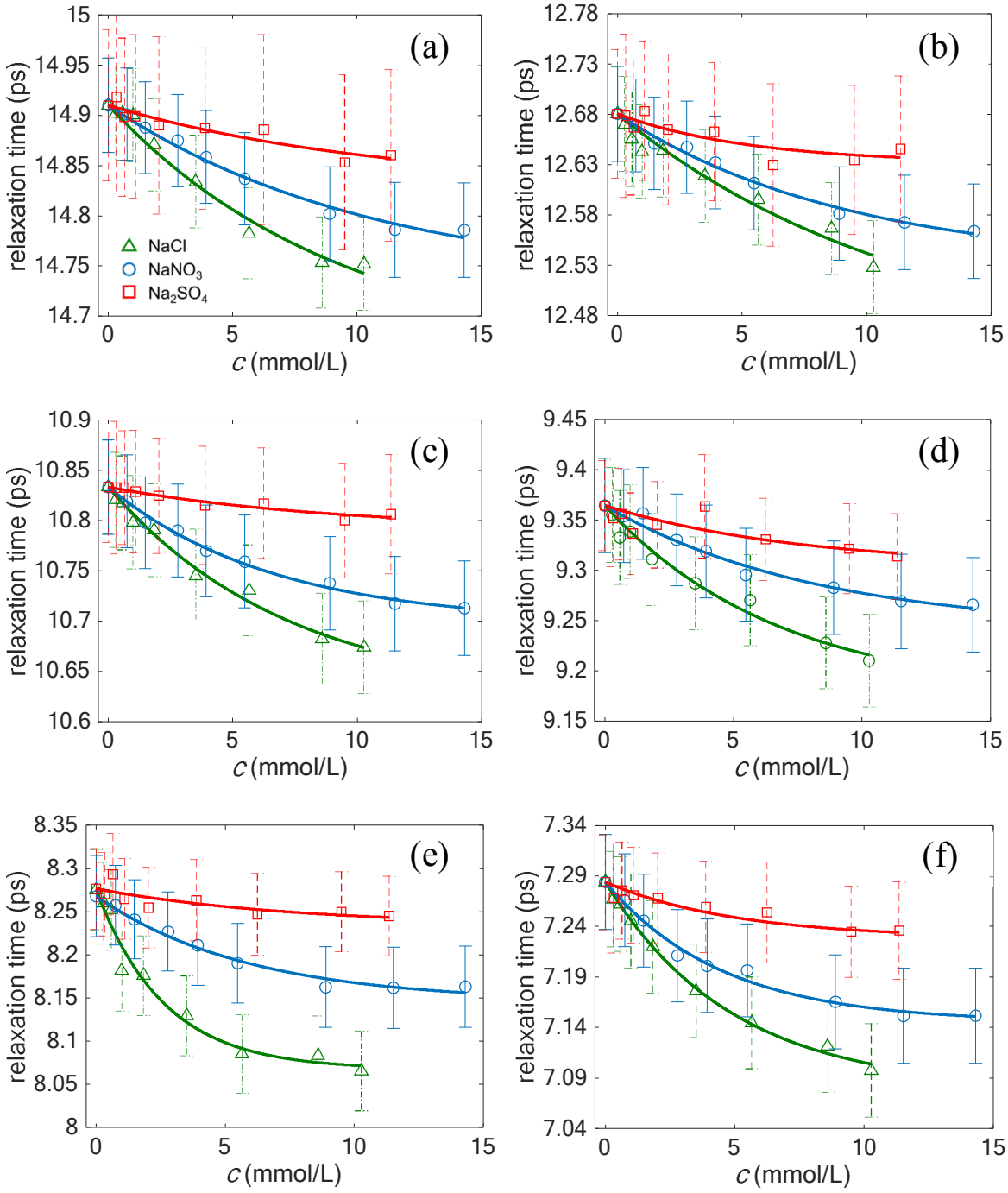

Figure 4.5 Experimental data (symbols), Tables 4.1 to 4.3, and empirical model (solid lines), (4.11) and Table 4.6, of relaxation time for aqueous solutions of NaCl, $NaNO_3$, and Na_2SO_4 at (a) 5 °C, (b) 10 °C, (c) 15 °C, (d) 20 °C, (e) 25 °C, and (f) 30 °C. The error bars represent the calculated standard uncertainty based on the Monte Carlo method (Tables 4.1 to 4.3) and reflect a level of confidence of approximately 68 %.

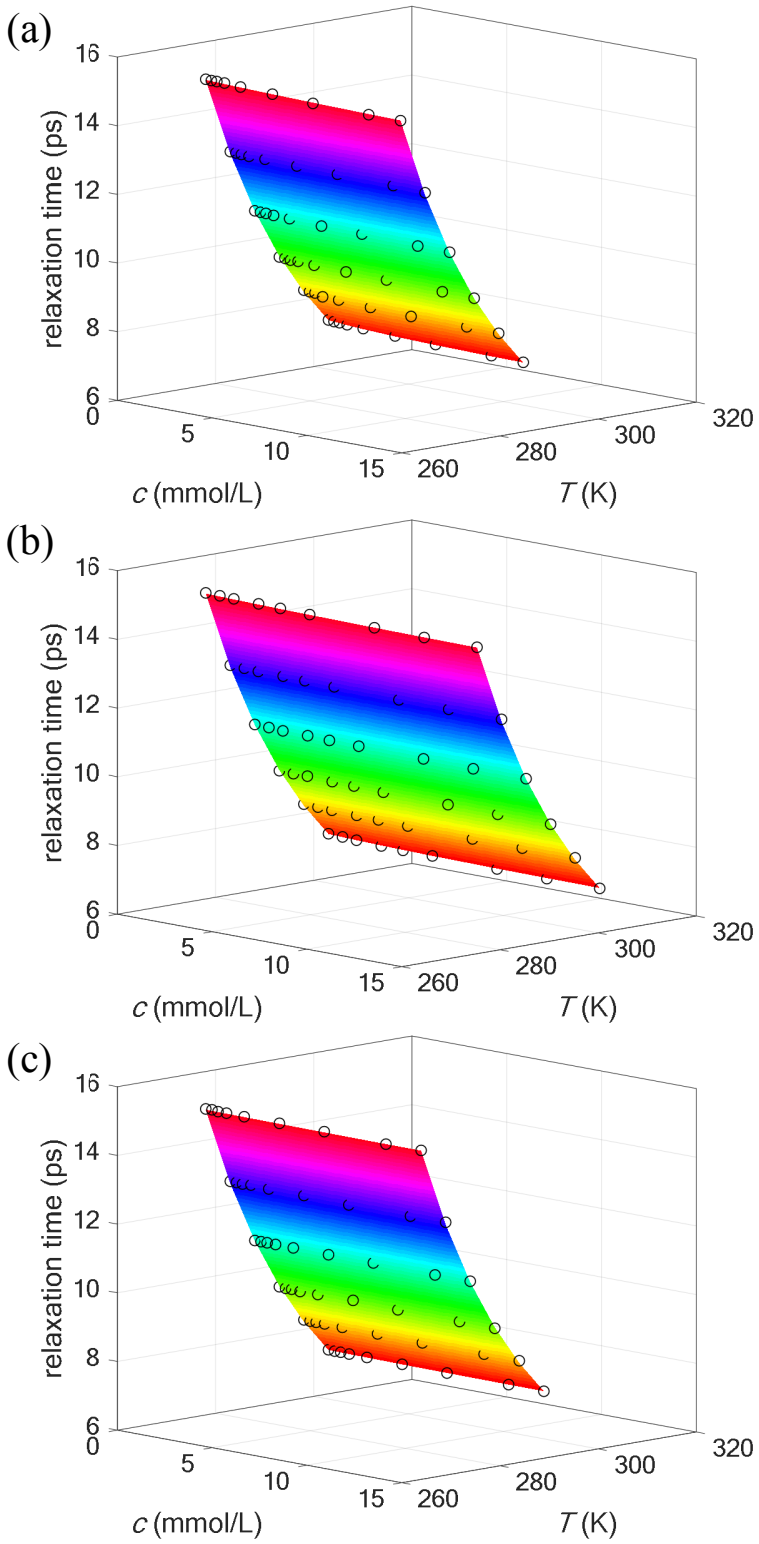

Figure 4.6 Surface plot of temperature- and concentration-dependent relaxation time model (4.12) and experimental data (Tables 4.1 to 4.3) for aqueous solutions of (a) NaCl, (b) $NaNO_3$, and (c) Na_2SO_4.

molecules) who contribute to the total polarization, and g is the Kirkwood correlation factor. After a few mathematical manipulations on (4.13), ε^0_{dc} can be written as

$$\varepsilon^0_{dc} = \frac{N_A g \mu^2 c_d \left(\varepsilon_\infty + 2\right)^2}{36 k_B \varepsilon_0 T} + \frac{\varepsilon_\infty}{4} + \sqrt{\left(\frac{N_A g \mu^2 c_d \left(\varepsilon_\infty + 2\right)^2}{36 k_B \varepsilon_0 T} + \frac{\varepsilon_\infty}{4}\right)^2 + \frac{\varepsilon_\infty{}^2}{2}} \tag{4.14}$$

in which ε_∞, g, μ, and c_d are all temperature-dependent parameters and must be treated separately, as discussed next.

4.7.1.1. Infinite permittivity

The infinite permittivity ε_∞ can be written from Kirkwood-Frohlich equation, (4.13), as

$$\begin{aligned} \varepsilon_\infty &= \frac{-\varepsilon^0_{dc}\left(1+4X\right) + \left(8X\varepsilon^0_{dc}{}^3 + 9\varepsilon^0_{dc}{}^2 + 8X\varepsilon^0_{dc}{}^2 - 16X\varepsilon^0_{dc}\right)^{0.5}}{2\left(1+X\varepsilon^0_{dc}\right)} \\ &= \frac{-\varepsilon^0_{dc}\left(1+4X\right) + \sqrt{8}X^{0.5}\varepsilon^0_{dc}{}^{1.5}\left[1 + \frac{\left(9+8X\right)\varepsilon^0_{dc} - 16X}{8X\varepsilon^0_{dc}{}^2}\right]^{0.5}}{2\left(1+X\varepsilon^0_{dc}\right)} \end{aligned} \tag{4.15}$$

where

$$X = \frac{N_A g \mu^2 c_d}{9 k_B \varepsilon_0 T} \tag{4.16}$$

Taking crude estimates for g = 1, c_d = 5.5 $\times 10^4$ (mol/m3), μ = 1.855×3.336×10^{-30} C.m (1.855 D), T = 25 °C, and ε^0_{dc} = 78.36 one would get $X \approx 4$, and the second term in the bracket of (4.15), $[(9+8X)\varepsilon^0_{dc} - 16X / 8X\varepsilon^0_{dc}{}^2] \approx 0.01$.Using the identity $(1+A)^n \approx 1+nA$ for A < 1, and approximating the bracket term, (4.15) can be written as

$$\varepsilon_\infty \simeq \frac{16\sqrt{8}X^{1.5}\varepsilon^0_{dc}{}^{3.5} + \sqrt{8}\left(9+8X\right)X^{0.5}\varepsilon^0_{dc}{}^{2.5} - 16\sqrt{8}X^{1.5}\varepsilon^0_{dc}{}^{1.5} - \left(1+4X\right)\varepsilon^0_{dc}{}^{0.5}}{32X^2\varepsilon^0_{dc}{}^3 + 32X\varepsilon^0_{dc}{}^2} \tag{4.17}$$

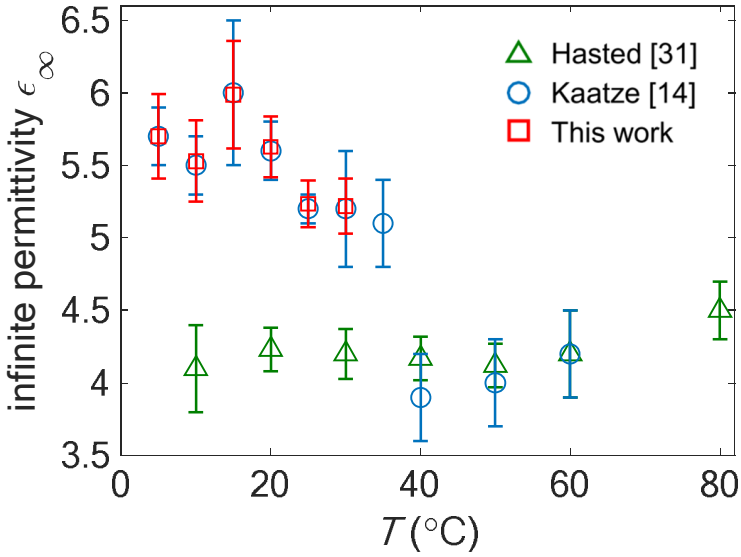

Figure 4.7 Measured ε_∞ values for the deionized water, various authors. The standard uncertainty ranges corresponding to 68% confidence interval are also shown.

Table 4.8 Estimates of ε_∞ (4.18) from available literature values for ε^0_{dc}, g, c_d, and μ within the lowest and highest reported temperature range available. c_d is approximated by analytical water concentration c_s (refer to Section 4.6.1.3).

T (°C)	ε^0_{dc} [14]	g [29]	μ (C.m) [30]	c_s (mol/m3) (4.25)	ε_∞ (4.18)
5	87.91	2.6	$2.45\times3.336\times10^{-30}$	5.55×10^{4}	3.01
62	66.7	2.49	$2.41\times3.336\times10^{-30}$	5.45×10^{4}	3.05

in which taking the highest powers of the fraction reduces (4.17) to

$$\varepsilon_\infty \simeq \sqrt{2}\left(\frac{\varepsilon^0_{dc}}{X}\right)^{0.5} \simeq \sqrt{2}\left(\frac{9k_B\varepsilon_0 T\varepsilon^0_{dc}}{N_A g\mu^2 c_d}\right)^{0.5} \tag{4.18}$$

The above equation is an approximation that gives underestimated values for ε_∞. However, the range of values that ε_∞ (4.18) may get within the temperature range of this work, i.e., 5 °C to 30 °C, can be obtained by inserting available literature values for ε^0_{dc}, g, μ ,and c_d that contain that temperature range, as listed in Table 4.8. Also shown in Figure 4.7 are the measured ε_∞ values for the deionized water by various authors. As interpreted from Table 4.8 and Figure 4.7, the variation in calculated ε_∞ (4.18)and measured ε_∞ within the

corresponding lowest (5 °C) and highest (30 °C) temperature range will be relatively small compared to the uncertainty range existent in each reported value. As a result, for the purpose of reducing the complexity in deriving a temperature- and concentration-dependent model for static permittivity (4.14), it will be both theoretically and experimentally reasonable to assume that ε_∞ is independent of variation in temperature. In the rest of this chapter, ε_∞ is taken as the average of the measured values from 5 °C to 30 °C which equals $\varepsilon_\infty = 5.55 \pm 0.11$.

4.7.1.2. Kirkwood correlation factor

The Kirkwood correlation factor, g, is a measure of intermolecular angular correlation between the dipole moments (water molecules) in material. The physical interpretation of this is that if one water molecule is aligned along the direction of the applied field, it tends to drag its neighbors (via the H-bonds) into line with it [29]. Increasing thermal agitation broadly speaking distorts or breaks down the H-bond network and so the angular correlation decreases.

A thorough discussion on the history of calculating g has been made by Hasted [31]. Accordingly, the first structural calculation of g was made by Oster and Kirkwood [32]. They assumed that only the N_1 nearest neighbors in the first hydration layer were correlated with the direction of the central water molecule. The number of nearest water molecules was calculated from X-ray diffraction methods [33]. The static permittivity calculated by Oster and Kirkwood, however, decrease too slowly with increasing temperature. Lennard-Jones and Pople [29] had put forward the alternative viewpoint of *bond-bending* model. In their model the correlation with water molecules outside the first hydration layer makes an appreciable contribution to the total alignments of water molecules due to hydrogen bonds. The *bond-bending* model shows to be adequate over a smaller temperature range, but at

higher temperatures, particularly above 100 °C, it would yield static permittvities systematically high [31].

Haggis *et al*. [20] made a statistical analysis of their *bond-breaking* model. In this model water is described as a structure in which each water molecule is striving to bond itself tetrahedrally to four neighboring molecules, but in which bonds are continually breaking and reforming. For a certain percentage p of hydrogen bonds broken at a given temperature T, there will be an equivalent percentage n_i of molecules forming i = 0, 1, 2, 3, or 4 bonds. The Kirkwood correlation factor g and the dipolar moment μ presented in (4.13) are then written as [20]

$$g\mu^2 = \sum_{i=0}^{4} \frac{n_i(T)}{100} g_i(T)\,\mu_i^2(T) \tag{4.19}$$

where $g_i(T)$ and $\mu_i(T)$ are the correlation factor and the dipolar moment of a water molecule connected to i hydrogen bond, which depend on temperature. From the data presented in [20] for n_i, g_i, and μ_i at five discrete temperatures (T = 0, 25, 60, 100, 200, and 300 °C) and corresponding percentage of hydrogen bonds broken (p = 9, 11.3, 15.8, 20.2, 34.1, and 61.3 %), the right hand side of (4.19) can be well approximated by a linear function with respect to p (R-squared = 0.9938) as

$$\sum_{i=0}^{4} \frac{n_i(T)}{100} g_i(T)\,\mu_i^2(T) \simeq -v_1' p + v_2' \tag{4.20}$$

where v'_1 and v'_2 are the fitting parameters of the linear model. The percentage of hydrogen bonds broken p is related to temperature T through [20]

$$p = 1 - \frac{L(T) - W_{273}}{2\Delta H_{273}} \tag{4.21}$$

where $L(T)$ (J/mol) is the latent heat of vaporization, W_{273} = 10.46×10^3 J/mol is the energy necessary to overcome the van der Waals forces at 0 °C (273 K), and ΔH_{273}= 18.83×10^3 J/mol is the activation enthalpy of hydrogen-bond breaking down at 0 °C (273 K). As in Haggis's time there were no available data for $L(T)$ for a broader range of temperatures, we can take our step from this point and employ a temperature-dependent model of $L(T)$. Xiang [34] constructed a three-parameter system-dependent physical model for the latent heat of vaporization $L(T)$ of water covering the entire range from the triplet point temperature T_t = 0.16 °C (273.16 K) to the critical point T_c = 374.096 °C (647.096 K) as

$$L = 6.847RT_c\left[\frac{\left(\frac{T_c}{T}-1\right)^{0.325}+1.738\left(1-\frac{T}{T_c}\right)^{0.435}}{1+1.391\left(1-\frac{T}{T_c}\right)}\right] \tag{4.22}$$

where T and T_c are in kelvin, and R = 8.3145 J mol^{-1} K^{-1} is the universal gas constant. Inserting (4.22) into (4.21) and then employing it in (4.20), we get

$$\sum_{i=0}^{4}\frac{n_i(T)}{100}g_i(T)\mu_i^2(T) \simeq \frac{6.847v_1'RT_c}{2\Delta H_{273}}\left[\frac{\left(\frac{T_c}{T}-1\right)^{0.325}+1.738\left(1-\frac{T}{T_c}\right)^{0.435}}{1+1.391\left(1-\frac{T}{T_c}\right)}\right]+\left[v_2'-v_1'\left(1+\frac{W_{273}}{2\Delta H_{273}}\right)\right] \tag{4.23}$$

Finally, employing (4.23) into (4.19), we can formulate a model for $g\mu^2$ as

$$g\mu^2 \simeq \left\{\frac{v_1 6.847RT_c}{2\Delta H_{273}}\left[\frac{\left(\frac{T_c}{T}-1\right)^{0.325}+1.738\left(1-\frac{T}{T_c}\right)^{0.435}}{1+1.391\left(1-\frac{T}{T_c}\right)}\right]+\left[v_2-v_1\left(1+\frac{W_{273}}{2\Delta H_{273}}\right)\right]\right\}\mu_0^2 \tag{4.24}$$

where v_1 and v_2 are the adjustable fitting parameters which will be used to fit the measured static permittivity within the temperature range of this work (5 °C to 30 °C), and μ_0 = $1.854\times3.336\times10^{-30}$ C.m (1.854 D) [35] is the dipolar moment of an unbonded water molecule which is unaffected by any neighboring molecule via hydrogen bond.

4.7.1.3. Hydrogen-bonded molecules concentration

The concentration of dipolar moments (water molecules) c_d, which contribute to the dominant relaxation process, is due to the concentration of hydrogen-bonded (H-bonded) water molecules. This concentration, however, is not directly accessible, because, in the water system, H-bonded and free (single) water molecules co-exist at the same time. The free water molecules, which are not connected to any hydrogen bond, are responsible for a weaker high-frequency relaxation process at around ~ 120 GH. The analytical solvent (water) concentration c_s, which can be calculated directly from the density ρ (g/L) and the molecular weight M = 18.0153 (mol/g) of water, as

$$c_s(T) = \frac{10^3 \rho(T)}{M} \tag{4.25}$$

comprises the total concentration of water molecules including H-bonded and free molecules. As a result, it is permissible to write c_d in terms of c_s as

$$c_d(T) = \xi c_s(T) \tag{4.26}$$

where $0 < \xi < 1$ is assumed to be constant. The temperature-dependent water density $\rho(T)$ (g/L) can be written based on Kell formula as [36]

$$\begin{aligned}\rho(T) = 999.8529 + 5.3787\times10^{-2}(T-273) - 7.5964\times10^{-3}(T-273)^2 \\ +4.2554\times10^{-4}(T-273)^3 - 1.3432\times10^{-7}(T-273)^4\end{aligned} \tag{4.27}$$

4.7.1.4. Model

After taking care of temperature dependence of ε_∞, g, μ, and c_d in Sections 4.6.1.1 to 4.6.1.3, the complete model temperature-dependent static permittivity model of the deionized water, $\varepsilon^0_{dc}(T)$, can be derived by employing (4.24) to (4.27) into (4.14) as

$$\varepsilon^0_{dc}(T) = \frac{N_A \mu_0^2 G\left(\frac{10^3 \rho(T)}{M}\right)(\varepsilon_\infty + 2)^2}{36 k_B \varepsilon_0 T} + \frac{\varepsilon_\infty}{4} + \sqrt{\left(\frac{N_A \mu_0^2 G\left(\frac{10^3 \rho(T)}{M}\right)(\varepsilon_\infty + 2)^2}{36 k_B \varepsilon_0 T} + \frac{\varepsilon_\infty}{4}\right)^2 + \frac{\varepsilon_\infty{}^2}{2}} \tag{4.28}$$

where G is

$$G = \frac{v_1 6.847 R T_c}{2\Delta H_{273}} \left[\frac{\left(\frac{T_c}{T} - 1\right)^{0.325} + 1.738\left(1 - \frac{T}{T_c}\right)^{0.435}}{1 + 1.391\left(1 - \frac{T}{T_c}\right)} \right] + \left[v_2 - v_1\left(1 + \frac{W_{273}}{2\Delta H_{273}}\right) \right] \tag{4.29}$$

and v_1 and v_2 are the adjustable fitting parameters (ξ is also captured by v_1 and v_2). The experimental static permittivities of deionized water (c = 0) as listed in Table 4.1 for temperature range from 5 °C to 30 °C are fitted using (4.28). The corresponding parameters are listed in Table 4.9. The resulting plot is also shown in Figure 4.8.

4.7.2. Temperature Dependence of Ionic Aqueous Solutions

The concentration-dependent empirical model of static permittivity at a constant temperature was proposed in Chapter 2. In this section the model is developed to include the temperature dependence of the static permittivity for NaCl, $NaNO_3$ and Na_2SO_4 aqueous solutions within the range of concentrations and temperatures studied in this work. The concentration-dependent static permittivity $\varepsilon_{dc}(c)$ at each temperature can be written as

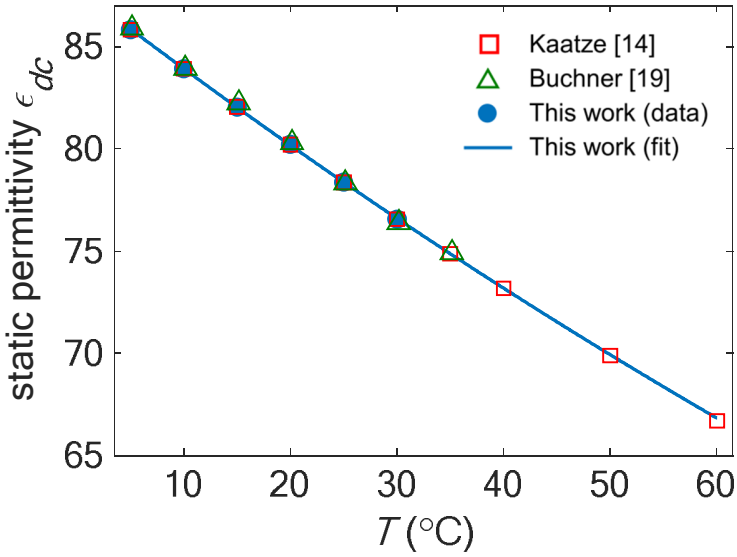

Figure 4.8 Static permittivity, data (symbols) of various authors, and temperature-dependent model (4.28) of deionized water as a function of temperature T.

Table 4.9 Fitting parameters for the temperature-dependent model of static permittivity $\varepsilon^0_{dc}(T)$, (4.28), of deionized water. The fitting procedure was performed for the measured data within 5 °C to 30 °C. The sum of squared errors (sse) of the fit is also shown. Also see Figure 4.8.

ν_1	ν_2	T_c (K)	W_{273} (kJ/mol)	ΔH_{273} (kJ/mol)	ε_∞	sse
0.6811 ± 0.013	0.753 ± 0.001	647.096	10.46	18.83	5.55	0.004

$$\varepsilon_{dc}(c) = \varepsilon^0_{dc} + \gamma_1 c^{0.5}\exp(-\gamma_2 c) - \left[\frac{3v(c)\varepsilon^0_{dc}\left(\varepsilon_e - \varepsilon^0_{dc}\right)}{2\varepsilon^0_{dc} + \varepsilon_e - v(c)\left(\varepsilon_e - \varepsilon^0_{dc}\right)}\right] - \left[\frac{2}{3}\frac{\varepsilon^0_{dc} - \varepsilon^0_\infty}{\varepsilon_0\varepsilon^0_{dc}}\tau^0\sigma(c)\right] - \gamma_3 c \tag{4.30}$$

where γ_1 ($L^{0.5}/mol^{0.5}$), γ_2 (L/mol), and γ_3 (L/mol) are adjustable fitting parameters extracted through the fitting procedure at each temperature, $\varepsilon_e = 2$ is approximated for nonpolar solutes [37], $v(c) = cM/\rho$ is volume fraction of the solute where c (mol/L), ρ (g/L), and M (g/mol)

are concentration of solute, water density, and solute molecular weight, respectively, $\sigma(c)$ (S/m) is the measured specific conductivity of the solution (Tables 4.1 to 4.3), and τ^0 (s) and ε^0_{dc} are the measured relaxation time and static permittivity of the deionized water (Table 4.1). The experimental static permittivities of NaCl, $NaNO_3$ and Na_2SO_4 aqueous solutions as listed in Tables 4.1 to 4.3 were fitted using (4.30) at each temperature (5 °C to 30 °C) and the fitting parameters γ_1, γ_2, and γ_3 were calculated as in Table 4.10. The resulting plots are also depicted in Figure 4.9.

The static permittivity behavior with respect to concentration has been thoroughly discussed for NaCl, $NaNO_3$, and Na_2SO_4 aqueous solutions in Chapter 2. Within the concentration range of this work (~ mmol/L), the Debye-Falkenhagen effect, characterized by γ_1, causes a slight increase in static permittivity with concentration for NaCl and $NaNO_3$ aqueous solutions. In addition, the eventual decline in static permittivity as concentration increases is represented by γ_3 (dielectric saturation effect) which is more pronounced for Na_2SO_4.

As temperature increases, the initial increase in static permittivities is more observable. One speculation is that the corresponding Debye length (Chapter 2) of the induced dipolar moment created by ionic atmosphere polarization increases with temperature. The resulting Debye-Falkenhagen effect (induced polarization), characterized in overall by $\gamma_1\exp(-\gamma_2 c)$, therefore, becomes stronger. The dielectric saturation effect, which is characterized by γ_3, on the other hand, decreases with temperature. This is because water molecules in the hydration layer of ions become more agile with increasing temperature and are no longer bonded to ions, and thus, can contribute to the total polarization (static permittivity) of the system.

Considering the range of uncertainties associated with γ_1, γ_2, and γ_3 (Table 4.10) for various temperatures, the temperature dependence of these parameters can be best modeled by a linear behavior. As a result, the complete temperature- and concentration-dependent model of the static permittivity $\varepsilon_{dc}(c, T)$ for NaCl, $NaNO_3$, and Na_2SO_4 aqueous solutions can be obtained as

$$\varepsilon_{dc}(T,c)=\varepsilon_{dc}^{0}(T)+\hat{\gamma}_1(T)c^{0.5}\exp\left[-\hat{\gamma}_2(T)c\right]-\left\{\frac{3v(c)\varepsilon_{dc}^{0}(T)\left[\varepsilon_e-\varepsilon_{dc}^{0}(T)\right]}{2\varepsilon_{dc}^{0}(T)+\varepsilon_e-v(c)\left[\varepsilon_e-\varepsilon_{dc}^{0}(T)\right]}\right\}$$
$$-\left[\frac{2}{3}\frac{\varepsilon_{dc}^{0}(T)-\varepsilon_{\infty}^{0}}{\varepsilon_0\varepsilon_{dc}^{0}(T)}\tau^{0}(T)\sigma(T,c)\right]-\hat{\gamma}_3(T)c \tag{4.31}$$

where $\hat{\gamma}_1(T)$, $\hat{\gamma}_2(T)$, and $\hat{\gamma}_3(T)$ are the temperature-dependent linear functions calculated for γ_1, γ_2, and γ_3 (Table 4.10), respectively, and are given in Table 4.11. $\sigma(T, c)$ (S/m) is the analytical specific conductivity (4.7), and $\tau^0(T)$ (s) and $\varepsilon^0_{dc}(T)$ are the temperature-dependent models for the relaxation time (4.9) and static permittivity (4.28) of deionized water.

The surface plots demonstrating the static permittivity (4.31) as a function of concentration and temperature, along with the measured data (Tables 4.1 to 4.3) for NaCl, $NaNO_3$ and Na_2SO_4 aqueous solutions are shown in Figure 4.10. The required parameters to fully describe the model for each ionic aqueous solution are listed in Table 4.11. The sum of squared errors (sse) of the surface-plot fits (4.31) and the measured data are also given in Table 4.11.

Table 4.10 Parameters of semi-empirical static permittivity model, (4.30), of aqueous NaCl (c = 0 to 10.275 mmol/L), $NaNO_3$ (c = 0 to 14.31 mmol/L), and Na_2SO_4 (c = 0 to 11.36 mmol/L) solutions for discrete temperatures from 5 °C to 30 °C. The specific conductivities σ for each solution are taken from Tables 4.1 to 4.3. The relaxation time τ^0 and static permittivity ε^0_{dc} of deionized water at each temperature are taken from Table 4.1. The standard uncertainties of the fitting parameters were calculated based on Monte Carlo method and provide a level of confidence of approximately 68 %.

NaCl						
T (°C)	5	10	15	20	25	30
γ_1 ($L^{0.5}/mol^{0.5}$)	0.47 ± 0.21	0.81 ± 0.36	1.45 ± 0.58	2.05 ± 0.76	2.31 ± 0.40	1.87 ± 0.53
γ_2 (L/mol)	190 ± 83	178 ± 92	192 ± 99	147 ± 83	115 ± 49	142 ± 60
γ_3 (L/mol)	5.7 ± 3.5	4.6 ± 3.0	2.8 ± 1.5	0.482 ± 0.079	0.0029 ± 0.0014	0.0040 ± 0.0021
$NaNO_3$						
γ_1 ($L^{0.5}/mol^{0.5}$)	0.56 ± 0.33	0.57 ± 0.33	0.44 ± 0.26	0.77 ± 0.41	0.96 ± 0.50	0.93 ± 0.45
γ_2 (L/mol)	144 ± 70	131 ± 61	60 ± 25	107 ± 49	29 ± 9	95 ± 48
γ_3 (L/mol)	13.3 ± 3.6	12.1 ± 4.0	10.1 ± 2.5	10.3 ± 4.2	10.4 ± 4.1	10.4 ± 3.6
Na_2SO_4						
γ_3 ($L^{0.5}/mol^{0.5}$)*	16.3 ± 3.1	11.8 ± 3.3	14.5 ± 2.8	12.4 ± 2.9	12.0 ± 2.7	8.3 ± 3.1

* For sodium sulphate data, γ_1 and γ_2 are set to zero.

Table 4.11 Parameters of temperature- and concentration-dependent static permittivity model, (4.31), for aqueous NaCl (c = 0 to 10.275 mmol/L), $NaNO_3$ (c = 0 to 14.31 mmol/L), and Na_2SO_4 (c = 0 to 11.36 mmol/L) solutions. In (4.31), $\sigma(T, c)$ (S/m) is calculated from (4.7), $\tau^0(T)$ (s) from (4.9) and the parameters in Table 4.5, and $\varepsilon^0_{dc}(T)$ from (4.28) and the parameters in Table 4.9. The standard uncertainties of the fitting parameters were calculated based on Monte Carlo method and provide a level of confidence of approximately 68 %. The sum of squared errors (sse) of the surface-plot fits and the measured data are also shown.

	$\hat{\gamma}_1(T)$ ($L^{0.5}/mol^{0.5}$)	$\hat{\gamma}_2(T)$ (L/mol)	$\hat{\gamma}_3(T)$ (L/mol)	sse
NaCl	(0.069 ± 0.020)(T - 273) + (0.28 ± 0.39)	(-2.7 ± 1.1)(T - 273) + (208 ± 21)	(-0.256 ± 0.044)(T - 273) + (6.76 ± 0.85)	0.073
$NaNO_3$	(0.020 ± 0.070)(T - 273) + (0.35 ± 0.13)	(-2.9 ± 2.1)(T - 273) + (145 ± 40)	(-0.108 ± 0.046)(T - 273) + (12.97 ± 0.90)	0.082
Na_2SO_4*	-	-	(-0.237 ± 0.094)(T - 273) + (16.7 ± 1.8)	0.126

* For sodium sulphate data, γ_1 and γ_2 are set to zero.

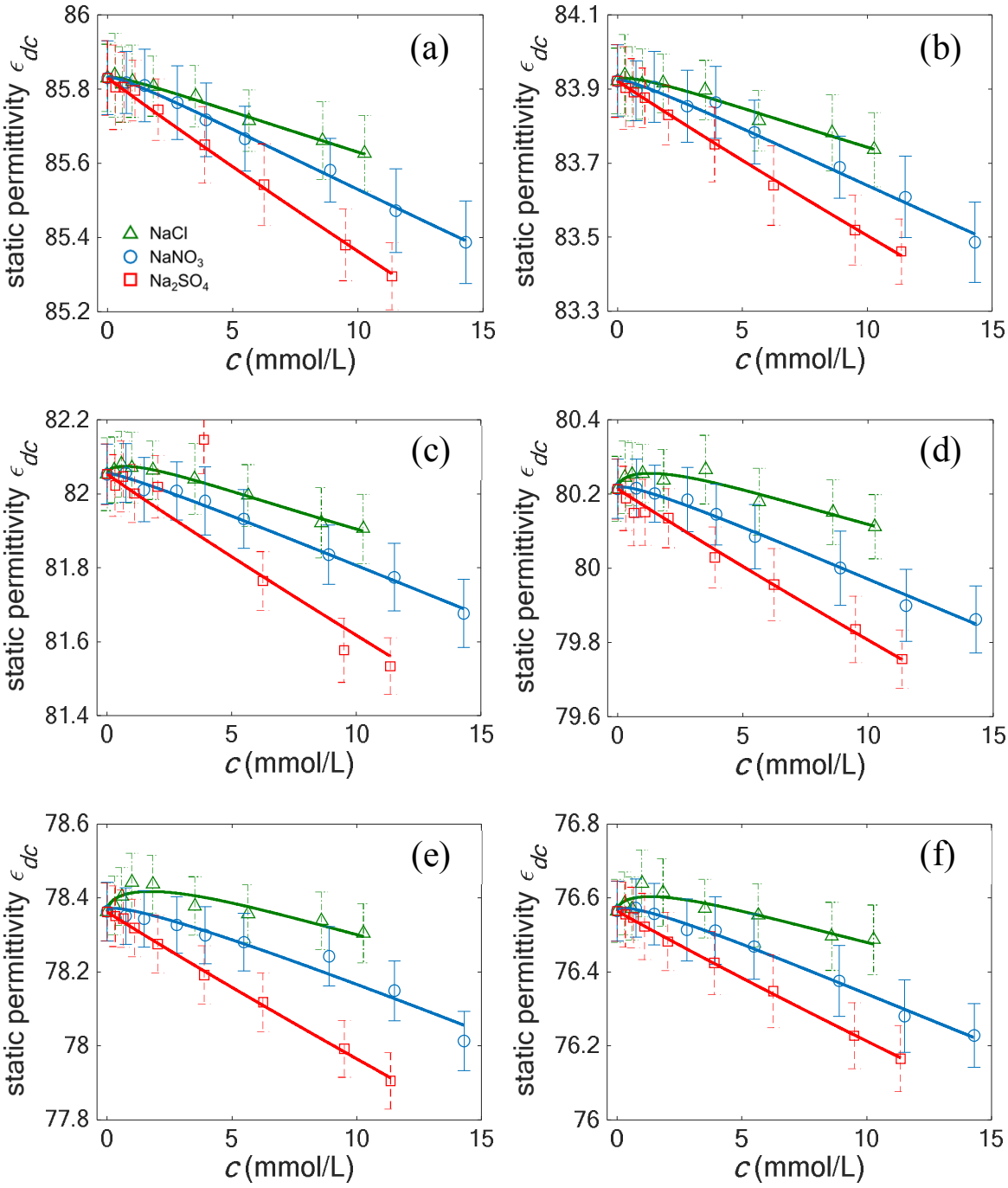

Figure 4.9 Experimental data (symbols), Tables 4.1 to 4.3, and semi-empirical model (solid lines), (4.30) and Table 4.10, of static permittivity for aqueous solutions of NaCl, $NaNO_3$, and Na_2SO_4 at (a) 5 °C, (b) 10 °C, (c) 15 °C, (d) 20 °C, (e) 25 °C, and (f) 30 °C. The error bars represent the calculated standard uncertainty based on the Monte Carlo method (Tables 4.1 to 4.3) and reflect a level of confidence of approximately 68 %.

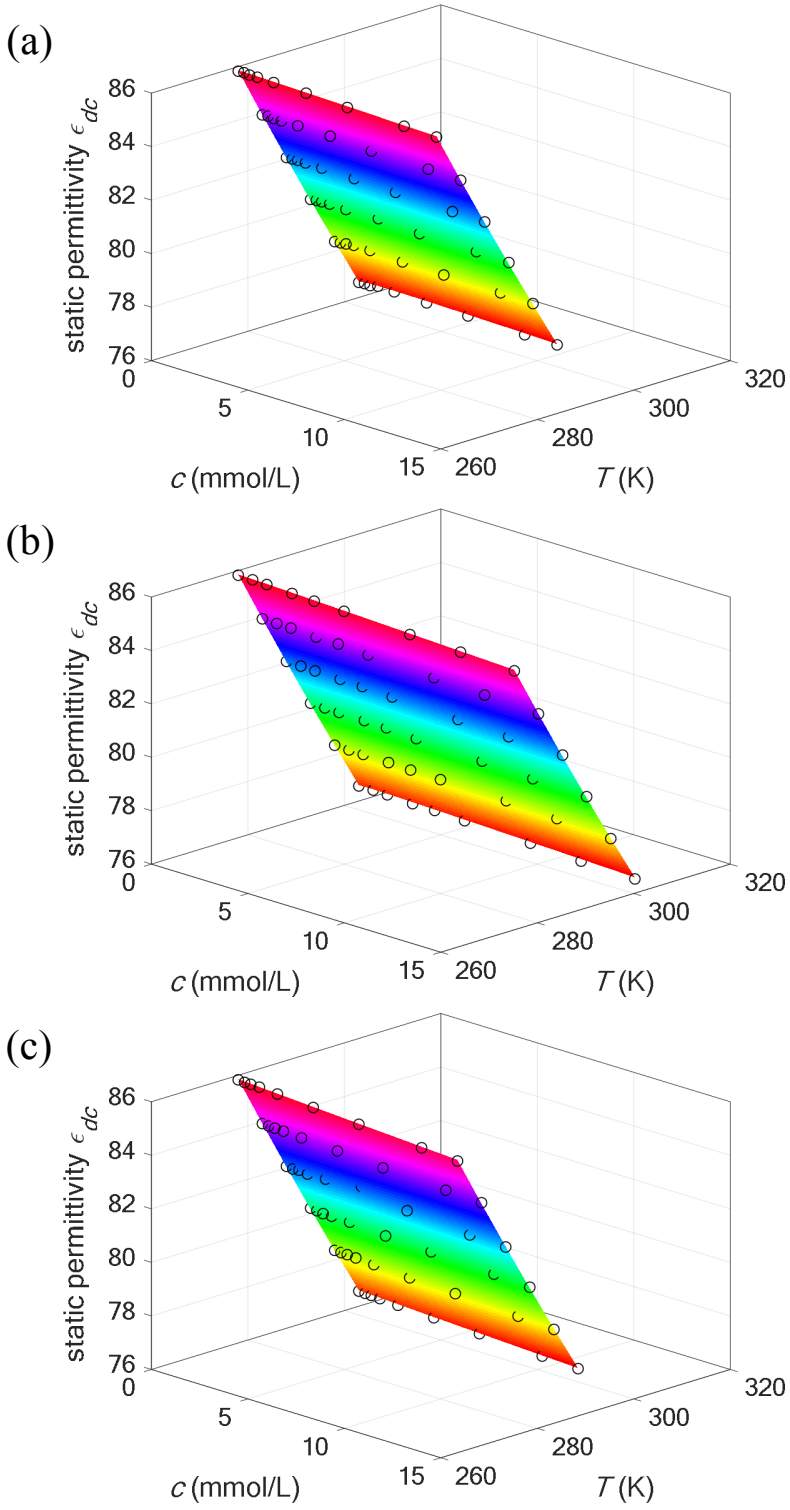

Figure 4.10 Surface plot of temperature- and concentration-dependent static permittivity model (4.31) and experimental data (Tables 4.1 to 4.3) for aqueous solutions of (a) NaCl, (b) $NaNO_3$, and (c) Na_2SO_4.

4.8. Three-Dimensional Trajectory Plots

As discussed in Chapter 3, static permittivity ε_{dc}, relaxation time τ, and specific conductivity σ are recognized as potential indicators of ion concentration and type. To identify an ion and measure its concentration, it was proposed to consider, simultaneously, three dimensions of data. Figure 4.11 shows a 3D trajectory plot of measured and fitted static permittivity ε_{dc}, relaxation time τ, and conductivity σ data for NaCl, $NaNO_3$, and Na_2SO_4 aqueous solutions for different temperatures from 5 °C to 30 °C. According to Figure 4.11, the 3D trajectory for each solution type is a unique curve in ε_{dc}-τ-κ space. This suggests that the ion type and concentration of an unknown electrolyte solution can be found by measuring its dielectric spectrum, extracting ε_{dc}, τ, and σ parameters, and mapping these indicators to a benchmark data set from which the ion type and concentration can be inferred.

4.9. Conclusion

The dielectric spectra of agriculturally-relevant low concentration aqueous solutions of sodium chloride (NaCl), sodium nitrate ($NaNO_3$), and sodium sulphate (Na_2SO_4) that are commonly found in tile drainage waters were analyzed through well-controlled laboratory experiments. The Debye fitting parameters including static permittivity ε_{dc}, relaxation time τ, and specific conductivity σ were carefully modeled as a function of concentration and temperature, based on existent molecular dynamics and mechanisms present in low-concentration ionic aqueous solutions. The analytical model presented for specific conductivity has accounted for the electrophoretic and asymmetric relaxation effects. Within the range of dilute concentrations (< 0.01 mol/L) the conductivity follows nearly a linear relationship with concentration. It was also shown that the specific conductivity increases with increasing temperature, due to increasing mobility of ions. The semi-empirical model

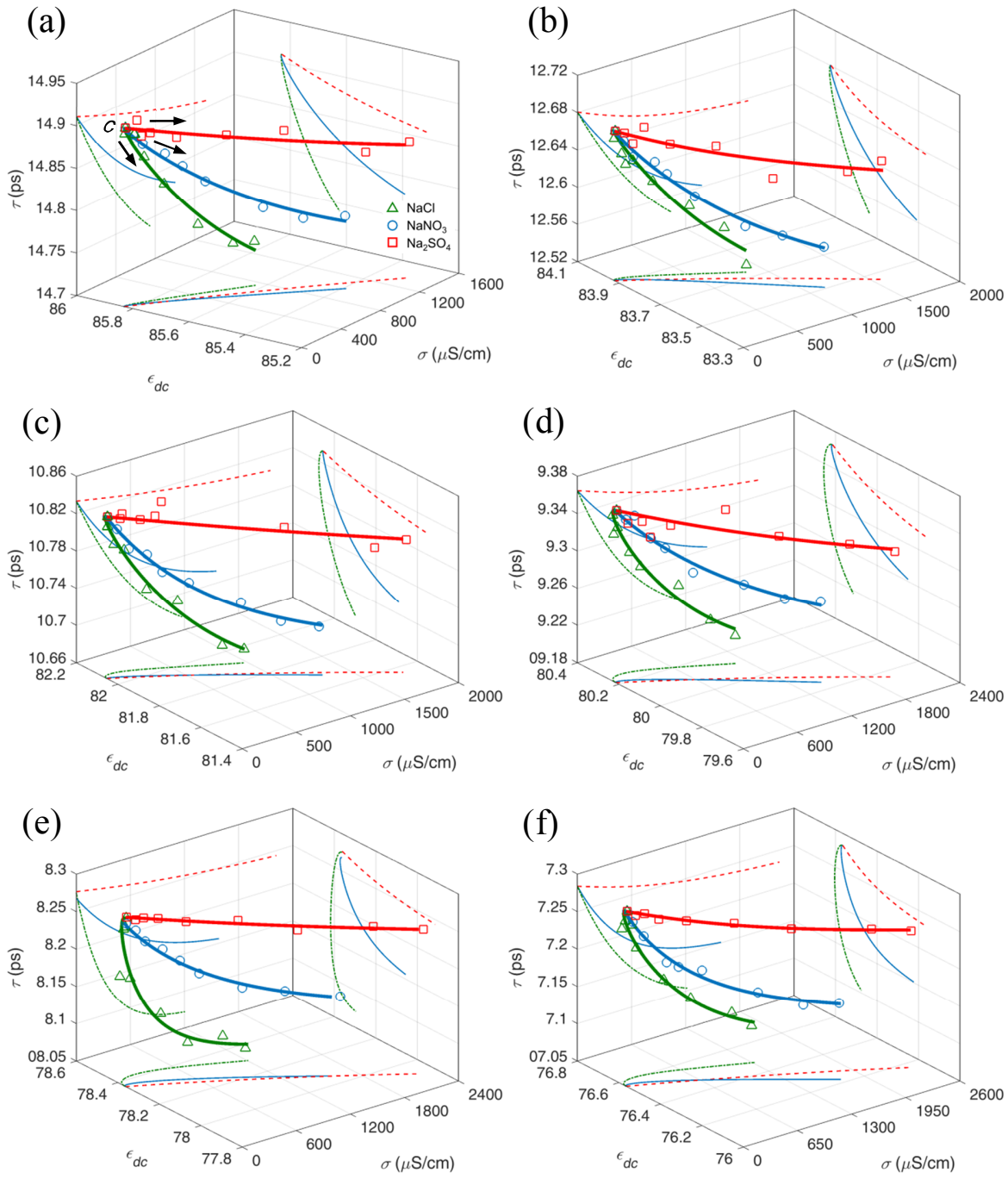

Figure 4.11 3D trajectory plot mapped from extracted measured (symbols) and fitted (solid lines) static permittivity ε_{dc}, relaxation time τ, and conductivity σ of NaCl (c = 0 to 10.275 mmol/L), $NaNO_3$ (c = 0 to 14.31 mmol/L) and Na_2SO_4 (c = 0 to 11.36 mmol/L) solutions at (a) 5 °C, (b) 10 °C, (c) 15 °C, (d) 20 °C, (e) 25 °C, and (f) 30 °C. For clarity, error bars that represent the standard uncertainty of the data (Tables 4.1 to 4.3) are not shown in the figures. The 2D contour plots of each pair of fitted parameters are projected onto the corresponding planes for NaCl (dashed-dotted line), $NaNO_3$ (solid line) and Na_2SO_4 (dashed line)

derived for the relaxation time has been developed on the basis of Eyring's approach. The model successfully estimates the resulting decrement in the relaxation time as a function of temperature and concentration. The resulting decrement in the relaxation time, in general, follows the trend NaCl > $NaNO_3$ > Na_2SO_4 at various temperatures, which can be attributed to structure maker and structure breaker ion effects. The semi-empirical static permittivity model has efficiently accounted for contributions due to dilution and internal depolarizing fields, kinetic depolarization, dielectric saturation, and the Debye-Falkenhagen effect. The results have shown that the Debye-Falkenhagen effect, which is observed as initial increase in static permittivity with concentration, is more pronounced for NaCl and $NaNO_3$ aqueous solutions, particularly at higher temperatures. The dielectric saturation effect, on the other hand, decreases with temperature, mainly because water molecules in the hydration layer of ions become more agile with increasing temperature and hence contribute to the total polarization characterized by static permittivity.

The methodology taken here is not only useful for ionic aqueous solutions presented in this work, but also other types of contaminant ions found commonly in water sources, such as bicarbonate HCO_3^-, calcium Ca^{2+}, magnesium Mg^{2+}, nitrite NO_2^-, and phosphate PO_4^{3-}. Highly accurate measurements and experimental data will be needed to derive appropriate models for these ions.

Acknowledgment

This work was funded by the USDA-National Institute of Food & Agriculture, Award Number 013025-00001. The authors gratefully acknowledge Amy L. Kaleita for her leadership on this project.

4.10. References

[1] B. A. Zimmerman, "Exploration of ion species in agricultural subsurface drainage waters," Iowa State University, 2016.

[2] K. Nörtemann, J. Hilland, and U. Kaatze, "Dielectric properties of aqueous NaCl solutions at microwave frequencies," *The Journal of Physical Chemistry A,* vol. 101, pp. 6864-6869, 1997.

[3] R. Buchner, G. T. Hefter, and P. M. May, "Dielectric relaxation of aqueous NaCl solutions," *The Journal of Physical Chemistry A,* vol. 103, pp. 1-9, 1999.

[4] E. Levy, A. Puzenko, U. Kaatze, P. B. Ishai, and Y. Feldman, "Dielectric spectra broadening as the signature of dipole-matrix interaction. I. Water in nonionic solutions," *The Journal of Chemical Physics,* vol. 136, p. 114502, 2012.

[5] A. Lileev, Z. Filimonova, and A. Lyashchenko, "Dielectric permittivity and relaxation in aqueous solutions of alkali metal sulfates and nitrates in the temperature range 288–313 K," *Journal of Molecular Liquids,* vol. 103, pp. 299-308, 2003.

[6] W. Wachter, W. Kunz, R. Buchner, and G. Hefter, "Is there an anionic Hofmeister effect on water dynamics? Dielectric spectroscopy of aqueous solutions of NaBr, NaI, NaNO3, NaClO4, and NaSCN," *The Journal of Physical Chemistry A,* vol. 109, pp. 8675-8683, 2005.

[7] J. Barthel, H. Hetzenauer, and R. Buchner, "Dielectric Relaxation of Aqueous Electrolyte Solutions II. Ion-Pair Relaxation of 1: 2, 2: 1, and 2: 2 Electrolytes," *Berichte der Bunsengesellschaft für physikalische Chemie,* vol. 96, pp. 1424-1432, 1992.

[8] R. Buchner, S. G. Capewell, G. Hefter, and P. M. May, "Ion-pair and solvent relaxation processes in aqueous Na2SO4 solutions," *The Journal of Physical Chemistry B,* vol. 103, pp. 1185-1192, 1999.

[9] B. A. Zimmerman and A. L. Kaleita, "Dissolved Constituents in Agricultural Drainage Waters," *Transactions of the ASABE,* vol. 60, pp. 847-859, 2017.

[10] A. Peyman, C. Gabriel, and E. Grant, "Complex permittivity of sodium chloride solutions at microwave frequencies," *Bioelectromagnetics,* vol. 28, pp. 264-274, 2007.

[11] J. Hasted, D. Ritson, and C. Collie, "Dielectric properties of aqueous ionic solutions. Parts I and II," *The Journal of Chemical Physics,* vol. 16, pp. 1-21, 1948.

[12] J. Hasted and G. Roderick, "Dielectric properties of aqueous and alcoholic electrolytic solutions," *The Journal of Chemical Physics,* vol. 29, pp. 17-26, 1958.

[13] U. Kaatze, V. Lönnecke, and R. Pottel, "Dielectric spectroscopy of aqueous ZnCl 2 solutions. Dependence upon solute concentration and comparison with other electrolytes," *Journal of Molecular Liquids,* vol. 34, pp. 241-255, 1987.

[14] U. Kaatze, "Complex permittivity of water as a function of frequency and temperature," *Journal of Chemical and Engineering Data,* vol. 34, pp. 371-374, 1989.

[15] R. Gulich, M. Köhler, P. Lunkenheimer, and A. Loidl, "Dielectric spectroscopy on aqueous electrolytic solutions," *Radiation and Environmental Biophysics,* vol. 48, pp. 107-114, 2009.

[16] M. R. Wright, *An introduction to aqueous electrolyte solutions: Ch12*: John Wiley & Sons, 2007.

[17] J. T. R. Watson, R. Basu, and J. V. Sengers, "An improved representative equation for the dynamic viscosity of water substance," *Journal of Physical and Chemical Reference Data,* vol. 9, pp. 1255-1290, 1980.

[18] A. L. Horvath, *Handbook of aqueous electrolyte solutions*: Halsted Press, 1985.

[19] R. Buchner, J. Barthel, and J. Stauber, "The dielectric relaxation of water between 0 C and 35 C," *Chemical Physics Letters,* vol. 306, pp. 57-63, 1999.

[20] G. Haggis, J. Hasted, and T. Buchanan, "The dielectric properties of water in solutions," *The Journal of Chemical Physics,* vol. 20, pp. 1452-1465, 1952.

[21] U. Kaatze, "Bound water: Evidence from and implications for the dielectric properties of aqueous solutions," *Journal of Molecular Liquids,* vol. 162, pp. 105-112, 2011.

[22] N. Agmon, "Tetrahedral displacement: The molecular mechanism behind the Debye relaxation in water," *The Journal of Physical Chemistry,* vol. 100, pp. 1072-1080, 1996.

[23] D. Loginova, A. Lileev, and A. Lyashchenko, "Dielectric properties of aqueous potassium chloride solutions as a function of temperature," *Russian Journal of Inorganic Chemistry,* vol. 47, pp. 1426-1433, 2002.

[24] J. Barthel, R. Buchner, P.-N. Eberspächer, M. Münsterer, J. Stauber, and B. Wurm, "Dielectric relaxation spectroscopy of electrolyte solutions. Recent developments and prospects," *Journal of Molecular Liquids,* vol. 78, pp. 83-109, 1998.

[25] E. V. Anslyn and D. A. Dougherty, *Modern physical organic chemistry*: University science books, 2006.

[26] T. Chen, G. Hefter, and R. Buchner, "Dielectric spectroscopy of aqueous solutions of KCl and CsCl," *The Journal of Physical Chemistry A,* vol. 107, pp. 4025-4031, 2003.

[27] U. Kaatze, R. Behrends, and R. Pottel, "Hydrogen network fluctuations and dielectric spectrometry of liquids," *Journal of Non-Crystalline Solids,* vol. 305, pp. 19-28, 2002.

[28] Wolfram|Alpha. [Accessed: 2018, March 27]. Available: http://m.wolframalpha.com

[29] J. A. Pople, "Molecular association in liquids II. A theory of the structure of water," *Proc. R. Soc. Lond. A,* vol. 205, pp. 163-178, 1951.

[30] C. Coulson and D. Eisenberg, "Interactions of H _2 O Molecules in Ice. II. Interaction Energies of H _2 O Molecules in Ice," *Proceedings of the Royal Society of London. Series A, Mathematical and Physical Sciences,* pp. 454-459, 1966.

[31] J. B. Hasted, *Aqueous dielectrics*: Chapman and Hall, 1973.

[32] G. Oster and J. G. Kirkwood, "The influence of hindered molecular rotation on the dielectric constants of water, alcohols, and other polar liquids," *The Journal of Chemical Physics,* vol. 11, pp. 175-178, 1943.

[33] J. Morgan and B. Warren, "X-Ray Analysis of the Structure of Water," *The Journal of Chemical Physics,* vol. 6, pp. 666-673, 1938.

[34] H. Xiang, "A new enthalpy-of-vaporization equation," *Fluid Phase Equilibria,* vol. 137, pp. 53-62, 1997.

[35] E. V. Tsiper, "Polarization forces in water deduced from single molecule data," *Physical Review Letters,* vol. 94, p. 013204, 2005.

[36] F. E. Jones and G. L. Harris, "ITS-90 density of water formulation for volumetric standards calibration," *Journal of Research of the National Institute of Standards and Technology,* vol. 97, p. 335, 1992.

[37] U. Kaatze, "The dielectric properties of water in its different states of interaction," *Journal of Solution Chemistry,* vol. 26, pp. 1049-1112, 1997.

CHAPTER 5. GENERAL CONCLUSION

5.1. Summary

The research presented in this dissertation is motivated by a need for an effective, real-time, and affordable sensing system for monitoring of contaminant ions and their concentrations in tile-drained water. High levels of nitrate, which is mainly due to efflux from agricultural lands, is a major contributor to hypoxic conditions in receiving waters and is expensive to remove from drinking water. In recent years, great efforts have been devoted to the development of effective ion monitoring systems that are capable of operating with very low (~ millimoles per liter), agriculturally relevant concentrations. Most of these systems, however, do not meet all the criteria mentioned above. The dielectric spectroscopy method within radio-frequency and microwave frequency ranges is proposed, here, as a potential tool to identify ions and estimate their concentrations in agriculturally-relevant aqueous solutions. The dielectric properties of agriculturally-relevant aqueous solutions of sodium chloride (NaCl), sodium nitrate ($NaNO_3$), and sodium sulphate (Na_2SO_4) that are among the most common ionic pollutants found in agricultural tile drainage waters in Iowa and the United States have been thoroughly investigated. Assessment of measurement uncertainties, which comprise random and systematic errors, has been conducted. It has been shown that systematic errors, which are due to non-ideal probe dimensions, imperfect instrument (VNA) calibration, calibration of the probe (short-air-load method), and cable phase instability, are the main contributors to the measurement uncertainty in both real ε' and imaginary ε'' permittivity values with relative standard uncertainties around or below 1 %, and are far larger than the random errors, whose relative standard uncertainties are around 0.1 %. Furthermore, covariance matrix and Monte Carlo methods have been conducted to

calculate the associated uncertainties of the extracted indicator parameters. The uncertainty values evaluated through the Monte Carlo method have been found to be slightly higher than those evaluated through the covariance matrix method. The Monte Carlo method, however, considerably reduces the tediousness of analytical calculations associated with the covariance matrix method. Dielectric spectra of samples of various concentrations have been measured at various temperatures and fitted using a single-term Debye relaxation model which is found to be the best model within the frequency range under consideration, i.e., 200 MHz to 20 GHz. The Debye relaxation parameters which include static permittivity ε_{dc}, relaxation time τ, infinite permittivity ε_{∞}, and specific conductivity σ, along with the associated uncertainties for each of NaCl, $NaNO_3$, and Na_2SO_4 aqueous solutions have been extracted from corresponding dielectric spectra. The static permittivity ε_{dc}, relaxation time τ, and specific conductivity σ have demonstrated useful trends as potential indicators of ion concentration and type. A method of judiciously exploiting the indicators, by means of 3D trajectory plot, has been proposed to uniquely identify an ion and infer its concentration. The 3D trajectory plot suggests that the ion type and concentration of an unknown ionic aqueous solution can be found by measuring its dielectric spectrum, extracting ε_{dc}, τ, and σ parameters, and mapping these indicators to a benchmark data set from which the ion type and concentration can be inferred. The benchmark data set for single-type ion systems of NaCl, $NaNO_3$, and Na_2SO_4 aqueous solutions within a broad range of agriculturally-relevant concentrations, i.e., 0 to 20 mmol/L, and temperatures, i.e., 5 °C to 30 °C in 5 °C increments have been provided by this research. Analytical and semi-empirical concentration- and temperature-dependent parametric models of specific conductivity $\sigma(c, T)$, static permittivity $\varepsilon_{dc}(c, T)$, and relaxation time $\tau(c, T)$, accounting for physical chemistry and molecular dynamics for each ionic

system of NaCl, $NaNO_3$, and Na_2SO_4 have been developed. The analytical conductivity model presented, which is based on Debye, Huckel, and Onsager (DHO) theory, accounts for the electrophoretic and asymmetric relaxation effects, and agrees well (~ 1% difference at most) with the experimental data within the concentration range studied. The conductivity increases with concentration and temperature and in general the conductivity magnitude follows $\sigma_{Na_2SO_4} > \sigma_{NaCl} > \sigma_{NaNO_3}$ at each temperature and concentrations. The semi-empirical relaxation time model, which is directly proportional to temperature and the number of hydrogen bonds needed to be broken for the ability of a water molecule, has been developed on the basis of Eyring's approach. The model successfully estimates the resulting decrement in the relaxation time as a function of temperature and concentration. The resulting decrement in the relaxation time, in general, follows the trend $\tau_{Na_2SO_4} > \tau_{NaNO_3} > \tau_{NaCl}$ at various temperatures. The semi-empirical static permittivity model has efficiently accounted for contributions due to dilution and internal depolarizing fields, kinetic depolarization, dielectric saturation, and the Debye-Falkenhagen effect. The results have shown that the decrements in static permittivity due to aggregation of dilution and internal depolarizing field, kinetic depolarization, and dielectric saturation follow the trend $\varepsilon_{dc_{NaCl}} > \varepsilon_{dc_{NaNO_3}} > \varepsilon_{dc_{Na_2SO_4}}$ at various temperatures. In addition, within the low concentration range studied, it has been observed that in NaCl and $NaNO_3$ solutions there is significant positive contribution due to the Debye-Falkenhagen effect that increases the static permittivity, particularly at lower concentrations. This effect becomes more pronounced as temperature increases. The Debye-Falkenhagen effect has also been discussed to be possibly related to the electrophoretic effect and the coordination number, leading to the Debye-Falkenhagen effect strength to follow $NaCl > NaNO_3 > Na_2SO_4$.

All in all, the research presented in this dissertation lays a foundation upon which an electrical sensing system can be designed for the efficient monitoring and analysis of agriculturally-relevant contaminant ions and their concentrations in tile drainage waters. A method based upon dielectric spectroscopy can potentially address the need for a fast, real-time, field-deployable, and economically feasible sensor, improving upon existing high-cost or non-durable monitoring systems.

5.2. Feasibility of Potential Sensor

Cost

A sensor capable of measuring the dielectric spectra of samples can be designed based on well-known resonant methods, such as, open-ended coaxial resonators. The manufacturing cost of such a sensor would be low, as it can be made of inexpensive and readily available coaxial cables. Bulk manufacturing would further lower the cost of production. In addition, it may be possible to measure the dielectric spectra at some, but enough, discrete frequencies (resonance frequencies) which make the sensor to be used in conjunction with a much simpler and less expensive measuring device than a broadband Vector Network Analyzer (VNA). A phase-locked loop (PLL) can be implemented to generate frequency stable signals at desired discrete frequencies. The use of such method would render the resonant sensor a much more economically viable system than broadband methods as well as the ultraviolet (UV) absorption sensors.

Sensitivity

The rather large uncertainties quantified in this research for the individual extracted dielectric indicators at these agriculturally-relevant low concentrations do not mask the general trends of the indicators when concentration and temperature change. In the real field environment, however, these may interfere with the successful interpretation of measured

data. A lot of care should then be devoted to designing a highly-sensitive sensor that properly characterizes the environment (e.g. temperature) as well as the solutions of interest. As a suggestion, this could be potentially overcome by providing a large input power to the system (in the order of a few Watts), or using a suitable Low Noise Amplifier (LNA) to increase the overall signal power, and making it easier to separate it from the noise background.

Field Deployment

A resonant sensor can be designed to fit into standard tile drains. The part of the sensor which interacts with the solution can be encapsulated in a thin chemically-inert polymer coating, for example, PTFE tape, to prevent the conductor from corroding. This will result in the sensor having high durability when compared to an ion-selective electrode (ISE) sensor. Another important factor which requires further research to make the sensor field deployable is the knowledge of performance of the sensor when the sample is flowing. Uneven flow in different parts of the sample may lead to turbulences, locally increasing the temperature of certain regions and thus deteriorating results. This can be avoided by placing the sensor in a tank storing the tile drainage water where the flow can be expected to be considerably less.

Real Time Operation

The interaction of the molecular dipoles and ions with an applied electric field is almost instantaneous at RF and MW frequencies (200 MHz to 20 GHz studied here). As a result, the operation would be real time for practical purposes. The speed of operation, indeed, is likely to be limited by the rate at which the data can be collected and read.

5.3. Future Directions

Mixture of Ions

Driven by the preceding section, the future work on dielectric spectroscopy and characterization of ionic aqueous solutions would involve measurements and highly accurate experimental data for other ionic pollutants, such as bicarbonate HCO_3^-, calcium Ca^{2+}, magnesium Mg^{2+}, nitrite NO_2^-, and phosphate PO_4^{3-} found commonly in tile-drainage waters. In a tile drain containing agricultural efflux, there would be multiple types of compounds dissolved in water. The next step could be further development of the dielectric spectroscopy method for multi-substance systems and distinguishing between multiple substances present simultaneously in a sample solution. In cases of ionic and non-ionic substances present in the sample simultaneously, one way possible can be employing multiple-term relaxation models to fit the dielectric spectra, in which, each relaxation term correspond to particular substance of interest. If the sample consists of multiple ions dissolved in water, it may be practically difficult to decompose the individual relaxation terms associated with each ion, as they nearly overlap each other within the low ionic concentrations. One speculative way of attacking such cases is suggested as follows. Let's assume there are three types of unknown ion systems with unknown concentrations c_1, c_2, and c_3 in the sample, and also, we already measured the benchmark relaxation parameters, i.e., static permittivity, relaxation time, and conductivity, for a pool of different ion systems (NaCl, $NaNO_3$, Na_2SO_4, $MgCl_2$, $CaCl_2$, $NaHCO_3$, $NaNO_2$, etc.) at different concentrations. We measure the dielectric spectra of the sample, extract its relaxation parameters, i.e., ε_{dc}, τ, and σ, and calculate the differences with respect to the relaxation parameters of deionized water (denoted by superscript 0), as

$$\begin{aligned}\Delta\varepsilon_{dc} &= \varepsilon_{dc}^{0} - \varepsilon_{dc} \\ \Delta\tau &= \tau^{0} - \tau \\ \Delta\sigma &= \sigma^{0} - \sigma\end{aligned} \tag{4.32}$$

We can then attempt to form various 'system of equations' based on calculated values in (4.32) and n different combinations of benchmark relaxation parameters, as

$$1.\begin{cases}\Delta\varepsilon_{dc} = \delta_{\varepsilon_{dc}}^{\mathrm{NaCl}}(c_1) + \delta_{\varepsilon_{dc}}^{\mathrm{NaNO_3}}(c_2) + \delta_{\varepsilon_{dc}}^{\mathrm{Na_2SO_4}}(c_3) \\ \Delta\tau = \delta_{\tau}^{\mathrm{NaCl}}(c_1) + \delta_{\tau}^{\mathrm{NaNO_3}}(c_2) + \delta_{\tau}^{\mathrm{Na_2SO_4}}(c_3) \\ \Delta\sigma = \delta_{\sigma}^{\mathrm{NaCl}}(c_1) + \delta_{\sigma}^{\mathrm{NaNO_3}}(c_2) + \delta_{\sigma}^{\mathrm{Na_2SO_4}}(c_3)\end{cases}$$

$$2.\begin{cases}\Delta\varepsilon_{dc} = \delta_{\varepsilon_{dc}}^{\mathrm{NaCl}}(c_1) + \delta_{\varepsilon_{dc}}^{\mathrm{NaNO_3}}(c_2) + \delta_{\varepsilon_{dc}}^{\mathrm{MgCl_2}}(c_3) \\ \Delta\tau = \delta_{\tau}^{\mathrm{NaCl}}(c_1) + \delta_{\tau}^{\mathrm{NaNO_3}}(c_2) + \delta_{\tau}^{\mathrm{MgCl_2}}(c_3) \\ \Delta\sigma = \delta_{\sigma}^{\mathrm{NaCl}}(c_1) + \delta_{\sigma}^{\mathrm{NaNO_3}}(c_2) + \delta_{\sigma}^{\mathrm{MgCl_2}}(c_3)\end{cases}$$

$$3.\begin{cases}\Delta\varepsilon_{dc} = \delta_{\varepsilon_{dc}}^{\mathrm{NaHCO_3}}(c_1) + \delta_{\varepsilon_{dc}}^{\mathrm{NaNO_3}}(c_2) + \delta_{\varepsilon_{dc}}^{\mathrm{MgCl_2}}(c_3) \\ \Delta\tau = \delta_{\tau}^{\mathrm{NaHCO_3}}(c_1) + \delta_{\tau}^{\mathrm{NaNO_3}}(c_2) + \delta_{\tau}^{\mathrm{MgCl_2}}(c_3) \\ \Delta\sigma = \delta_{\sigma}^{\mathrm{NaHCO_3}}(c_1) + \delta_{\sigma}^{\mathrm{NaNO_3}}(c_2) + \delta_{\sigma}^{\mathrm{MgCl_2}}(c_3)\end{cases}$$

$$\vdots$$

$$n.\begin{cases}\Delta\varepsilon_{dc} = \delta_{\varepsilon_{dc}}^{\mathrm{NaHCO_3}}(c_1) + \delta_{\varepsilon_{dc}}^{\mathrm{NaNO_2}}(c_2) + \delta_{\varepsilon_{dc}}^{\mathrm{CaCl_2}}(c_3) \\ \Delta\tau = \delta_{\tau}^{\mathrm{NaHCO_3}}(c_1) + \delta_{\tau}^{\mathrm{NaNO_2}}(c_2) + \delta_{\tau}^{\mathrm{CaCl_2}}(c_3) \\ \Delta\sigma = \delta_{\sigma}^{\mathrm{NaHCO_3}}(c_1) + \delta_{\sigma}^{\mathrm{NaNO_2}}(c_2) + \delta_{\sigma}^{\mathrm{CaCl_2}}(c_3)\end{cases} \tag{4.33}$$

where $\delta(c)$s represent the difference of corresponding benchmark relaxation parameters for each ion system and those of deionized water, e.g., $\delta_{\tau}^{\mathrm{NaCl}}(c) = \tau^{0} - \tau_{\mathrm{NaCl}}(c)$. As models for δs are non-linear (Chapter 4), each system of equation might not be well-posed and have a unique solution for c_1, c_2, c_3. A conducive approach, therefore, is to employ methods of

optimization (simply meaning to play around with variables, but in a judicious way) to find a set of c_1, c_2, c_3 that satisfies one of the n systems of equations, i.e., (4.33), in the best way possible. We can then refer to that system of equation as the system representing the unknown ions (which are now found) with corresponding c_1, c_2, and c_3 concentrations found from the optimization method.

Low-Concentration Measurements

In terms of physical chemistry, the experimental observance of the Debye-Falkenhagen (DF) effect, predicted to exist at low ionic concentrations, has been a topic of debate for a long time. In this research the initial increase in measured static permittivity of sodium chloride (NaCl) and sodium nitrate ($NaNO_3$) has been attributed to the DF effect. Further measurements and highly accurate experimental data for other ionic systems are desirable to extend our knowledge of ionic atmosphere polarization and the positive contribution of the DF effect to static permittivities in low concentration ionic solutions. One idea to improve the accuracy of measurements at low ionic concentrations which can also be beneficial in a potential practical system, could include the idea of manipulating the sample to be more amenable to measurements by deliberately polarizing the sample through a direct-current (DC) bias field generated from designed electrodes. This may amplify the response of the sample in the dielectric spectra, particularly, at lower frequencies where static permittivity and conductivity are pronounced, so a better resolution can be obtained. As measurement systems and dielectric spectra are more responsive to high-concentration samples, another idea could include driving off the water through heat which results in increased concentration (per unit volume) of the sample.

Other Applications

The concept of employing dielectric spectroscopy in identifying substances and their concentrations can be extended to other applications and is likely to be particularly successful when the target substances are of high concentration (~ mol/L) such as in wastewater treatment.